SUBSONIC FLOW PAST ROTATING BODIES.

Brahman Sivaprakasapillai, B.Sc., (Eng.)

October, 1964.

A thesis for the Degree of Doctor of Philosophy in the Faculty of Engineering of the University of London.

ABSTRACT.

This thesis describes an experimental investigation of the flow past a rotating circular cylinder placed in a wind stream. The cylinder was rotated about a diameter in its mid-plane, with the axis of rotation parallel to the wind stream. The Reynolds numbers at the different cross-sections were such as to have laminar separation of the flow from the cylinder surface.

The investigation consisted of measuring the pressures and examining the streamlines at the cylinder surface.

The object of the investigation was to obtain an understanding of the flow past a particular rotating body with a view to laying the framework for a better understanding of the flows past fans and propellers.

The investigation revealed that the pressure profiles, at all sections, were asymmetrical about the stagnation point and that the peak suction pressure coefficients obtained at sections near the axis of rotation were much larger than those

obtained on the stationary cylinder. It was also found that the radial component of velocity at the cylinder surface in the region of attached flow was small at all sections. Further, the pressure in the separated region was not uniform around the circumference. It is argued that the changes observed in the pressure profile, on rotating the cylinder, are due to secondary effects in the wake arising from the fluid being centrifuged towards the ends of the cylinder.

ACKNOWLEDGEMENTS.

The author wishes to acknowledge with grateful thanks the many valuable criticisms made by Mr. G. Jackson, particularly whilst writing this thesis.

The author acknowledges most gratefully his indebtedness to Prof. P.R.Owen for the valuable criticisms made after reading an initial draft.

Grateful acknowledgement must also be made of the help given by Mr. W.C.Wilson, Education Officer, Vickers-Armstrongs (Engineers) Limited, in making arrangements for having this thesis typed and duplicated.

Thanks are also due to the workshop staff of the Department of Aeronautics and in particular to Messrs. W.H. Davies, F. Fone and J. Coles.

Finally, the author thanks Mrs. F. Fawcett for typing this thesis.

LIST OF CONTENTS.

LIST OF ILLUSTRATIONS.

PART.	FIG.NO.	TITLE.
II	9	V = 96 ft.sec.$^{-1}$. N = 983 r.p.m.
II	10	V = 60 ft.sec.$^{-1}$. N = 502 r.p.m.
II	11 to 13	PRESSURE DISTRIBUTION ON THE STATIONARY CYLINDER.
II	11	V = 60 ft.sec.$^{-1}$. $R_E = 0.77 \times 10^5$.
II	12	V = 79 ft.sec.$^{-1}$. $R_E = 1.0 \times 10^5$.
II	13	V = 96 ft.sec.$^{-1}$. $R_E = 1.2 \times 10^5$.
II	14 to 19	PRESSURE DISTRIBUTION IN SEPARATED REGION OF ROTATING CYLINDER.
II	14	V = 60 ft.sec.$^{-1}$. N = 1190 r.p.m.
II	15	V = 79 ft.sec.$^{-1}$. N = 1190 r.p.m.
II	16	V = 96 ft.sec.$^{-1}$. N = 1190 r.p.m.
II	17	V = 60 ft.sec.$^{-1}$. N = 983 r.p.m.
II	18	V = 79 ft.sec.$^{-1}$. N = 983 r.p.m.
II	19	V = 96 ft.sec.$^{-1}$. N = 983 r.p.m.
II	20 to 26	DEVELOPED VIEW OF SURFACE FLOW PATTERNS.
II	20	V = 60 ft.sec.$^{-1}$. N = 1190 r.p.m.
II	21	V = 79 ft.sec.$^{-1}$. N = 1190 r.p.m.
II	22	V = 96 ft.sec.$^{-1}$. N = 1190 r.p.m.
II	23	V = 60 ft.sec.$^{-1}$. N = 983 r.p.m.
II	24.	V = 79 ft.sec.$^{-1}$. N = 983 r.p.m.
II	25	V = 96 ft.sec.$^{-1}$. N = 983 r.p.m.
II	26	V = 60 ft.sec.$^{-1}$. N = 502 r.p.m.

PART.	FIG.NO.	TITLE.
II	27	Circumferential pressure distribution in attached region of rotating cylinder.
II	27a	Pressure distribution on circular cylinder (Two-dimensional flow).
II	28	Magnitude and position of the minimum pressure on the rotating cylinder.
II	29	Location of separation points on rotating cylinder.
II	30	Variation of k with advance ratio.
II	31	Variation of H with $(V/\Omega a)^2$.
II	32a	Co-ordinate systems used in investigation.
II	32b	Isometric view of flow pattern around the rotating cylinder.
II	32c	Proposed flow model for rotating cylinder.
II	32d	Flow model for stationary cylinder.
II	33	Lift and drag coefficients on rotating cylinder.
II	34	Thrust and Torque coefficients on rotating cylinder.
II	35	Estimated pressure distribution on rotating cylinder: $V = 60$ ft.sec^{-1}, $N = 1190$ r.p.m., $y = 6$ ins.

LIST OF SYMBOLS.

V = wind velocity of undisturbed stream in tunnel (ft.sec.$^{-1}$).

$p_{stat.}$ = static pressure upstream of model (mm. H_2O).

$2a$ = diameter of cylinder (ft.)

(x,y,z) = rectangular cartesian co-ordinates, vide Fig.32.

$(u,v,w.)$ = velocity components in the (x,y,z) directions.

N = speed of rotation of cylinder (r.p.m.)

(ϕ,y,s) = cylindrical polar co-ordinates, vide Fig.32

(u^1,v,w^1) = velocity components in (ϕ,y,s) directions.

C_p = $\dfrac{p - p_{stat}}{\frac{1}{2}\rho(V^2+\Omega^2 r^2_{stag})}$

r = perpendicular distance from axis of rotation of a point.

R_E = $\dfrac{2a\sqrt{V^2 + \Omega^2 r^2_{stag}}}{\nu}$

θ = angle measured from stagnation point (degrees).

λ = $V/\Omega r_{stag.}$

Ω = speed of rotation of cylinder. (rad.sec.$^{-1}$)

ϱ = density of air in tunnel. (slug.ft^{-3})

Θ = air temperature in tunnel. (^{o}C absolute).

ν = kinematic viscosity (ft^{2}.sec.$^{-1}$)

k = constant, vide Appendix V.

H = arbitrary function of y, vide Appendix V.

α' = $90 - \tan^{-1} V/\Omega r = \tan^{-1}\frac{\Omega r}{V}$

α = Angular displacement of maximum pressure point on rotating cylinder, relative to its position on the stationary cylinder.

LIST OF SUFFICES.

s	=	separation point, e.g. θ_s
W-W	=	windward face, e.g. $\theta_{s_{W-W}}$
L-W	=	leeward face, e.g. $\theta_{s_{L-W}}$
p-s	=	minimum pressure (peak suction) point, e.g. $C_{p_{p-s}}$
stag.	=	stagnation point, e.g. $C_{p_{stag.}}$
max.	=	maximum pressure point, e,g. $C_{p_{max.}}$

1.0 INTRODUCTION.

The design of airscrews, ships' propellers, axial blowers and other similar rotodynamic machines is usually based on the assumption that the flow past the blades may be simulated by a two-dimensional cascade of aerofoils. This approach to the design has been due, in part at least, to the difficulties of making experimental investigations of the flow past rotating components. For example, the first experimental investigation had to await the development of suitable rotating seals that would enable the surface pressures to be measured by a stationary manometer. A further reason is the relative simplicity of the two dimensional model. The two-dimensional model has been found to be reliable for blades operating at low section angles of attack. The two-dimensional model cannot, however, predict the peak section lift coefficient or the angle of incidence at which a section stalls.

Himmelskamp (1945) reported an experimental investigation of the flow past a rotating impeller. He found that peak lift coefficients

at sections near the hub were much higher than those on the equivalent cascade and he also stated that stalling had been delayed. He suggested that the boundary layer in regions of adverse pressure gradient was thinner than that in two-dimensional flow, as a result of radial velocities in the boundary layer. He proceeded to argue that thinner boundary layers are less likely to separate and, therefore, there must be a delay in the onset of stall.

Himmelskamp succeeded in establishing two points. First, that it was possible to make experimental investigations on rotating blades. Second, that it was possible to design turbo-machines to operate at larger angles of attack than had previously been thought possible on the basis of two-dimensional studies. His work, however, had two weak points. The first was that, though he had succeeded in developing a technique to measure pressures, his technique was not completely reliable. This proved to be a drawback in so far as he was only able to make a qualitative analysis of his painstaking boundary layer total

head traverses. The second was that his use of wool tufts for flow visualization meant that there was no reliable indication of surface flow patterns in regions of possible separation. This was because the equilibrium position of a tuft is governed by the shear forces on it and the centrifugal forces arising from the motion. In regions of low velocity, that is in regions immediately upstream of a separation point and in the separated region itself, the tuft is likely to settle along a blade generator under the dominant influence of the centrifugal accelerations. Thus on a rotating body a tuft is not a reliable indicator of the onset of flow separation. An attempt is made later in this thesis to argue that in Himmelskamp's work there was, at the highest rate of advance, flow breakaway from the surface of the impeller blade which Himmelskamp had not detected and an alternative interpretation of Himmelskamp's results is proposed.

Harvey (1960) developed a pressure pick-up that was suitable for use on rotating bodies. It had the advantage that it did not use rotating seals

to transmit pressures to a stationary manometer. The pressure pick-up consisted of a transducer situated within the rotating system, linked to stationary measuring equipment through a system of brushes and slip-rings. This scheme of transmitting an electrical signal to an outside measuring system has proved to be both reliable and accurate.

The development of a flow visualization technique suitable for use on rotating bodies is described in Part I of this thesis. This method shows up the limiting stream-lines in regions of attached flow and consequently the position of flow separation. It does not suffer from the limitations of a tuft in that it is insensitive to centrifugal accelerations.

With the aid of these newer techniques for the measurement of surface pressures and the visualization of surface flow patterns, an experiment was designed to bring out the changes in the flow structure caused by rotation. This experiment is described in Part II of this thesis.

P A R T I.

1. INTRODUCTION.

Pictures of flow patterns at the surface of rotating blades would be useful in the design of fan and propeller blades. Conventional flow visualization techniques using smoke[1] or wool tufting[2] have been used to obtain such pictures. These techniques, however, are not very convenient to use because of the difficulty of illuminating regions of interest satisfactorily. Further, their indications are not easy to interpret because the photographs used to record them must show views oblique to at least some parts of the blade surface. Lastly, wool tufts cannot be used to trace out limiting streamlines. There is then, a need for a technique that is reliable in its indications of laminar flow, turbulent flow and separation and is also convenient to use.

A technique has been developed in which acidified air fed into the boundary layer is made to trace its path over a specially prepared coating on the body surface. A laminar boundary layer gives a trace different from a turbulent boundary layer and separation is clearly shown.

This technique is, however, not confined to rotating blades and could be used in any boundary layer investigation.

2. DETAILS OF THE STAIN TECHNIQUE.

A sheet of blue litmus paper is wrapped around the body and punctured at points of interest to allow the escape of air carrying moist hydrogen chloride into the boundary layer. The subsequent motion of the air is then recorded as a salmon pink stain on an azure background.

The litmus paper is prepared by air-drying a sheet of chromatography paper dipped into a saturated aqueous solution of litmus. The paper is then attached along its edges to the body by means of sellotape. To prevent the flow of acidified air between the paper and the body surface a strip of double coated bonding tape is placed between the paper and the body.

The acidified air is produced by bubbling air through a 32% w./w. solution of hydrochloric acid. The apparatus used is shown in fig.1. A coarse adjustment to the rate of bubbling is obtained by adjusting the height of the two water bottles

relative to one another and a finer adjustment by means of the screw clip. The rate of bubbling should be kept at a low steady level in order that fine well-developed streaks may be obtained.

The stain technique is most suitable for bodies fitted out for pressure plotting because the network of pressure tubes and holes can then be used to inject the acidified air.

3. PRELIMINARY TRIALS WITH THE STAIN TECHNIQUE.

The stain technique was used on two bodies, one a stationary yawed wing and the other a rotating circular cylinder. The yawed wing was chosen because it provided a means of comparing the indications of the stain technique with those of the conventional techniques. The rotating cylinder was chosen to show up any limitations of the technique on rotating bodies and because the flow past a rotating body is of some interest per se. All the tests were made in the 3' x 2' wind tunnel at Imperial College.

3.1 The Yawed Wing.

The yawed wing has a 9.75in. chord and spans the working section of the wind tunnel. The

chordwise profile of the wing is as shown in fig.3. The streamwise incidence of the wing can be varied between $\pm 10^{\circ}$. The angle of sweepback of the leading edge, i.e. the angle which the leading edge makes with a plane normal to the axis of the working section when the leading edge is horizontal, is 30°. The wing has a set of pressure tappings lying on a chordwise line in the position shown in fig.2.

Two incidences $+5\frac{1}{2}^{\circ}$ and $-5\frac{1}{2}^{\circ}$ and a wind speed of 84 ft/sec. were used. Experimental pressure distributions for these two incidences are given in figs.6a and 6b. The Reynolds number based on the chord was 4.25×10^5. The positive incidence gave a large extent of attached turbulent flow and the negative incidence a large extent of attached laminar flow on the upper surface of the wing. Figs.4a and 5a show photographs of the flow patterns obtained by using the Stain Technique, at $-5\frac{1}{2}^{\circ}$ and $+5\frac{1}{2}^{\circ}$ respectively. Figs.4b and 5b show for purposes of comparison photographs of the flow patterns, under the same conditions as figs. 4a and 5a respectively, obtained by painting the wing surface with a suspension of Dayglo in Paraffin.

In obtaining figs.4a and 5a it was found that a rate of injection of acidified air of 0.16 in^3/min. i.e. a bubble every 3 seconds, maintained over a period of $1\frac{1}{2}$ to 2 minutes gave satisfactory streaks. A slower rate of injection caused the streaks to be too fine, a faster rate too wide. Lastly, it was found that the time between commencement of staining and the formation of a complete streak was only 15 secs., the balance of the time being required for driving the air out of the connecting leads. Thus the amount of acidified air actually injected into the boundary layer was about 0.04 $ins.^3$

3.2 The Rotating Cylinder.

The cylinder used in this experiment was a wooden bar $16\frac{1}{2}$ ins. long x $2\frac{3}{4}$ ins. diameter. It was made to windmill about an axis through a diameter in its mid-plane by screwing a spoiler to one end as in fig.7. The steady rotational speed was 400 r.p.m. at a wind speed of 84 ft/sec.

The cylinder was screwed to the forward end of a hollow shaft mounted in bearings. The bearings were held in a housing fixed rigidly in the centre of the working section of the tunnel by four struts.

The acidified air was fed through a tube running loosely in the after-end of the hollow shaft. The air passed from the forward end of the hollow shaft through a tube embedded in the surface of the cylinder and out into the boundary layer at a point 6 ins. from the axis of rotation and very close to the stagnation line. A strip of litmus paper bearing a stain obtained in this way forms fig.8.*

4. DISCUSSION.

Inspection of fig.5b reveals that three regions of flow could be differentiated in the picture, viz. a small region of attached laminar flow, followed by a region covered by a separation bubble and last a region of attached turbulent flow. Comparison with fig.5a reveals that all three points of injection of acidified air have been in the turbulent region and that the streaks widened as they travelled aft as is to be expected. Further, if the geometric centre lines of the streaks are considered these lines are seen to reproduce the direction and the curvature of the limiting streamlines as faithfully as the Dayglo technique. The validity of this last statement

* Not given here in view of Figs.20 - 26 in Part II of this thesis.

can be amply confirmed by superposing a trace of the shortest streak in fig.5a on fig.5b whereupon a surprisingly good measure of agreement can be noted.

Inspection of fig.4b reveals two regions of flow, viz. a large region of attached laminar flow followed by a region of separated flow. The inference of attached laminar flow preceding separation is justified because the existence of attached turbulent flow must be accompanied either by separation bubble or by a transition of the flat plate type. Inspection of fig.4b reveals that there was no separation bubble. Inspection of fig.6a reveals a favourable pressure gradient which together with the fact that the Reynolds number for transition on a flat plate is 5×10^5 must be taken to imply that the transition again was unlikely. Inspection of fig.4a, in the light of these observations, reveals that all points of injection are in the region of attached laminar flow and that the width of the three shorter streaks in particular remain unchanged along their length. Further, the stained band running in a spanwise direction,

near the trailing edge in fig.4a, corresponds to the region of separated flow in fig.4b. The forward edge of the stained band corresponds to the line of separation indicated by the Dayglo technique in fig.4b. The formation of the stained band must be attributed to the spanwise component of flow and the turbulence in the separated region.

The formation of the stained band is a relatively slow process compared to the formation of the streak itself and if sufficient time is not given separation is indicated by the termination of the streak and not by the formation of the stained band. Separation in 2-d boundary layers was found to be indicated by the termination of the streak.

The stain technique is, therefore, capable of differentiating between regions of laminar flow and turbulent flow and also of indicating the commencement of separation.

If a technique such as the stain technique is to be used on rotating bodies it is essential that errors due to the difference in density between air and the acidified air used be small.

Some confidence on this score may be derived from two observations on the wing, viz. (1) the reasonably faithful reproduction of the curvature and the direction of the limiting streamlines and (2) the fact that the molecular weight of hydrogen chloride is 36.5 and that of water vapour is 18, whereby the molecular weight of the mixture must be quite near that of air, viz. 28.

In the case of the rotating cylinder the Reynolds number at the point of injection was 1.2×10^5. The Reynolds number for this purpose was based on the relative velocity far upstream and the cylinder diameter. The lower critical Reynolds number for a circular cylinder placed in the tunnel is 2×10^5 and a value of 1.2×10^5 would be in the high drag range. Inspection of fig.8* reveals that laminar separation occurred 79° aft of the stagnation line and that in the attached laminar boundary layer the radial component of velocity was small compared to the chordwise component. These observations agree with Graham's theoretical work as reported by Sears[3]. However, injection at a point 2" from the axis of rotation where the Reynolds

* Not given here in view of Figs.20 - 26 in Part II of this thesis.

number was substantially unchanged reveals separation 71^{o} aft of the stagnation line and even smaller ratios of radial to chordwise components of velocity in the attached laminar boundary layer. This would suggest that it would be difficult to use Himensz' cross-flow potential in the boundary layer calculations, as Graham did, in regions near the axis of rotation. The observations based on the stain technique are in accord with those of Himmelskamp[2] who found the effect of rotation more pronounced in regions nearer the hub than in regions nearer the tips of his airscrew. It must be emphasized, however, that too much reliance should not be placed on these preliminary observations of the stain technique because this experiment was not set up with a view to obtaining a detailed picture. A careful study of the flow past rotating circular cylinders will shortly be commenced.

It is found that flow patterns obtained by using the stain technique are capable of being preserved and, therefore, eliminates the need of photographing the indications either with a view to recording or with a view to preserving the indications.

The stain technique is in fact a modification of the smoke filament technique. However, the stain technique does not suffer from limitations either on the score of photography or on the score of clogging of the pipework with tarry deposits. Further, the smoke filament technique is found to be unsuitable for boundary layers where the free stream velocity exceeds 150-200 ft/sec. The stain technique has been tested on such a boundary layer at a speed of 200 ft/sec. and was found satisfactory.

CONCLUSION.

The stain technique has been tested on a stationary yawed wing and on a rotating cylinder and found to be a satisfactory method of flow visualization. The stain technique is capable of differentiating between laminar and turbulent boundary layers and of also indicating the commencement of separation. The amounts of hydrogen chloride actually released are very small and no ill effects have been observed.

REFERENCES.

1. LIPPISCH, A.M. Flow Visualization in two and three dimensional flow fields by use of Smoke Filaments. A.S.M.E. Symposium on Flow Visualization (1960).

2. HIMMELSKAMP, H. Profile investigations on a rotating airscrew. M.A.P. volkenrode.

3. SEARS, W.R. Boundary layers in three dimensional flow. A.M.R. 7. (1954).

APPENDIX.

It has been brought to the attention of the author, by Mr. D.F. Pilkington, of the possibility of developing a variant of the stain technique using the colour-foam-kit supplied by M/S Johnsons of Hendon. In this variant, the litmus paper is replaced by a sheet of 'fogged' photographic paper developed in the blue dye-coupler. This gives a very good contrast since bright yellow streaks are obtained against a deep blue background. The surface of the photographic paper being smoother

than that of the litmus paper is an added attraction. However, the method suffers a serious drawback in that very long exposures to acid vapours are required for the stain to be produced and to date a complete streak has not been produced at all.

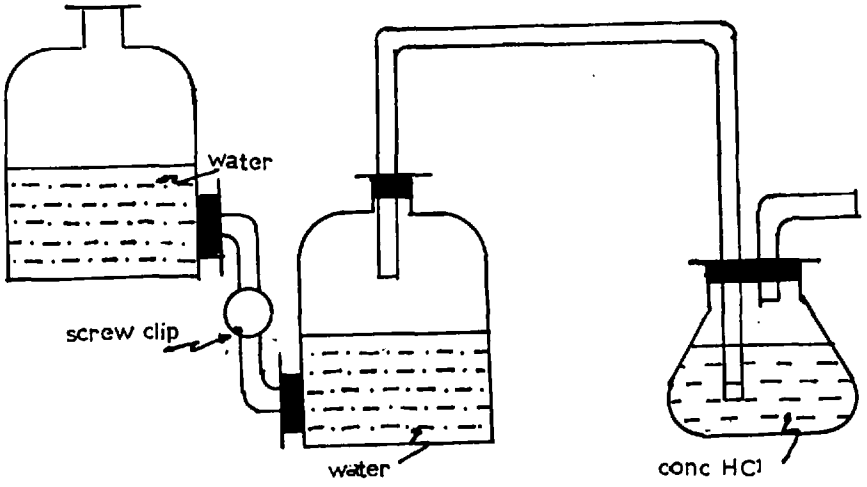

FIG.1: THE BUBBLING APPARATUS

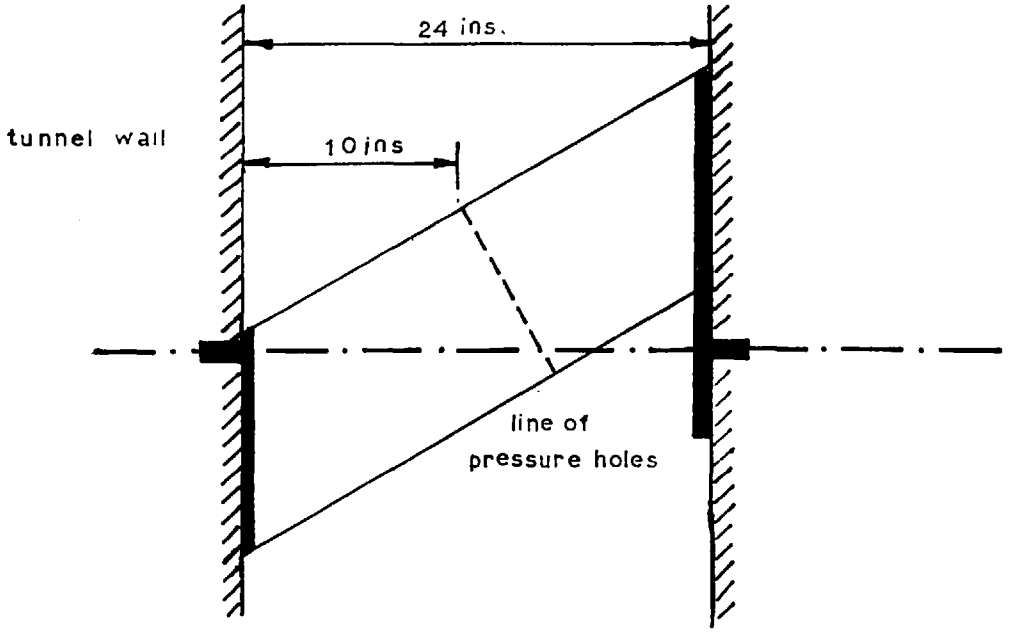

FIG. 2: PLAN VIEW OF YAWED WING

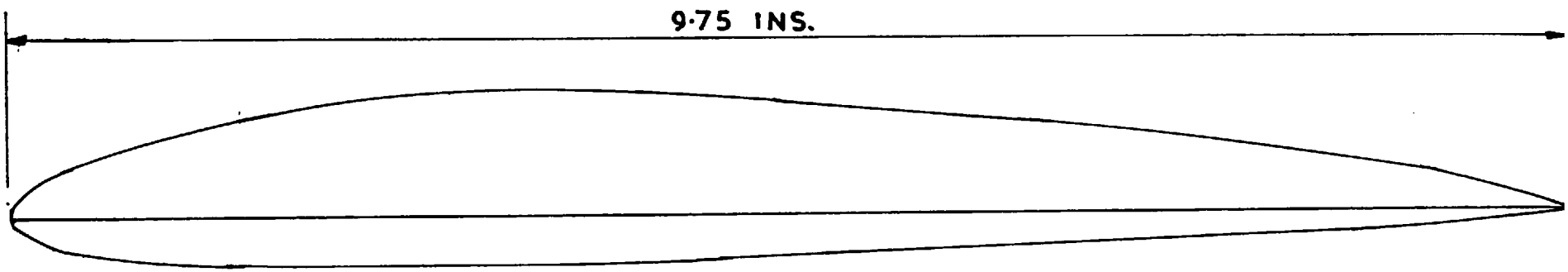

FIG.3: CHORDWISE PROFILE OF YAWED WING

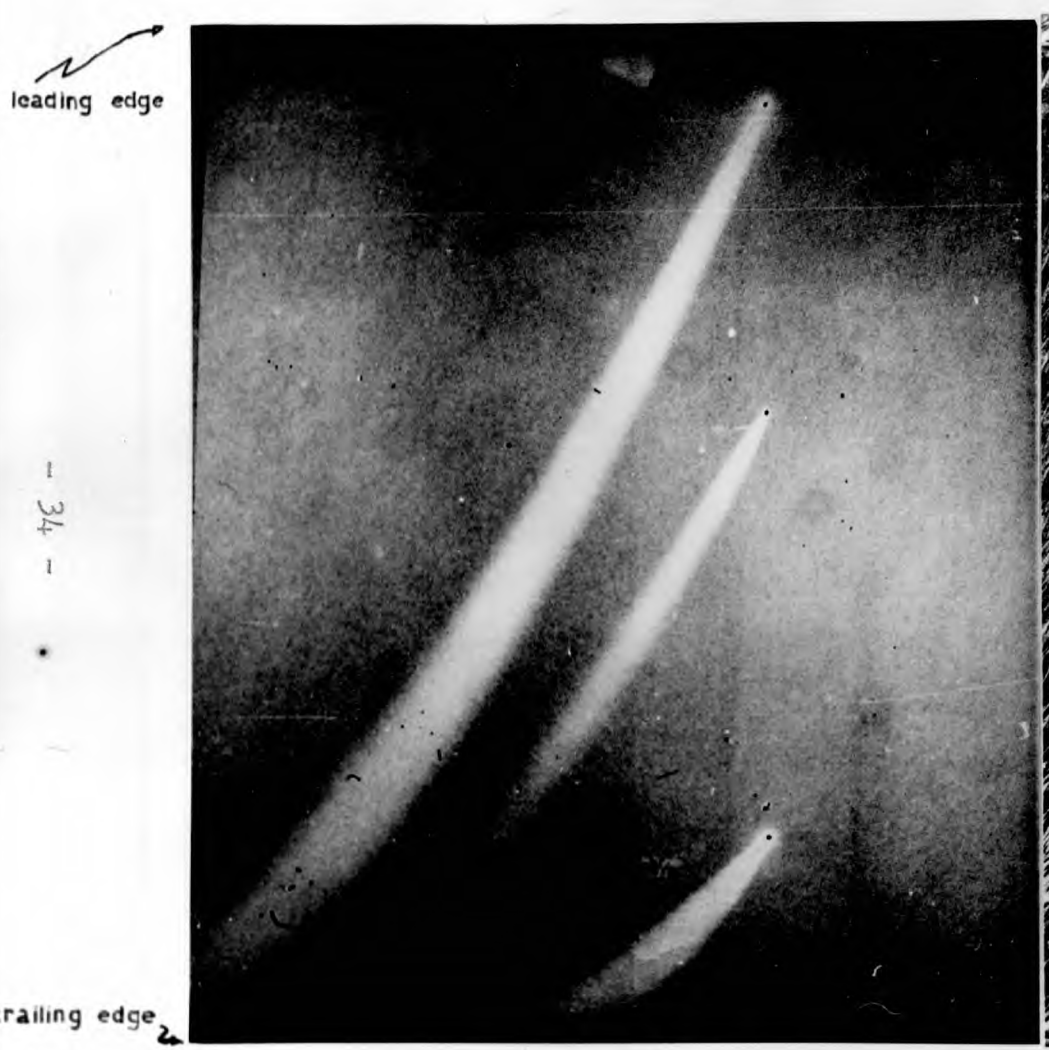

FIG: 5 a

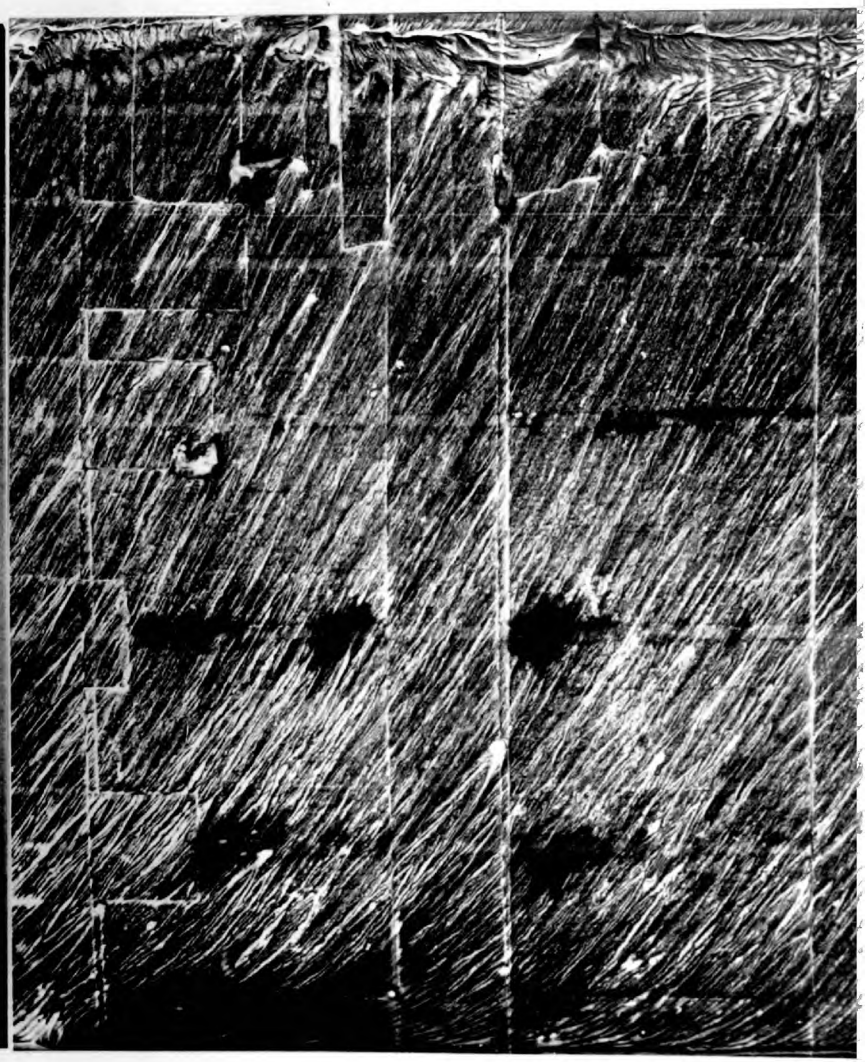

FIG: 5 b

FLOW PATTERN ON WING AT α = + 5·5°

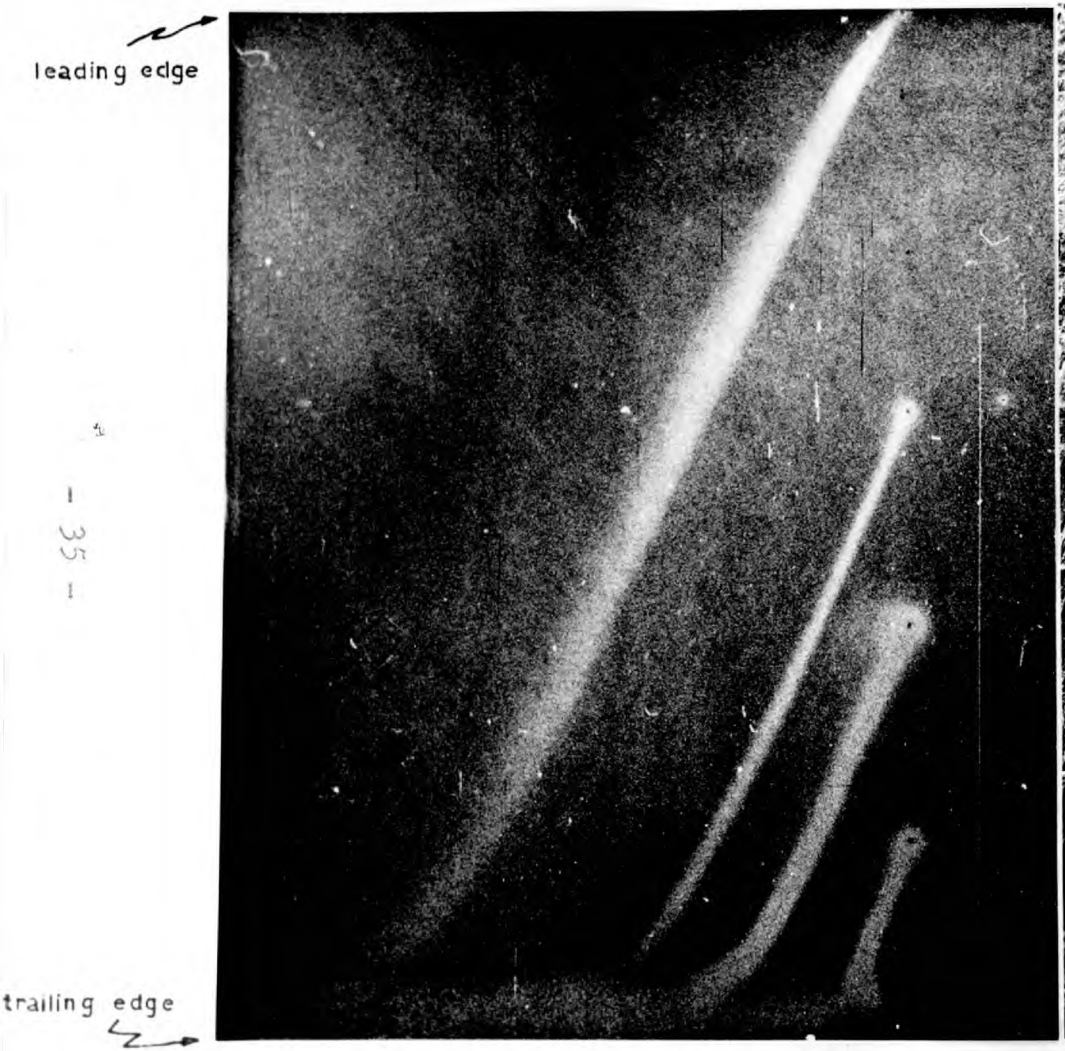

FIG: 4 a

FIG: 4 b

FLOW PATTERN ON WING AT $\alpha = -5{\cdot}5°$

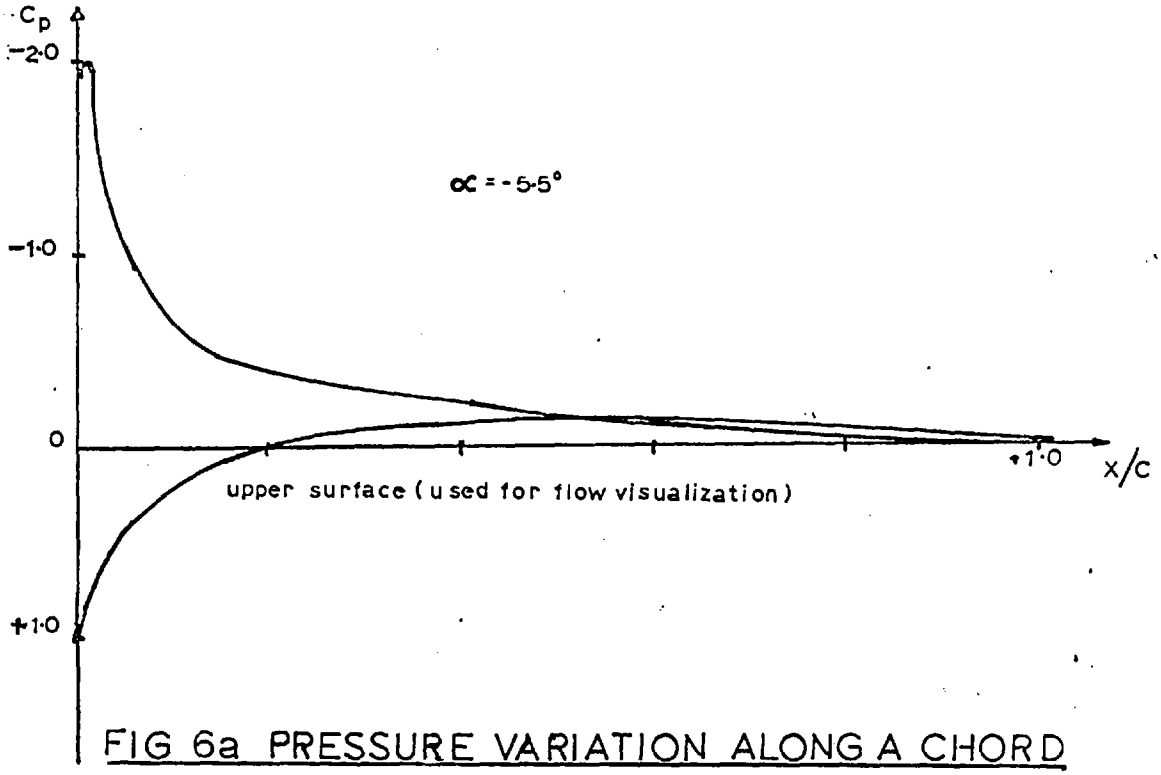

FIG 6a PRESSURE VARIATION ALONG A CHORD

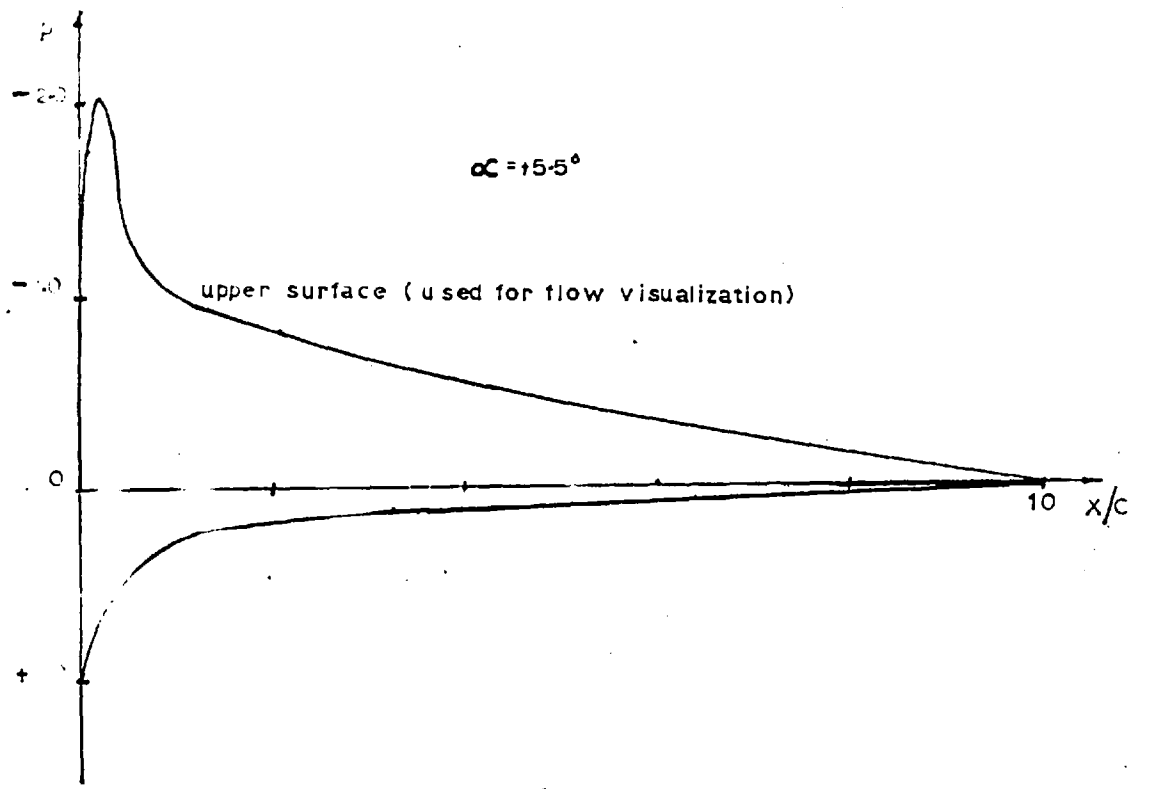

FIG 6b PRESSURE VARIATION ALONG A CHORD

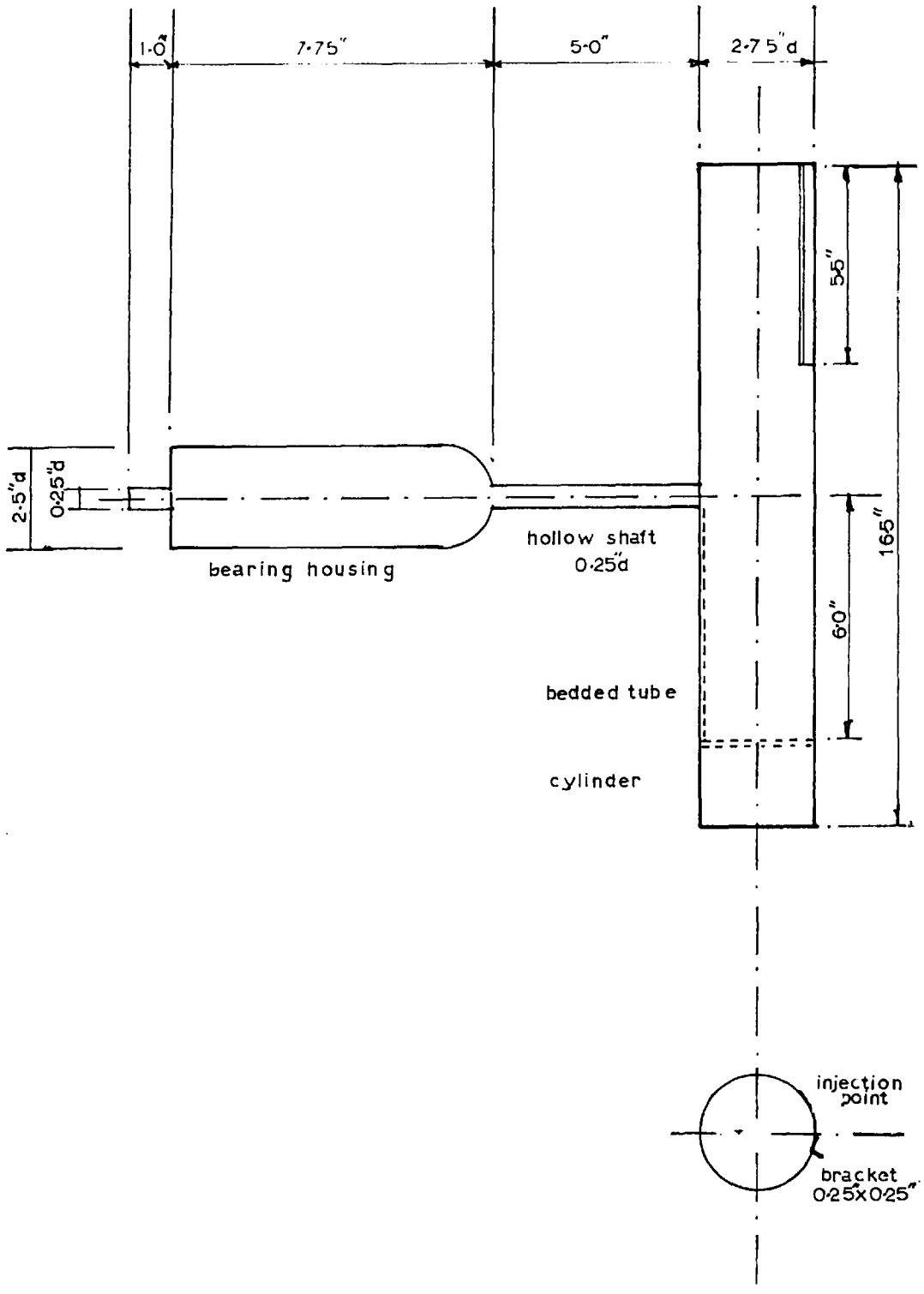

FIG: 7. ROTATING CYLINDER RIG

P A R T II.

1.0 INTRODUCTION.

The experiment described in this part of the thesis consisted of a series of observations of the surface flow, using the technique described in Part I, and of the pressure distributions, using Harvey's pressure pick-up, on a circular cylinder 16 ins. long and $2\frac{3}{4}$ ins. diameter rotating like a propeller in the 3 ft. x 2 ft. low speed wind tunnel at Imperial College. Some of the tests were repeated in the 5 ft. x 4 ft. tunnel to give an indication of whether there were serious interference effects. The reasons for selecting this particular model were as follows:-

1. A two-bladed impeller, was preferable to a multi-bladed fan because it minimised the effects of blade interference. The trivial case of a single bladed impeller having a counterweight on the far side of the axis of rotation was considered unsuitable for a preliminary study because the flow in regions near the axis of rotation would be influenced by the presence of the free end.
2. With circular cylindrical blades, the blade root or hub design no longer influences the

flow since the generators can be continuous across the axis of rotation, the impeller being mounted on, and driven by, a slender shaft lying in the wake.

3. The flow past any station of a blade with an aerofoil section would depend on - (a) thickness, (b) camber and (c) incidence of the section. The effective incidence would vary from section to section depending on the peripheral velocity of the section and on the induced flow. It is, in general, difficult to estimate accurately the effective incidence of a section. If the rotating blade were a circular cylinder then the parameters (a) and (b) would be the same at all sections and, furthermore, changes of incidence will not in themselves produce changes of pressure distribution. Changes in the flow past a circular cylindrical blade must, therefore, arise from centrifugal and Coriolis forces whereas for an aerofoil section it would be difficult to distinguish between changes caused by changes in incidence per se and changes caused by the centrifugal and Coriolis forces.

4. Previous studies (Himmelskamp (1945)) indicated that boundary layer separation phenomena were of particular interest on rotating bodies. Working with a circular cylinder and keeping the section Reynolds number always in the laminar separation range has the advantage that the basic two-dimensional flow has been the subject of extensive investigations, experimental and theoretical, in the region of attached flow and after separation.

5. With a circular cylinder it is possible to obtain as detailed a survey of the surface pressure distribution as is required over any part of the periphery by having only a few pressure tappings and arranging for the cylinder to be rotated about its own axis.

6. Two observations made in Part I of this thesis indicate that an experiment on a circular cylinder would be fruitful. First, it was observed that a circular cylinder could be made to auto rotate. This meant that the pressure distribution was not symmetrical about a stagnation point. The second was that the surface flow patterns on the cylinder did not reveal large radial velocities in the boundary layer.

2. APPARATUS.

2.1 The Model.

The model consisted of a circular cylinder, 16 ins. long x $2\frac{3}{4}$ ins. o/d. x $2\frac{1}{2}$ ins. i/d, fitted with flat end pieces, (Fig.3). It was possible to dismantle the cylinder into three separate cylindrical pieces. The centre piece will be referred to as the hub and the two outer pieces as the blades. One of these blades was fitted with 108 pressure tapping points and will be referred to as the measuring blade. A hollow shaft was used to attach the hub to the forward end of the rotating apparatus.

27 pressure tubes were laid, as shown in figs. 2 and 3, along generators of the measuring blade. 4 pressure tappings, each 0.020 ins. dia. were located along each tube to permit the scanning of the pressure distribution at four cross-sections, distant 2 ins. 4 ins. 6 ins. and $7\frac{1}{2}$ ins. from the axis of rotation. A transparent plastic ('Fablon') sheet was wrapped around the entire model and the tappings selected for measurement were exposed by puncturing the 'Fablon'.

This scheme of providing the model with a replaceable outer skin ensured that a smooth unscratched surface with no edges or ridges was presented to the flow at all times.

Finally, it was possible to rotate the measuring blade about its axis relative to the hub and secure it at any desired position. The position of the measuring blade was determined with the aid of vernier scales engraved on the mating edges of the blade and hub, (vide Fig.2).

2.2 The Model mounting and the Driving Motor.

The drive used in this investigation has been described by Harvey (1960). It consisted essentially of a gearbox mounted in the tunnel and a synchronous motor mounted outside the tunnel.

The gearbox had a streamlined casing and was held in the tunnel working section as shown in fig.1. The supports were designed (a) to cause a minimum of interference to the flow downstream of the model and (b) to enable the axis of rotation to be correctly aligned to the

tunnel windstream direction. To achieve the first objective one of the four supports was built as a space frame having three longitudinal members cross braced with tubes. Each of the other three supports consisted of two longitudinal members held together by end fastenings.

The motor used was a three phase, ½ H.P., synchronous motor with a speed of 1500 r.p.m. The speed of this motor was independant of the load within the power rating.

The motor was coupled to the streamlined gear box through an infinitely variable hydraulic gear box. The output speed of this gear box could be set at any value between 0 and 1500 r.p.m. The fluctuation in speed about the mean value did not exceed 1% at the maximum speed of 1500 r.p.m. Further, there was no observable drifting of the mean speed when the tunnel speed was changed (thus changing the load on the motor) nor during the warming up period when the viscosity of the oil was changing.

2.3 The Pressure Pick-Up.

The pressure pick-up used was developed by Harvey (1960). It consists of a pressure switch, diaphragm and inductive displacement pick-up built into a single unit attached to the after end of the output shaft of the streamlined gear box, The ancillary measuring equipment needed to meter the output of the displacement pick-up is situated outside the tunnel and is linked to the displacement pick-up by brushes and slip-rings.

The pressure to be measured acts on one face of the diaphragm and a known pressure on the other. The resulting deformation of the diaphragm is detected by the displacement pick-up and measured as a change of mutual inductance.

2.3.1. The Pressure Switch.

Twenty 'Schrader' car tyre valves mounted with their axes normal to the axis of rotation are used in this switch. The valves are opened one at a time by a rotating cam. The actuator

mechanism for the cam is controlled from outside the rotating system and is linked to the control gear by brushes and slip-rings. A telephone dial was employed in the control gear because it enabled the cam to be advanced by more than one step at a time by the dialling of the appropriate number. The position of the cam, and, therefore, the identity of the valve currently held open, was displayed on an electromagnetic counter situated on the control panel. Finally, the disposition of the valves was such as to (a) cause no unbalanced centrifugal forces and (b) use the centrifugal forces to help keep the valves closed.

2.3.2. The Transducer.

A 2 in. dia. diaphragm was cemented on to the end of a pressure-tight cell enclosing the pressure switch. The displacement pick-up was mounted along the axis of rotation in contact with a hardened pad soldered to the centre of the diaphragm. The pick-up was enclosed in a sealed compartment maintained at a standard reference pressure supplied through rotating seals. Thus one face of the diaphragm was

exposed to a known pressure and the other to the pressure at the valve currently held open.

The diaphragm used was of crinkled, 0.005 ins. thick, Berylium-Copper.

The displacement pick-up used the principle that displacements could be measured as changes in mutual inductance. The pick-up consisted essentially of a primary coil, two secondary coils and a movable core. The core consists of a 'Feroxcube' attached to a spring loaded shaft in contact with the hardened pad on the diaphragm. Thus, the deflection of the diaphragm was detected as a change in the mutual inductance of the secondary coils. This change in the mutual inductance was measured on an A.C. bridge. The pick-up and measuring bridge used were manufactured by M/s. Philips Ltd., (types P.R.9310 and 9312).

Finally silver graphite brushes and silver slip rings were used to link the pick-up to the measuring bridge. These were chosen on account of their constant electrical properties.

2.4 Measurement of the Speed of Rotation.

It was necessary to reproduce the speed of rotation of the model accurately for the different runs and consequently it was necessary to measure this speed accurately.

It was measured by two independant instruments. A tachometer was used to set the speed approximately to the desired value; in addition, an electronic device was capable of timing a single revolution of the model. This timer consisted of a ten toothed capacitative pick-up placed around the output shaft of the hydraulic gear box. An integrating circuit was linked to the capacitative pick-up and transmitted one single pulse to a microsecond chronometer for every ten pulses received from the capacitative pick-up. Successive pulses started and stopped the chronometer thereby giving the time for a single rotation.

2.5 Flow Visualization.

Acidified air, from the apparatus described in Part I of this thesis, was introduced into the rotating cylinder via a hypodermic tube, rotating

in seals, attached to the after end of the streamlined gear box. The air was transmitted along a pressure tube and released into the boundary layer through a pressure tapping. This procedure had the disadvantage that it was necessary to dismantle the pressure measuring equipment and therefore, no simultaneous pressure measurements could be made; also a picture of the overall flow pattern on the model had to be built up from a series of traces obtained by injection at different points. It was advisable to keep the injection rate for the acidified air low in order that no localized disturbances should be set up by the injection. In consequence, it took about 3 minutes to obtain each trace.

In this particular investigation, two holes were punctured on each strip of litmus paper. Both the holes lay on the same cross-section and acidified air was injected out of only one of them. The other hole was some distance away and served to provide a line of reference for observing the spanwise displacement

of the limiting streamline. This enabled a composite picture of the flow pattern to be built by copying the traces obtained on to a sheet of transparent paper.

It was decided that the width, viz. 3 ins. of the strips of litmus paper used was adequate because the spanwise flow appeared to be quite small, and, therefore, unlikely to have been affected by the presence of the paper on the surface of the model.

3.0 EXPERIMENTAL PROGRAMME.

The sequence of tests was as follows:-

(a) The pressure distribution at the station 2 ins. from the axis of rotation was obtained in the 3 ft. x 2 ft. tunnel at wind speeds of 60, 79 and 96 ft.sec. for each of the model speeds of rotation of 0, 983 and 1190 r.p.m.

(b) The above procedure was repeated for the stations 4, 6 and 7½ ins. from the axis of rotation.

(c) The stain technique was used to obtain the limiting streamlines on either side of the 'stagnation' line for the speeds listed in (a).

(d) Some of the pressure measurements were repeated in the 5 ft. x 4 ft. wind tunnel.

4.0 RESULTS.

The results obtained in the 3 ft. x 2 ft. tunnel are presented in Figs. 4 - 26. The results obtained in the 5 ft. x 4 ft. tunnel agree closely with those obtained in the 3 ft. x 2 ft. tunnel, except at the station 2 ins. from the axis of rotation, and have, therefore, not been presented. The differences observed at the station 2 ins. from the axis of rotation ~~is~~ are discussed in Section.5.3.

The experimental points are not shown in Figs.4 - 13. The pressures in the wetted region had very little scatter. The experimental pressures in the separated region where there was some scatter, are given separately in Fig. 14 - 19.

5.0 DISCUSSION.

5.1 Accuracy of the pressure measurements.

Harvey (1960) reports that the pressure pick-up was calibrated in the speed range 0 - 1000 r.p.m. and the variation in calibration with r.p.m. found to fit the empirical law:-

$$\frac{\text{observed pressure} - \text{true pressure}}{\text{observed pressure}} = 6 \times 10^{-14} \times (\text{r.p.m.})^4$$

where the observed pressure was obtained from the calibration at zero r.p.m. This shows that at 1200 r.p.m. the correction would be 12% of the observation.

It was decided, in these circumstances, to calibrate the pressure pick-up at each of the speeds 0, 500, 1000 and 1200 r.p.m. This was done as follows.

The calibrations were performed when all the apparatus had been mounted into the wind tunnel. The pressure to be measured was fed to the pick-up via a hypodermic tube, rotating in seals, attached to the forward end of the hollow shaft which was subsequently used to

hold the model. This pressure was measured with the aid of a Betz manometer graduated to 0.1 mm water pressure, before it was fed into the hypodermic tube. The best straight line approximations were drawn to the calibration curves. These straight lines all passed through the origin. The accuracy of calibration was estimated as $\pm$ 3%.

A troublesome feature of the apparatus was the zero-drift which took place with changes of temperature. This was overcome by feeding the reference pressure to two of the tappings on the pressure switch enabling, thereby, frequent corrections to be made for the zero drift.

The possibility of there being a change in the calibration during the experiment is commented on in **Section 5.3.**

It was necessary to make a correction to the pressure readings, to allow for the centripetal pressure gradients in the pressure tubes, linking the surface tappings on the model to the pressure switch. This was made by the method shown in Appendix I.

5.2. Calibration of the 3 ft. x 2 ft. wind tunnel.

It was observed that the static pressure in the working section upstream of the model was greater than atmospheric pressure for the two cases of model stationary and model rotating. The tunnel was, therefore, calibrated with the model rotating at speeds of 0, 500, 1000 and 1200 r.p.m. at tunnel fan-speeds of 800, 1000 and 1500 r.p.m.

For each of the twelve cases considered pitot static traverses were made in planes normal to the tunnel axis, upstream of the model. It was observed that over planes distant more than 10 ins. upstream of the cylinder axis, there was no significant variation in static pressure or total head. Thus the static pressure for purposes of calculating the surface pressure coefficient was taken to be that obtaining at the plane 10 ins. upstream of the model.

The fact that the static pressure in the free stream was greater than the atmospheric pressure was held to be due to the large drag

of the rolling apparatus and model. The static pressure was found to be greater than atmospheric pressure even in the 5 ft. x 4 ft. tunnel.

5.3. Pressure Distribution on the Stationary Cylinder.

The length/diameter ratio of the cylinder tested was $\frac{16 \text{ ins.}}{2\frac{3}{4} \text{ ins.}}$, i.e. approximately 5.8. Pressure distributions at sections 25%, 50%, 75% and 93.75% of the half length of the model out from the axis of rotation (i.e. 2 ins., 4 ins., 6 ins., and 7.5 ins. from the mid-span of the model) are plotted in Figs.11 - 13 at Reynolds numbers of 0.77, 1.00 and 1.21 x 10^5 respectively. Also plotted are the two-dimensional pressure distributions obtained with a 6 ins. diameter circular cylinder completely spanning the same wind-tunnel and operating at the same Reynolds numbers. All the pressure distributions on the finite span cylinder deviate from the two-dimensional results, in particular, the wake suction is much less with finite spans. The maximum pressure and the wake pressure both showing a tendency to

fall towards the tips as shown in Table I.

TABLE I.

	$R_E = \frac{V.2a}{\nu} = 0.77 \times 10^5$		1.0×10^5		1.2×10^5	
	Cp max.	Cp wake	Cp max.	Cp wake	Cp max.	Cp wake.
2 - d	1.00	-1.05	1.00	-1.02	1.00	-0.97
y = 2 ins.	*1.05	*-0.61	*1.02	*-0.65	*1.00	*-0.71
y = 4 ins.	1.00	-0.72	0.97	-0.72	0.94	-0.65
y = 6 ins.	1.00	-0.75	0.97	-0.84	1.00	-0.92
y = 7.5 ins.	0.95	-0.70	-0.91	-0.72	0.94	-0.83

The results are consistent with other published data. For example, Sykes (1962), testing relatively long cantilever cylinders at a fixed Reynolds No. of 8.6×10^4, found that the pressure in the wake was almost constant along the length and around the circumference and also that these values were higher than the two-dimensional wake pressure. In the attached-flow

* These values are approximately 5% too large due to a fault in the instrumentation. See below.

i.e. forward facing, region the pressures fell off within a distance of two cylinder diameters from the free end, which in Table I would correspond roughly to the sections from y = 2.4 ins. to y = 8 ins. This falling off in pressure is due to the velocity component along the forward face of the cylinder, directed towards the free end, which is induced by the end itself. The decrease of maximum pressure with increase of Reynolds number is consistent with the simultaneous decrease in wake pressure, which would be expected to cause an increase in this spanwise velocity component. This decrease in wake pressure with increasing Reynolds number does not occur in two-dimensional flow, as shown in Table I.

The anomalous pressure coefficients in excess of unity in Table I are due to a shift in the calibration of the pressure pick-up caused by a deposition of oil and dust on the slip-rings. Once this error had been noticed and, with some difficulty, its source identified, great care was taken to keep the slip-rings clean.

The magnitude of the error, about +5%, was found by making a few check tests. This error affects the row of observations marked with an asterisk in Table I and also the observations at the same station on the rotating cylinder. It is unlikely to be present in the remainder of the tests. Even if there were errors of this order, they are small enough compared with the pressure changes brought about by rotation not to affect the subsequent discussions and conclusions.

5.4. Pressure Distribution on the rotating cylinder.

5.4.1. The position of the maximum-pressure point.

Pressure distributions about the rotating cylinder for various rotational and forward speeds are plotted in figs. 4 to 10 inclusive. In all these figures, the co-ordinate θ denotes the peripheral angular position in a plane perpendicular to the cylinder axis measured from the point of maximum pressure. It might be expected that the locus of the maximum pressure

points could be accurately estimated from a simple consideration of the relative velocities. On this basis the maximum pressure point would be displaced from the zero-rotation position through an angle $\alpha' = \tan^{-1} \frac{\Omega r}{V}$ where V is the tunnel speed, Ω the rotational speed and r the perpendicular distance from a point on the periphery to the axis of rotation. Round a section normal to the cylinder axis the distance r varies from a minimum at the ends of a diameter parallel with the axis of rotation to a maximum at the ends of a perpendicular diameter and hence α' varies. In fact for values of α more than about 10 degrees, the experimental shift in maximum pressure point lies below the minimum value of α' predicted on this simple basis. Some of these results are illustrated in figs. 20 to 26 inclusive and a few are given in Table II.

TABLE II.

	V ft.sec.$^{-1}$	Estimated movement of maximum pressure point (degrees) Upper Limit.	Lower Limit.	Observed Movement (degrees)
0.75a from axis = 1190 r.p.m.	96.	33.5.	32.8.	32.0.
	79.	38.8.	38.1.	35.0.
	60.	46.4.	45.8.	44.8.
0.9375a from axis = 1190 r.p.m.	96.	40.4.	39.8.	38.0.
	79.	45.6.	45.0.	43.0.
	60.	53.2.	52.6.	50.0.

Although only small, this discrepancy of a degree or two is nonetheless significant. It is important because it is in the sense that corresponds to a circulation about the cylinder which would give rise to a cross-wind force with a component in the direction of rotation, a component required for the autorotation observed in Part I of this thesis.

5.4.2. The location of the separation points.

The separation points were taken to be indicated by the termination of the streaks produced by the flow visualization method (see Part I). Some of the streak patterns are reproduced in Figs.20 to 26 inclusive.

In the cases examined, the separation points are marked with the letter S on the pressure distribution graphs, Figs.4 to 13 inclusive. In almost every case examined, the region of adverse pressure gradient continues well beyond the separation point on the rotating cylinder, contrasting with separation point positions obtained by the same method in the same tunnel shown in figs. 11 to 13 for the stationary cylinder. In the latter case the region of adverse pressure gradient terminates at the separation point and is followed by a constant pressure plateau. This difference is of interest because it shows that while a separated region is shown up as a constant pressure plateau in linear motion, there is no similar indication of the presence

of a separated region on a rotating body.

The assertion made above about the pressure distribution in separated regions on the rotating cylinder rests on the reliability of the flow visualization technique used. Since no boundary layer traverses were made it is necessary to use indirect means to check on the reliability of the flow visualization technique, when used on the rotating cylinder. The following points may be noted.

(a) The critical Reynolds number for a circular cylinder placed in the 3 ft. x 2 ft. tunnel is 2×10^5. The Reynolds numbers used in this investigation lay in the range 0.77×10^5 to 1.2×10^5. In these circumstances turbulent reattachment would appear to be unlikely.

All the streaks obtained had an appearance suggesting that there was a laminar boundary layer everywhere.

(b) The flow visualization technique is capable of showing up flow reattachment and no evidence of reattachment was observed on the rotating cylinder.

(c) Separation points always lay at or downstream of the pressure minima, i.e. they lay either at the upstream end of or inside the region of unfavourable pressure gradient.

(d) The pressure, on the basis of the fluctuations of the meter needle, was unsteady in the region downstream of the separation points, whereas there was no observable unsteadiness elsewhere. It is unlikely that a region of attached flow could have unsteady surface pressures. The pressure fluctuations observed were of small amplitude and relatively low frequency viz. 1 - 10 c.sec.$^{-1}$.

(e) The pressures in the region between the maximum pressure point and a point just upstream of the observed separation point were repeatable. The pressures downstream of this point were not exactly repeatable.

These arguments support the view that the flow visualization technique gave a reliable indication of the separation point.

In the case of the station $7\frac{1}{2}$ ins. from the axis of rotation the streaks obtained were almost

parallel to the cylinder generators. This showed that the flow past this particular station was dominated by the presence of the free-end. The streak-patterns obtained at this station are not reproduced in this report.

The reliability of the flow visualization technique, discussed in this section, is important because the flow patterns could be used to determine the structure of the flow past the rotating cylinder. It is, therefore, useful to summarize the conclusions that could be drawn about the structure of the flow:-

The structure of the flow past the rotating cylinder is similar to that of the two-dimensional flow past a circular cylinder in the high-drag range of Reynolds numbers. The boundary layer is laminar in the region between the maximum pressure points and the separation points, i.e. in the attached flow region. Shear layers spring from the separation lines, i.e. the lines joining the separation points, on each face. These shear layers are probably unstable and disintegrate into eddies and vortices.

5.4.3. Extent of the attached flow region.

Fig.29 shows $|\theta s|$, the angular spacing between the maximum pressure point and the point of flow separation, plotted against the advance ratio λ $(= \frac{V}{\Omega r_{stag.}})$. The experimental points display too much scatter to permit any conclusions to be drawn from Fig.29. The values of $|\theta s|$ are also given in Appendix VI. Table III shows both the average value and the greatest observed departure from this value for different combinations of tunnel wind speed V and speed of rotation N.

TABLE III.

	V = 60 ft.sec.$^{-1}$		V = 79 ft.sec.$^{-1}$		V = 96 ft.sec.$^{-1}$	
	θs_{W-W}	θs_{L-W}	θs_{W-W}	θs_{L-W}	θs_{W-W}	θs_{L-W}
N = 0 r.p.m.	$78^{\pm 0}$	$78^{\pm 0}$	$78^{\pm 0}$	$78^{\pm 0}$	$78^{\pm 0}$	$78^{\pm 0}$
N = 983 r.p.m.	$76^{+5.0}_{-8.5}$	$76.4^{+4.2}_{-6.7}$	$84^{+9.8}_{-6.0}$	$75^{+13.7}_{-11.0}$	$83.5^{+5.5}_{-8.5}$	$89.0^{+5.0}_{-6.0}$
N = 1190 r.p.m.	$75^{+8.0}_{-10.0}$	$76^{+1.0}_{-0.5}$	$76^{+6.0}_{-4.0}$	$70^{+2.5}_{-2.0}$	$78^{+7.0}_{-6.0}$	$69^{+7.0}_{-8.0}$

It is seen that there is a trend for increasing rotational speed to decrease the extent of the attached flow region on both faces. The observed trend on the leeward face conflicts with the observation made on Himmelskamp's impeller where rotation was found to delay flow separation.

5.4.4. The pressure distribution and flow pattern in the attached region.

The experimental minimum pressure point locations and the minimum pressure coefficients are shown plotted against λ in Fig.28.

The angular spacing between the maximum and minimum pressure points does not change much along the span, this angle, θ_{p-s}, tends to be larger on the windward face than on the leeward face. The value of θ_{p-s} is 64^{o} on the stationary cylinder which is less than almost all the observations on the rotating cylinder.

Compared with the stationary cylinder the favourable pressure gradients tend to be steeper on the rotating cylinder. The gradients on the

windward face tend to be steeper than those on the leeward face and are steeper at the hub than at the tips. These trends can be seen in Figs.4 - 13. The minimum pressure on the leeward face is less strongly dependant on the advance ratio than are those on the windward face, where the minimum pressure decreases as λ increases. In some cases the changes are large; for example at the station 2 ins. from the axis of rotation with a tunnel speed of 60 ft.sec.$^{-1}$, the ratio of the minimum pressure at 1198 r.p.m. to the corresponding value at zero r.p.m. is 3.0 on the windward face and 1.6 on the leeward face.

The surface flow patterns (Fig.20 - 26) show little evidence of spanwise flow except in the region near the tip.

5.4.5. Attached flow : comparison with Woods' Theory.

Woods (1955) modified the classical Helmholtz theory by prescribing a pressure variation along the 'free-streamline' and calculated, as an

example, the two-dimensional flow of an ideal fluid past a circular cylinder. He used as data the experimental values of the sub-critical (laminar) separation point position and of the surface pressure in the separated region. Agreement between the calculated and experimental pressure distribution is very good as can be seen in Fig.27a (reproduced from fig.6 of Woods' paper). A complete theory would, of course, set out to predict separation and to predict the wake pressure, but it was not Woods' intention (nor is it the present author's) to attempt this much more difficult problem.

If Woods' method is used to obtain the pressure distribution for a rotating cylinder the observed asymmetry of the pressure distribution and the progressive change in pressure in the separated region raises a difficulty. If the experimental separation position and the pressure at separation are used then Woods' theory gives a poor fit, arising essentially from the shape of the experimental pressure distribution aft of the minimum pressure point being markedly

different from that which is given by Woods' method. A good fit is, however, obtained as far as the minimum pressure point by choosing one of Woods' family of curves to have its minimum pressure, rather than separation pressure, at the place and of the magnitude observed in the experiments.

It appears, therefore, that a method exists for constructing the pressure distribution between the maximum pressure point and the minimum pressure points. Some comparison between experiment and calculations made on this basis are given in Fig.27. The calculation being lengthy, not every set of observations has been checked against Woods' theory but the only serious difficulty appears to be near the tips where the three-dimensional nature of the flow cannot be ignored, and where, for instance, $C_{pmax} < 1.0$.

5.5 The pressure distribution and flow pattern in the separated region on the rotating cylinder.

It is evident that rotation decreases the pressure in the separated region at the stations

2 ins., 4 ins. and 6 ins. from the axis of rotation. This is seen by comparing Figs 4, 7 and 11, or 5, 8 and 12, or 6, 9 and 13.

The pressure in the separated region on a rotating cylinder is not constant as in the case of two-dimensional flow or of the stationary cylinder of finite span. At any station, the pressure is lower at the separation point on the windward face than at the separation point on the leeward face. This again, is best seen from Fig. 4 - 11.

The surface pressure (in m.m. H_2O, measured from the static pressure far upstream) in the separated region is replotted against an angular co-ordinate ϕ in Figs.14 - 19. The angle ϕ (vide Fig.32) is measured from the generator on the windward face and 90° away from the leading generator. The curves drawn in these figures were obtained by calculation. The method for calculating the surface pressures in the separated region will be discussed in Section 5.6.

From Figs.14 - 19, it is evident that there is a local pressure maximum near $\phi = 180^{\circ}$. This is of consequence because in the event of there being finite spanwise velocities in the wake, the resolved part of the attendant Coriolis pressure-gradient would be zero at the point $\phi = 180^{\circ}$. This is discussed further in Section 5.6.

Examples of the surface flow patterns in the separated regions are seen in Figs.23 and 24. These show that the predominant component of velocity, at the points examined, is the spanwise component. It was not possible in the time available to obtain more of these flow patterns, but the evidence suggests that the wall shear in the separated region is small and that the spanwise velocities are of order 10 ft.sec^{-1}, i.e. of order one tenth of the free stream speed.

5.6. Calculation of the pressure distribution in the separated region of the rotating cylinder.

In seeking a theoretical model of the flow, we can at the outset dismiss the possibility that the flow is two-dimensional, with the two-dimensional pressure coefficient, at each section,

since this would imply a wake pressure which decreased with increasing distance from the axis of rotation whilst the equation of motion requires the pressure to increase (vide Appendix III).

Consider therefore how the two-dimensional flow pattern behind and in the immediate vicinity of a stationary cylinder, such as depicted in Fig.32.d, might distort when the cylinder is rotated. It seems highly likely from the experimental results that the symmetry is not retained.

In order to give results consistent with the experimental results, it appears to the author that the pattern should be distorted in the sense of Fig.32.c, the region D swinging towards the windward face rather than the leeward face of the cylinder. If also as seems likely from the experiments there is a substantial spanwise flow in the wake, the resulting flow would be as sketched in Fig.32.b. Alternatively, if we first postulate the spanwise flow then, as argued in Appendix IV, there must be secondary flow from D to C in Fig.32.c. The spanwise

velocity component would by symmetry be zero on the axis of rotation.

In order to render the flow pattern amenable to simple analysis, suppose that the region D is very close to the windward separation line (S_{W-W} in Fig.32.c.) so that the major part of the flow near the surface may be thought of as spiralling out along the surface from the windward separation line to the leeward separation line. This assumption is likely to become less good for relatively low rotational speeds. Suppose also that the flow is steady and inviscid, this last assumption is equivalent to assuming that viscous effects are confined to a thin 'boundary-layer' at the back of the cylinder through which pressures are transmitted unaltered from an essentially inviscid external flow. Finally, suppose that the velocity components (u,v,w) in the (x,y,z.) directions (the co-ordinate system shown in Fig.32.a) are all linear functions of position, and of the form

$$\left.\begin{aligned} u &= -k\Omega z(\phi+\beta) \\ v &= +k\Omega y \\ w &= +k\Omega x(\phi+\beta) \end{aligned}\right\} \quad \ldots\ldots\ldots\ldots (1)$$

These expressions represent a flow of the type postulated, and also satisfy the equation of continuity and the condition $\frac{u}{w} = -\frac{z}{x}$ i.e. there is no component velocity perpendicular to the cylinder surface. Essentially, the constants k and β define the magnitude and extent of the secondary flow near the cylinder in the separated region. The proposed model of the flow over-simplifies, indeed ignores, the actual flow in the neighbourhood of the windward separation line (S_{W-W} in Fig.32.c) so in the ensuing analysis β has been chosen equal to $-\phi_{S_{L-W}}$, making $u = w = o$ at the leeward separation line (S_{L-W} in Fig.32.c). Substituting from (1) into the equation of motion and integrating to find the pressure distribution on the surface of the cylinder in a plane y = constant (vide Appendix V), the following expression is obtained.

$$\frac{p - p_{stat}}{\frac{1}{2}\rho\Omega^2 a^2} = k^2(\phi+\beta)^2 - 4k\frac{V}{a}\cos\phi + \cos^2\phi + H \quad \ldots (2)$$

where p is the gauge pressure and the constant of integration H is a function of y, V and Ω.

In the ensuing comparisons of the experimental results with this equation, the values of k and H

for each value of y have been found by making (2) fit the experimental pressure distribution at the point $\phi = 180^{\circ}$ and one other arbitrarily chosen point well removed from both separation points. The point $\phi = 180^{\circ}$ was chosen in preference to the leeward separation point because it was likely that the streamlines in the immediate vicinity of the latter point would have small radii of curvature and consequently the circumferential pressure gradients in this region would be different from those obtaining elsewhere in the wake. The values of k obtained in this investigation are plotted against the rate of advance, λ , in Fig.29. It will be seen that, except for high rates of advance, i.e. high values of $\lambda \left(= \frac{V}{\Omega r_{stag}}\right)$, k can be taken as constant with a value of about 0.6. The values of H are plotted against $V^2/\Omega^2 a^2$ in Fig.31. A straight line has been drawn through 11 of the 15 points, using the method of least squares. The four points omitted correspond to high values of $\lambda \left(=V/\Omega r_{stag}\right)$ and the corresponding values of k too are larger than 0.6.

The equation of the line is

$$H = -0.60 \frac{V^2}{\Omega^2 a^2} - 32.4$$

In Appendix V, it was shown that H could be expressed as follows:-

$$H = C_{p_w} \cdot \frac{V^2}{\Omega^2 a^2} + A_1\left(\frac{y}{a}\right) \cdot \frac{V}{\Omega a} + A_o\left(\frac{y}{a}\right)$$

C_{p_w} is a function of (y/a) and R_E. The range of variation C_{p_w} in Table 1 is small when compared to the range of variation observed on the rotating cylinder. If, therefore a simple expression for H was being sought, it would be reasonable to take C_{p_w} as being constant. The mean value of C_{p_w} in Table 1 is -0.73, and is lower than the value of -0.60 obtained from Fig.31. Further $A_o\left(\frac{y}{a}\right)$ and $A_1\left(\frac{y}{a}\right)$ turn out to be -32.4 and 0 respectively. Inspection of Fig.31 shows that three curves could be drawn, one for each value of y. These curves would merge into the straight line drawn there at high values of $V^2/\Omega^2 a^2$. This line of thought was not pursued because the straight line is a good enough approximation at low rates of advance λ (= $V/\Omega r_{stag}$).

The pressure distributions calculated from equation (2) are compared with the observed pressure distributions in Figs.14 - 19. The agreement is encouraging and as is to be expected the experimental and calculated results diverge as the windward separation point is approached, the experimental and calculated pressures in the region of impact D (Fig.32.c) and the extent of the divergence would be expected to diminish with decrease in the advance ratio λ ($=V/\Omega r_{stag}$). These trends are present.

Three terms, apart from H, occur in the right hand side of equation (2) above. The first of these terms arises from the term $\underline{v}.\nabla\underline{v}$. in the momentum equation and might be looked on as the pressure distribution required to maintain the postulated flow relative to the cylinder, the second and third terms are required to maintain the Coriolis and centripetal accelerations. The second term is important everywhere in the separated region. The first term is important only in the windward half of the separated region. The third term which arises from the varying distance from the axis of rotation in a plane y = constant, is relatively small unless

y and k are both small. Values of ϕ for the wake lie between approximately 220^0 and approximately 0^0. The Coriolis term alone therefore has a maximum in the wake at $\phi = 180^0$. The presence of a pressure maximum in the experimental results around $\phi = 180^0$ is clearly evident in Figs.14 - 19. This together with the fact that k is roughly constant and the fact that H depends primarily on $(V/\Omega a)^2$ gives support to the proposed model of the flow.

5.7. Estimating the pressure distribution on a rotating cylinder.

The object of this section is to show that it is possible to calculate the pressure distribution at any cross-section on a rotating circular cylinder, provided that the advance ratio λ $(=V/\Omega r_{stag})$ does not exceed 3.0, say. In order that this be achieved it is necessary to divide the cross-section of the cylinder into two portions, viz. (a) the portion of the wetted region lying between the peak suction points and (b) the rest of the cross-section.

The pressure distribution in the first of these regions is calculated as follows. The

stagnation point could be taken to be displaced by $\tan^{-1}\frac{V}{\Omega y}$ with respect to its position on the stationary cylinder. Table II in Section 5.4.1. shows that the resulting error would be less than 3°. The values of $C_{p_{p-s}}$ and θ_{p-s} for the two faces are then obtained from Fig.29 by interpolation. Thus the pressure distribution could be calculated by using Woods' theory as shown in Section 5.2.4.

The pressure distribution in the separated region could be calculated once the values of k, H and β are known. The appropriate values of k and H could be obtained from Figs.28 and 31 respectively. It was pointed out in Section 5.6 that the values of k and H differed from the values of 0.6 and $(-0.6\frac{V^2}{\Omega^2 a^2} - 32.4)$ for values of the advance ratio λ $(=V/\Omega r_{stag})$ greater than about 3.0. It is not possible, however to obtain the appropriate value of β from Fig.29. It is possible to obtain reasonably good values for the surface pressures by taking β to be given by the following relation:-

$$-\beta = 270 + \tan^{-1}\frac{V}{\Omega y} + \theta_s.$$

where θ_s° is the value of $\theta_{s_{L-W}}$ occurring on

stationary cylinder. The maximum error incurred when using this simplification could be estimated:- From equation (5) of Appendix V

$$\Delta \bar{p} = -2k^2(\phi+\beta).\Delta\beta$$

Fig.29 shows that $|\Delta\beta| \leqslant 20^0 \doteq +0.35^c$

Now, the extent of the region of separated flow is unlikely to exceed 270^0, i.e. $(\phi+\beta) \not< -270^0 \doteq -4.7^c$

Thus $|\Delta \bar{p}| \not> 3.3k^2$ and taking $k \doteq 0.6$, we have

$$|\Delta\bar{p}| \not> 1.2$$

i.e. at $\Omega = 125$ rad.sec.$^{-1}$, say, the error is unlikely to exceed 1.5 mm. H_2O. Inspection of Figs.14 - 19 shows this to be a permissible error.

A typical example of the pressure distribution on the rotating cylinder obtained by using the above method is shown in Fig.35. The agreement between the calculated and experimental values in Fig.35 is good.

It is therefore possible to calculate the pressure distribution at any cross-section of the rotating circular cylinder provided that the advance ratio is less than 3.0 at that section.

5.8. Lift and Drag Coefficients on the rotating cylinder.

It is pertinent to take the drag at any section of the rotating cylinder to be the resolved part of the force acting on that section along the diameter through the stagnation point. This definition of drag is in keeping with that employed in two dimensional flow past circular cylinders. Thus, the lift would be the component at right angles to the drag.

Hence, $C_L = \dfrac{\text{Lift}}{\frac{1}{2}\rho(V^2+\Omega^2 r_{stag}^2).2a.} = \int_0^{2\pi} C_p \sin\theta.d\theta$

and $C_D = \dfrac{\text{Drag}}{\frac{1}{2}\rho(V^2+\Omega^2 r_{stag}^2).2a} = \int_0^{2\pi} C_p \cos\theta.d\theta$

where $2a$ = diameter of cylinder.

and θ = angular co-ordinate measured from the stagnation point.

C_L and C_D are shown plotted against α (angular diaplacement of maximum pressure point) in Fig.33.

Two further non-dimensional quantities, the tangential and thrust components, C_S and C_t are shown plotted against α in Fig.34,

where $C_S = -C_D\sin\alpha + C_L\cos\alpha$

$-C_t = C_D\cos\alpha + C_L\sin\alpha$

C_S, the tangential component is taken to be positive when it acts in the same direction as the peripheral velocity vector, $y\underset{\sim}{\Omega}$.

Figs.33 and 34 show that C_L, C_D, C_S and C_t remain at their values on the stationary cylinder till α reaches 10°. At stations y = 4 and 6 ins. C_L, C_D and C_S appear to increase almost linearly with α. These curves do in fact resemble the corresponding curves on Himmelskamp's impeller. At the stations y = 2 ins. the curves of C_L, C_D and C_S rise quite steeply and seem to approach maxima.

At the stations y = 7½ ins. the curves of C_L, C_D and C_S appear to have reached maxima and seem to be falling off.

The curves of C_L and C_D at the four stations support Himmelskamp's assertion that increments in C_L obtained on impellers are derived at the expense of increments in C_D.

The maximum values of C_L and C_D obtained in this investigation were at N = 1190 r.p.m., V = 60 ft.sec.$^{-1}$ and are +1.17 and +3.23 respectively and occurred at the station y = 2 ins.

Figs.33 and 34 suggest that the dynamics of the flow past the circular cylinder may be similar to that past Himmelskamp's impeller.

5.9. Significance of the Flow Model proposed for the rotating cylinder.

It has been shown in Section 5.6 that the following flow model for the rotating cylinder is reasonable at the Reynolds Numbers examined:- The boundary layer in the region between the stagnation line and the separation lines is laminar. Shear layers spring from the separation lines, and the air entrained between the shear layers is swept out towards the free-ends of the cylinder. The air in this region is also swept circumferentially, from the shear layer springing from the windward face towards the shear layer springing from the leeward face.

It was observed in Section 5.8 that values of lift and drag coefficients of 1.17 and 3.23 were obtained on the rotating cylinder as compared to the corresponding values of 0 and 1.0 on the stationary cylinder. It was observed in Section 5.4.4. that the maximum value of the ratio

of the minimum pressure on the rotating cylinder to the corresponding value on the stationary cylinder, was 3.0 on the windward and 1.6 on the leeward face. The changes quoted above, are comparable with those obtained on Himmelskamp's impeller. For instance, the highest values of lift and drag coefficients observed on the impeller were 3.2 and 0.25 while the corresponding values from measurements made in a wind tunnel on an isolated aerofoil were 1.45 and 0.05, respectively. Further, the extreme values quoted were recorded in both instances at the stations nearest to the axis of rotation. The similarity between the two investigations does not, however, extend further. Himmelskamp claimed that the effect of rotation was to delay the onset of flow separation on the leeward (suction) face of the aerofoil. He went on to say that the mechanism responsible for this was large radial (spanwise) velocities in an attached boundary layer. The Coriolis forces, associated with these spanwise velocities, were thought to cause the boundary layer on the impeller to be thinner than

that on the isolated aerofoil.

In the case of the rotating cylinder the spanwise velocities in the wetted region were found to be negligibly small. Large spanwise velocities in the separated region were shown to be quite likely. In Section 5.4.3. it was pointed out that increasing the speed of rotation while keeping the tunnel speed constant probably reduced the extent of attached flow on the leeward face.

It is evident that similar trends of lift, drag and minimum pressure coefficients have been observed in the two investigations in spite of the, nominally, very different conditions found to obtain. It would therefore be opportune to re-examine some of Himmelskamp's work.

It is advisable to consider the assertion that there was no separation of the flow from the impeller surface on the occasions when high lift coefficients were obtained. Himmelskamp made this assertion on the basis of three observations. First, the pressure profile resembled that on a stationary blade with attached flow, in so far as the pressure was seen to rise

continuously from the minimum pressure point till the trailing edge. There is no a priori reason for assuming that a separated region on an impeller would be characterized by a constant pressure plateau. Even if a constant pressure plateau did indicate the presence of a region of separated flow on the impeller, too much reliance cannot be placed on Himmelskamp's pressure profiles. Himmelskamp did not trust his pressure measurements completely and he left out any points that did not lie on a smooth curve. This would have been permissible had he had in fact a large number of pressure tappings at each station and only a few of them gave results that appeared to be wrong. He had in fact only 18 tappings distributed equally on both faces, at any station.

It has been pointed out in Part 1 of this thesis that wool tufts are unsatisfactory in a region just upstream of flow separation or in a region of separated flow. Himmelskamp assumed that tufts pointing in a radial direction implied radial flow in the boundary layer. This was partially substantiated by measurements of flow

direction made near the blade surface.

A small cylindric tube with a hemi-spherical cap and a lateral borehole was used to measure the total head. This tube was pushed out of the inner chamber of the hollow impeller blade through a hole in the blade surface. It could be moved along its own axis, which was normal to the wall. It could also be rotated about its own axis. Both these movements could be executed while the impeller was rotating. This tube employed the fact that when the pressure measured at the bore hole was a maximum, the axis of the hole was parallel to the local flow direction. This device was subjected to a series of tests from which Himmelskamp concluded that its indications were reliable.

Finally, using this device he obtained boundary layer type velocity profiles in a region close to the wall. This region was found to be thinner than the boundary layer on the isolated aerofoil. On analyzing these traverses it is found that in some instances the total-head at the edge of this 'boundary-layer' was considerably

less than that obtaining far upstream.

Table V below has been compiled from Himmelskamp's results.

r/R	p_{tot} at A-p_o	p_{tot} at B-p_o	$V/\Omega R$
0.5	0.28	-0.05	0.124.
0.6	0.50	+0.30	0.124.
0.7	0.50	+0.47	0.124.

where the points A and B lay on generators of the measuring blade; distant 0.347 chord and 0.641 chord from the leading edge. Three points have been examined on each generator, and r is the distance of any point from the axis of rotation. p_o and U_o are the static pressure and axial component of velocity obtaining far upstream of the impeller; R is the tip radius of the impeller. $(p_{tot} - p_o)$ has been obtained from the values of the velocity at the edge of the boundary layer and the surface static pressure at the station, supplied by Himmelskamp.

Now, Himmelskamp thought that his surface pressure measurements were reliable. Since he used the same apparatus for traversing the region close to the blade surface, these measurements

must have been equally reliable. Now in some of the instances shown in Table V ($P_{tot} - P_o$)<<$\frac{1}{2}\rho U_o^2$.. This is repeated at other instances where relatively high values of C_L were obtained. This implies that the high lift coefficients were obtained with separated flow and not, as Himmelskamp asserted, with attached flow.

It must be that spanwise velocities on both the cylinder and the impeller occur only in the wake and not in the attached region. This view is confirmed by the photographs of the wool tufts on the impeller. These show that the tufts lie in a chordwise direction on the forward portion of the impeller and point radially only on the rear portion.

The evidence available seems to suggest that flow separation is a pre-requisite to the production of high lift and drag coefficients. It is conceivable that the higher lift coefficients result from the overall reduction of wake pressure caused by rotation. This reduction of wake pressure probably causes a lower unfavourable pressure gradient and the secondary flow causes

this pressure gradient to be maintained right to the trailing edge increasing thereby the area of the C_p vs x/c profile.

It was mentioned in Section 5.6 that the surface pressures in the wake on the rotating cylinder were much lower than those on the stationary cylinder. It is seen in Fig.27 that reducing the wake pressure causes a reduction of the minimum pressure, when the pressure distribution is calculated by Woods' theory.

Roshko (1954) points out that reducing the wake pressure causes an increase in the curvature of the free streamlines in the two-dimensional flow problem. It is therefore likely that increasing the curvature of the shear layer (free streamline) will result in reducing the minimum pressure on a circular cylinder. The flow model postulated in Section 5.6 can now be used to explain the relatively greater unsteadiness observed in the vicinity of the separation line on the windward face of the rotating cylinder. This is because the overall reduction of pressures in the wake caused by

rotation leads to an increase in the curvature of the shear layers springing from both faces of the rotating cylinder. The secondary circumferential flow, directed from the shear layer on the windward face to that on the leeward face, would cause an increase in the curvature of the shear layer on the windward face and a reduction in the curvature of the shear layer on the leeward face. Since the minimum pressure coefficient on leeward face of the rotating cylinder stays at approximately 1.2, the two opposing influences on the curvature must be balancing out. The minimum pressure coefficient on the windward face varies considerably with λ and this means that the curvature of the shear layer must also be changing considerably. Since the stability of the shear layer decreases with increase of curvature, the shear layer on the windward face could be expected to break up quite soon into eddies and vortices. This could then be the reason for the unsteadiness observed in the vicinity of the separation line on the windward face.

The flow model postulated could also be used

to account for the asymmetry of the pressure distribution on the rotating cylinder. The curvature of the shear layer on the windward face is increased by the overall reduction of wake pressure and the secondary flow. This must cause lower minimum pressures to be developed on the windward face than on the leeward face where these two effects would be opposing each other.

6.0 CONCLUSION.

The flow past a circular cylinder rotating, after the fashion of a propeller, in a wind stream has been studied. It was found that non zero section lift coefficients and unexpectedly large section drag coefficients were developed on the rotating cylinder. No evidence of significant spanwise velocities in the boundary layer were found.

A flow model for the secondary flow in the wake has been proposed. It has been argued that the Coriolis forces associated with this flow are responsible for the observed non-zero circumferential pressure gradients. The secondary flow in the wake is also suggested as the mechanism

responsible for changing unequally the shape of the shear layers springing from the two separation lines and thereby producing an asymmetrical pressure distribution about the line of maximum pressure (stagnation line).

Quasi-theoretical methods have been suggested for calculating the surface pressure distribution in the region of attached flow and the wake.

Finally, an earlier investigation on the flow past an impeller has been re-examined in the light of the findings of the current investigation. It has been shown that there was probably flow separation in the instances where the highest section lift coefficients were obtained. This is seen to cast doubt on the original finding that high lift coefficients are produced by spanwise velocities in the boundary layer causing a delay in the onset of flow separation.

7.0 SUGGESTIONS FOR FUTURE WORK.

It would be necessary to verify, experimentally, the model proposed in this thesis for the secondary flow in the wake. An attempt has

been made in this thesis to establish its plausibility but direct experimental evidence is necessary. This could be done by traverses in the wake using pitot-static tubes or hot wire anemometers.

An investigation similar to that made by Himmelskamp using Harvey's pressure pick-up would be helpful. This would be invaluable if the flow model suggested for the wake of the rotating cylinder was found to obtain in practice. It would then be possible to resolve the doubts expressed in this thesis about the conclusions reached by Himmelskamp.

REFERENCES.

HARVEY, J.K. — An experimental investigation of the flow past a slender delta wing in yaw and in roll. Ph.D. Thesis, University of London. (1960).

HIMMELSKAMP, H. — Profil untersuchungen an einem umlaufenden Propeller. Dissertation, Gottingen (1945).

ROSHKO, A. — A new hodograph for free streamline theory. NACA, TN.3168. (1954).

SYKES, D.M. — The supersonic and low speed flows past circular cylinders of finite length supported at one end. Vol.12, J.F.M. (1962).

WOODS, L.C. — Two-dimensional flow of a compressible fluid past given curved obstacles with infinite wakes. Vol.227.A. Proc.Roy.Soc. (1955).

APPENDIX I.

CORRECTION FOR CENTRIPETAL PRESSURE GRADIENTS.

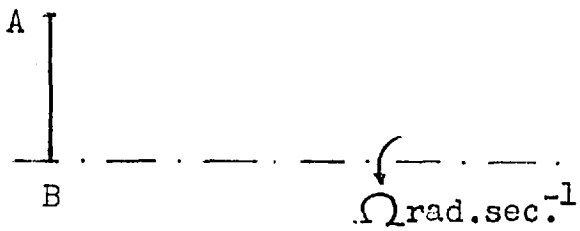

It is necessary to make a correction to the observed pressure readings to allow for the centripetal pressure gradients in the pressure tubes.

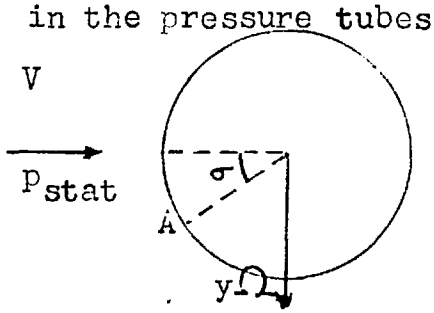

Suppose it is necessary to estimate the true pressure at the point A, lying on the cylinder surface. Suppose, further that A is displaced from the leading generator and lies on a section distant y from the axis of rotation. Then the perpendicular distance, r, of A from the axis of rotation is given by

$$r^2 = y^2 + a^2\sin^2\sigma = (y^2 + \tfrac{1}{2}a^2) - \tfrac{1}{2}a^2\cos 2\sigma$$

Let p_A = pressure at A

p_B = pressure at B = pressure measured by pick up.

Then $\frac{\partial p}{\partial r} = \rho r \Omega^2$

i.e. $p = \frac{1}{2}\rho r^2 \Omega^2 + \text{constant}$

using $p = p_B$ at $r = o$, we have

$$p_A = p_B + \tfrac{1}{2}\rho r^2 \Omega^2$$

Now $$\overline{\rho} \simeq \frac{p_{atm}}{R\Theta}$$

where p_{atm} = atmospheric pressure.

Θ = tunnel temperature.

R = constant for air.

Thus $p_A = p_B + \frac{1}{2} \frac{p_{atm}}{R\Theta} \cdot r^2 \Omega^2$

i.e. $p_A - p_{stat} = (p_B - p_{atm}) + \frac{\Omega^2 r^2}{2R} \cdot p_{atm} - (p_{stat} - p_{atmos})$.

This then is the required result.

A specimen set of calculations is shown in Appendix II.

APPENDIX II.

SPECIMEN CALCULATION.

R.P.D. = 50.5 mm. H_2O.

t = 0.06075 sec.

$135.5\Omega^2/2R\Theta = 0.77$

$p_{stat} - p_{atm} = \Delta p$ = 2.6 mm. H_2O

Ω = 103.4 rad./sec.

$\Omega^2 p_{atm}/2R\Theta$ = 58.6 mm. H_2O/ft^2.

y = 6 ins.

p_{atm} = 76.25 cm. Hg.

Θ = 305°k.

σ	+0	+10	+30	+50	+70	+90	+120	+130	+140	−155	−115	−95	−75	−65	−55	−45	−35	−20
$10^4 x \frac{1}{2} a^2 \cos^2\sigma$	+66	+62	+33	−12	−51	−66	−33	−12	+12	+42	−42	−65	−57	−42	−23	0	+23	+51
r^2	0.2500	0.2504	0.2533	0.2578	0.2617	0.2632	0.2599	0.2578	0.2554	0.2524	0.2608	0.2631	0.2623	0.2608	0.2589	0.2566	0.2543	0.2515
$\frac{\Omega^2 r^2}{2R\Theta} p_{atm} = p^1$	14.7	14.7	14.8	15.1	15.3	15.4	15.2	15.1	15.0	14.8	15.3	15.4	15.4	15.3	15.2	15.0	15.0	14.7
$p^1 - \Delta p$	12.1	12.1	12.2	12.5	12.7	12.8	12.6	12.5	12.4	12.2	12.7	12.6	12.8	12.7	12.6	12.4	12.4	12.1
$p_{meas.}$	+17.1	+38.2	+51.5	+20.8	−17.1	−85.5	−63.5	−62.0	−62.0	−59.0	−61.2	−58.0	−58.0	−59.0	−59.0	−66.6	−71.2	−40.2
$p - p_{stat}$	+29.2	+50.3	+63.7	+33.3	−4.4	−72.7	−50.9	−49.5	−49.6	−46.8	−48.5	−45.2	−45.2	−46.3	−46.4	−54.2	−58.8	−28.1

APPENDIX III.

CONSEQUENCES OF TWO-DIMENSIONAL FLOW PAST ROTATING CYLINDER.

It is possible to show by the reasoning given below, that there is no possibility that the flow past the rotating cylinder is two-dimensional, with the two-dimensional wake pressure coefficient obtaining at all sections.

If the flow was two-dimensional and the two-dimensional wake pressure coefficient obtained at all sections, then the wake pressure would be given by

$$p = p_{stat} + \tfrac{1}{2} C_{p_W} \cdot \rho (V^2 + \Omega^2 r^2_{stag}) \quad ..(1)$$

where p_{stat} = static pressure far upstream of model.

V = tunnel wind velocity.

C_{p_W} = two-dimensional wake pressure coefficient.

r_{stag} = perpendicular distance of stagnation (pressure maximum) point from axis of rotation.

It has been shown in Appendix I that

$$r^2_{stag} = y^2 + a^2 \sin^2 \alpha$$

Thus differentiating equation (1), we have

$$\frac{\partial p}{\partial y} = C_{p_W} \cdot \rho \, y \Omega^2$$

Now the average value of C_{pw} obtained from the measurements made on the 6 ins. dia. cylinder is -1.02.

Thus $\frac{\partial p}{\partial y} = -1.02 \rho y \Omega^2$ .....(2)

A further consequence of two-dimensional flow would be that the fluid within the wake may be assumed to have negligibly small velocity components relative to the cylinder as in the Helmholtz model. Thus the centripetal forces must be equal to the spanwise (radial) pressure gradients.

i.e. $\frac{\partial p}{\partial y} = + \rho y \Omega^2$.....(3)

Clearly, equations (2) and (3) are incompatible.

It is therefore reasonable to deduce that the flow past the rotating cylinder will not be two-dimensional.

A further consequence of the incompatibility of equations (2) and (3) is that it adds plausibility to the postulate of finite spanwise velocities in the wake (vide Section 5.6).

APPENDIX IV.

PROOF OF THE EXISTENCE OF A CIRCUMFERENTIAL VELOCITY COMPONENT.

Suppose cylindrical polar co-ordinates (ϕ, y, s) (vide Fig.32), were used to examine the flow in the wake.

Let the velocity be given by (u^1, v, w^1).

Then, the equation of continuity may be written as

$$\nabla . \underline{v} = \frac{1}{s}\frac{\partial u^1}{\partial \phi} + \frac{\partial v}{\partial y} + \frac{\partial w^1}{\partial s} + \frac{w^1}{s} = 0$$

At the surface of the cylinder

$$w^1 = 0.$$

$$\frac{\partial w^1}{\partial S} \geqslant 0$$

Considering the incompatibility of equations (2) and (3) shown in Appendix III, it is reasonable to take $v \geqslant 0$, and since $v = 0$ at $y = 0$ it is reasonable to take $\frac{\partial v}{\partial y} > 0$.

Thus, from the equation of continuity,

$$\frac{\partial u^1}{\partial \phi} < 0. \text{ at the cylinder surface.}$$

This could imply that

either $u^1 > 0$ and decreases continuously

or $u^1 \leqslant 0$ and becomes increasingly negative.

The first of these corresponds to the flow from D to C (vide Fig.32.c) and the second for the flow from D to B.

APPENDIX V.

INTEGRATION OF THE EQUATIONS OF MOTION.

The equations of motion may be written:-

$$\underline{V}.\nabla\underline{v} + 2\underline{\Omega}\wedge\underline{v} + \underline{\Omega}\wedge(\underline{\Omega}\wedge\underline{r}) = -\frac{1}{\rho}\nabla p \quad \ldots\ldots\ldots(1)$$

and

$$\nabla.\underline{v} = 0 \quad \ldots\ldots\ldots(2)$$

Suppose rectangular cartesian co-ordinates (x,y,z) (vide Fig.32.a) are used to examine the flow in the wake of the rotating cylinder

Let $\underline{v} = (u,v,w.)$

Look for a solution of the kind

$$u = -k\Omega z(\tan^{-1}\frac{x}{z}+\beta) \equiv -k\Omega s.(\phi+\beta).\cos\phi \ldots(3a)$$

$$v = +k\Omega y = +k\Omega y \quad \ldots\ldots\ldots\ldots(3b)$$

$$w = +k\Omega x(\tan^{-1}\frac{x}{z}+\beta) \equiv +k\Omega s.(\phi+\beta).\sin\phi \ldots(3c)$$

Equivalently, $u^1 = -k\Omega s.(\phi+\beta)$

$$v = k\Omega y.$$

$$w^1 = 0.$$

where (u^1,v,w^1) is the velocity when using the cylindrical polar co-ordinates (ϕ,y,s) (vide Fig.32.a).

This solution satisfies the equation of continuity and the condition that $w^1 = 0$ i.e. the component of velocity normal to the surface of the cylinder is zero. Clearly the relation $v = k\Omega y$ would

not hold near the free ends of the cylinder.

Equation (1) may be rewritten:-

$$\frac{1}{\rho}\frac{\partial p}{\partial x} = u\frac{\partial u}{\partial x} + v\cancel{\frac{\partial u}{\partial y}}^{\circ} + w\frac{\partial u}{\partial z} \quad \ldots\ldots\ldots(1a)$$

$$\frac{1}{\rho}\frac{\partial p}{\partial y} = u\cancel{\frac{\partial v}{\partial x}}^{\circ} + v\frac{\partial v}{\partial y} + w\cancel{\frac{\partial v}{\partial z}}^{\circ} - 2\Omega w - \Omega^2 y \quad (1b)$$

$$\frac{1}{\rho}\frac{\partial p}{\partial z} = u\frac{\partial w}{\partial x} + v\cancel{\frac{\partial w}{\partial y}}^{\circ} + w\frac{\partial w}{\partial z} + 2\Omega v - \Omega^2 z \quad (1c)$$

It follows from equations (3a) and (3c) that

$$\frac{\partial u}{\partial z} = \frac{\partial w}{\partial x} - 2k\Omega.(\phi+\varepsilon)$$

It is then possible to write

$$\frac{\partial}{\partial x}(p/\rho + \tfrac{1}{2}(u^2+w^2)) = 2k\Omega.w.(\phi+\varepsilon) \quad \ldots\ldots(1d)$$

$$\frac{\partial}{\partial y}(p/\rho + \tfrac{1}{2}v^2) = 2\Omega w + \Omega^2 y \quad \ldots\ldots\ldots(1e)$$

$$\frac{\partial}{\partial z}(p/\rho + \tfrac{1}{2}(u^2+w^2)) = -2k\Omega u.(\phi+\varepsilon) - 2\Omega v + \Omega^2 z \ldots(1f)$$

It is convenient at this stage, to transform from rectangular cartesian co-ordinates (x,y,z) to the cylindrical polar co-ordinates (ϕ,y,s.)

This is done:-

$$s^2 = x^2 + z^2 \quad ; \quad \tan\phi = x/z.$$

i.e. $$\frac{\partial}{\partial x} = \sin\phi\frac{\partial}{\partial s} + \frac{1}{s}.\cos\phi\frac{\partial}{\partial \phi}$$

and, $\frac{\partial}{\partial z} = \cos\phi . \frac{\partial}{\partial s} - \frac{1}{s} . \sin\phi \frac{\partial}{\partial \phi}$

Substituting in equations (1d) to (1f) we have:-

$$(\sin\phi \frac{\partial}{\partial r} + \frac{1}{s}\cos\phi . \frac{\partial}{\partial \phi}).(p/\rho + \tfrac{1}{2}u_1^2)$$

$$= 2k^2\Omega^2 s.(\phi+\beta)^2.\sin\phi \quad .....(1g)$$

$$\frac{\partial}{\partial y}(p/\rho + \tfrac{1}{2}v^2)$$

$$= 2k\Omega^2 s.(\phi+\beta).\sin\phi + \Omega^2 y..(1h)$$

and, $(\cos\phi.\frac{\partial}{\partial r} - \frac{1}{s}.\sin\phi \frac{\partial}{\partial \phi}).(p/\rho + \tfrac{1}{2}u_1^2)$

$$= 2k^2\Omega^2 s,(\phi+\beta).\cos\phi -2\Omega v + \Omega^2 s.\cos\phi..(1j)$$

From equations (1g) and(1j) we have,

$$\frac{1}{s}\frac{\partial}{\partial \phi}.(p/\rho + \tfrac{1}{2}u_1^2) = 2\Omega v \sin\phi - \Omega^2 s.\tfrac{1}{2}\sin 2\phi$$

Integrating with respect to ϕ:-

$$\frac{1}{s}(p/\rho + \tfrac{1}{2}u_1^2) = -2\Omega v \cos\phi + \Omega^2 s.\frac{1}{4}\cos 2\phi + H_1$$

i.e. $p/\rho + \tfrac{1}{2}u_1^2 = -2\Omega s.v.\cos\phi + \tfrac{1}{2}\Omega^2 s^2\cos^2\phi - \frac{1}{4}\Omega^2 s^2 + H_1$

where $H_1 = H_1(y.s.V,\Omega)$.

Thus $p/\rho = -\frac{1}{2}.k^2\Omega^2s^2(\phi+\beta)^2 - 2\Omega s.v.\cos\phi + \frac{1}{2}\Omega^2s^2\cos^2\phi + H_2$

where $H_2 = H_2(y,s,V,\Omega) = H_1 - \frac{1}{4}\Omega^2s^2$

Since the tunnel static pressure p_{stat} is a function of V and Ω only, it is possible to write

$$\frac{p-p_{stat}}{\rho} = -\tfrac{1}{2}k^2\Omega^2s^2(\phi+\beta)^2 - 2\Omega s.v.\cos\phi + \tfrac{1}{2}\Omega^2s^2\cos^2\phi + H_3(y,s,V,\Omega).$$

At the surface of the cylinder

$$\bar{p} = -k^2(\phi+\beta)^2 - 4k.\frac{y}{a}\cos\phi + \cos^2\phi + H(y,V,\Omega) \quad \ldots\ldots(5)$$

where $\bar{p} = \dfrac{p-p_{stat}}{\frac{1}{2}\rho\Omega^2a^2}$

It is possible to obtain an insight into the nature of the arbitrary function $H(y,V,\Omega)$ as follows

Now when $\Omega = 0$,

$$\frac{p-p_{stat}}{\rho} = H_3(y,a,V,o)$$

but $\dfrac{p-p_{stat}}{\rho} = C_{p_W}.\frac{1}{2}V^2$

$\therefore H_3(y,a,V,o) = C_{p_W}.\frac{1}{2}V^2$ .....(6)

where C_{p_W} is the wake pressure coefficient at

the station distant y from the axis of rotation, and is from Table 1 a function of (y/a) and V.

It would be plausible to state that on a rotodynamic machine, the pressure coefficient at a point would depend on (a) its location and (b) the advance ratio ($V/\Omega 1$) where 1 is the tip diameter. The validity of this statement for the circular cylinder will be examined later, but will be assumed unquestioningly for the immediate purpose.

Thus $C_p = fn(y/a, \phi, V/\Omega a)$

Now $$C_p = \frac{p-p_{stat}}{\frac{1}{2}\rho(V^2+\Omega^2 r^2_{stag})}$$

$$= \frac{p-p_{stat}}{\frac{1}{2}\rho\Omega^2 a^2} \cdot \frac{1}{\frac{V^2}{\Omega^2 a^2} + \frac{y^2}{a^2} + \sin^2\alpha}$$

where α is the displacement caused by rotation of the stagnation point. α is in turn a function of y/a and $V/\Omega a$.

Thus for any point

$$\frac{p-p_{stat}}{\frac{1}{2}\rho\Omega^2 a^2} = fn(y/a, \phi, V/\Omega a)$$

Equation (5) of this Appendix gives

$$\frac{p-p_{stat}}{\frac{1}{2}\rho\Omega^2a^2} = -k^2(\phi+\beta)^2 - 4k.\frac{y}{a}\cos\phi + \cos^2\phi + H(y,a,V,\Omega) \quad ...(5)$$

Thus $H = fn(y/a, V/\Omega a)$

Since k is very nearly a constant.

Thus $H = A_0(y/a) + A_1(y/a).\frac{V}{\Omega a} + A_2(y/a).\frac{V^2}{\Omega^2a^2} + \sum_{n=3}^{\infty} A_n(y/a).\left(\frac{V}{\Omega a}\right)^n$

Now, $H_3(y,a,V,\Omega) = \frac{1}{2}\Omega^2a^2.H(y,a,V,\Omega)$

i.e. $H_3(y,a,V,\Omega) = A_0(y/a).\frac{1}{2}\Omega^2a^2 + A_1(y/a).\frac{1}{2}V.\Omega a + A_2(y/a).\frac{1}{2}V^2 + \frac{1}{2}\Omega^2a^2 \sum_{n=3}^{\infty} A_n(y/a).\left(\frac{V}{\Omega a}\right)^n$

Equation (6) of this Appendix gives,

$H_3(y,a,V,o) = C_{pW}.\frac{1}{2}V^2$, i.e. finite .....(6)

then, $A_n(y/a) = o$, $n \geqslant 3$

and $A_2(y/a) = C_{pW}$

$\therefore\ H(y,a,V,\Omega) = A_0(y/a) + A_1(y/a).\frac{V}{\Omega a} + A_2(y/a).\frac{V^2}{\Omega^2a^2}$

$= A_0(y/a) + A_1(y/a).\frac{V}{\Omega a} + C_{pW}.\frac{V^2}{\Omega^2a^2}$

This then is a convenient expression for H.

It is now necessary to examine the validity of the assumption

$$C_p = fn(y/a, \phi, V/\Omega a)$$

An allowance was made in choosing the values of V and Ω for this investigation to analyse such a situation. The two cases N = 1190 r.p.m., V = 97 ft.sec.$^{-1}$, and N = 983 r.p.m., V = 79 ft.sec.$^{-1}$, have the same value of $V/\Omega a$. It would therefore be advantageous to compare the different values of θ_{p-s}, $C_{p_{p-s}}$, etc. for the same values of y/a, ϕ and $V/\Omega a$. This is done in Table VI below.

TABLE VI.

y	V	Ω	λ	$10^{-5} \times R_E$	α	β	H	k	W-W Face		L-W Face	
									θ_{p-s}	$C_{p_{p-s}}$	θ_{p-s}	$C_{p_{p-s}}$
ins.	Ft.sec.$^{-1}$	Rad.sec.$^{-1}$	-	-	deg.	deg.	-	-	deg.	-	deg.	-
2	97	125	4.64	1.26	11°	-212°	-	-	70°	-1.75	-68°	-1.22
2	79	103	4.60	1.04	10°	-214°	-	-	70°	-1.52	-67°	-1.24
4	97	125	2.32	1.34	22°	-216°	-57.1	-0.60	70°	-1.33	-69°	-1.10
4	79	103	2.30	1.10	22°	-214°	-57.6	-0.52	68°	-1.32	-66°	-1.10
6	97	125	1.54	1.46	32°	-214°	-60.5	-0.62	67°	-1.26	-62°	-0.96
6	79	103	1.52	1.21	31°	-214°	-55.4	-0.48	67°	-1.20	-65°	-0.90

Comparing the values at the station y = 6 ins. it is seen that α, β, H, k, θ_{p-s} and $C_{p_{p-s}}$ are approximately the same in the two cases. A more detailed comparison could be made by comparing Figs 6 and 8. It is seen that there is a small but significant difference in the pressure distribution in the attached flow region. This suggests that the pressures depend to a small extent on the Reynolds no. as well. The pressures in the separated region are different (about 15%) but the curves appear to be displaced vertically with respect to one another. If allowance is made for the scatter of the points in Figs.16 and 18, it may be said that the results obtained at the station y = 6 ins. support the statement that $C_p = fn(y/a, V/\Omega a)$.

At the station y = 4 ins. the comparison shows that all the remarks made for the station y = 6 ins. apply with the exception of one. The pressures in the separated region are almost the same in both cases. Thus the results obtained at this station support very strongly the statement that $C_p = fn(y/a, V/\Omega a)$.

Finally at the station y = 2 ins. the comparison shows that the values of α, β, θ_{p-s} and $C_{p_{p-s}}$ are approximately the same. The pressures in most of the attached region (vide Figs.6 and 8) and the leeward half of the separated region are nearly the same. There is however a difference (about 25%) in the pressure distributions in the immediate vicinity of the peak suction point on the windward face and in the windward half of the separated region between the two cases. There is insufficient evidence to conclude that this difference is dependant solely on the Reynolds no.

It is therefore reasonable to infer that the pressure distribution at any station depends markedly on the advance ratio $V/\Omega a$, but depends also on the section Reynolds no.

APPENDIX VI.

RESULTS OF THE FLOW VISUALIZATION TECHNIQUE.

y	θs_{L-W}	θs_{W-W}	V.	N.	λ
2	77	83	60	1190	2.9
4	76	78	60	1190	1.45
6	76	65	60	1190	0.97
2	72.5	82	79	1190	3.81
4	65	74	79	1190	1.91
6	63	72	79	1190	1.27
2	69	72	96	1190	4.64
4	76	85	96	1190	2.32
6	61	77	96	1190	1.54
2	79.5	81.5	60	983	3.5
4	69.7	67.5	60	983	1.75
6	80.6	81	60	983	1.17
2	66	78	79	983	4.6
4	70	80	79	983	2.3
6	88.7	93.8	79	983	1.53
2	89	85.5	96	983	5.58
4	94	89	96	983	2.79
6	83	75	96	983	1.85

APPENDIX VII.

ILLUSTRATIONS

FIG.1: VIEW OF THE ROLLING APPARATUS

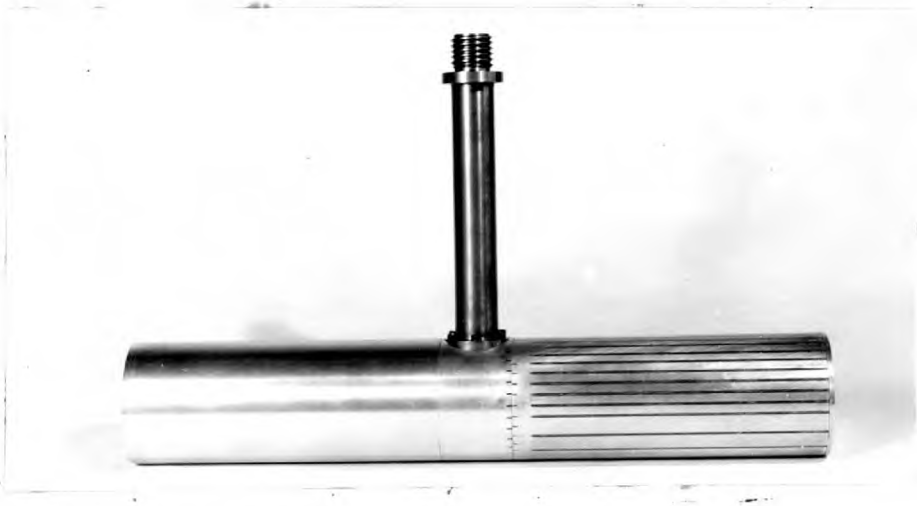

FIG. 2: THE CIRCULAR CYLINDER

FIG. 1 & 2

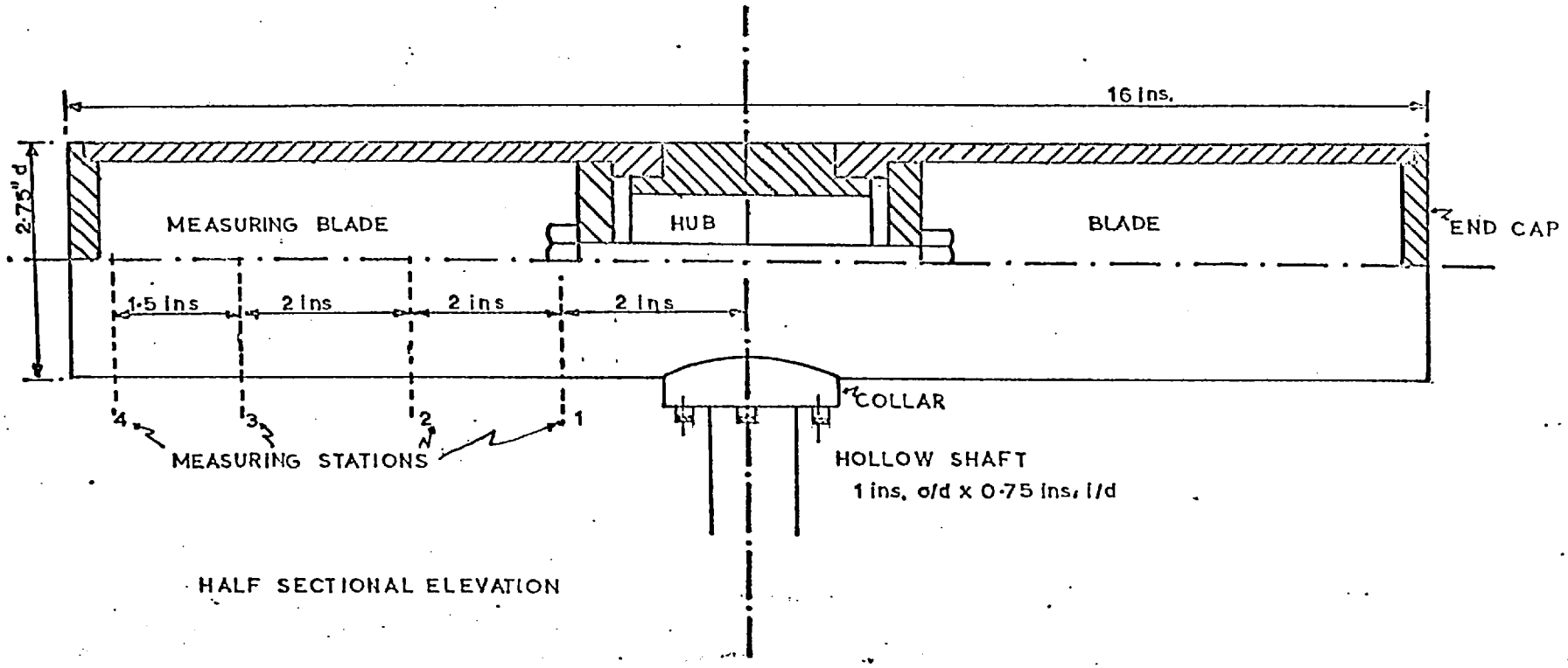

FIG. 3 :

PRESSURE TUBE SERIAL NUMBER	1	2	3	4	5	6	7	8	9	10	11	12	13	14	15	16	17	18
PRESSURE TUBE LOCATION deg.	0	10	30	50	70	90	120	130	140	205	245	275	285	295	305	315	325	340

DISPOSITION OF PRESSURE TUBES ALONG CIRCUMFERENCE OF MEASURING BLADE

FIG. 3 : DETAILS OF ROTATING CYLINDER

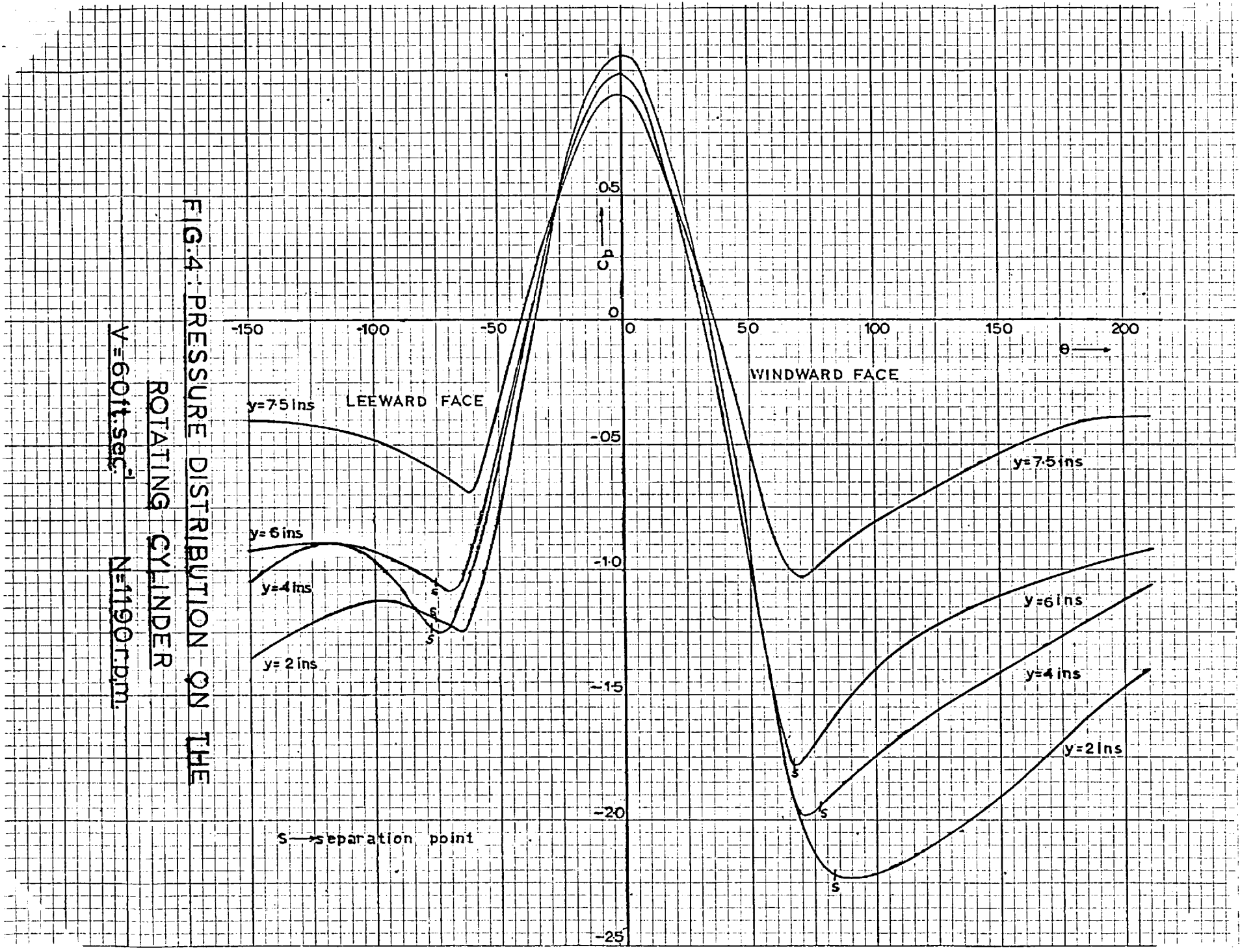

FIG.4: PRESSURE DISTRIBUTION ON THE ROTATING CYLINDER

V=60 ft.sec^{-1} N=1190 r.p.m.

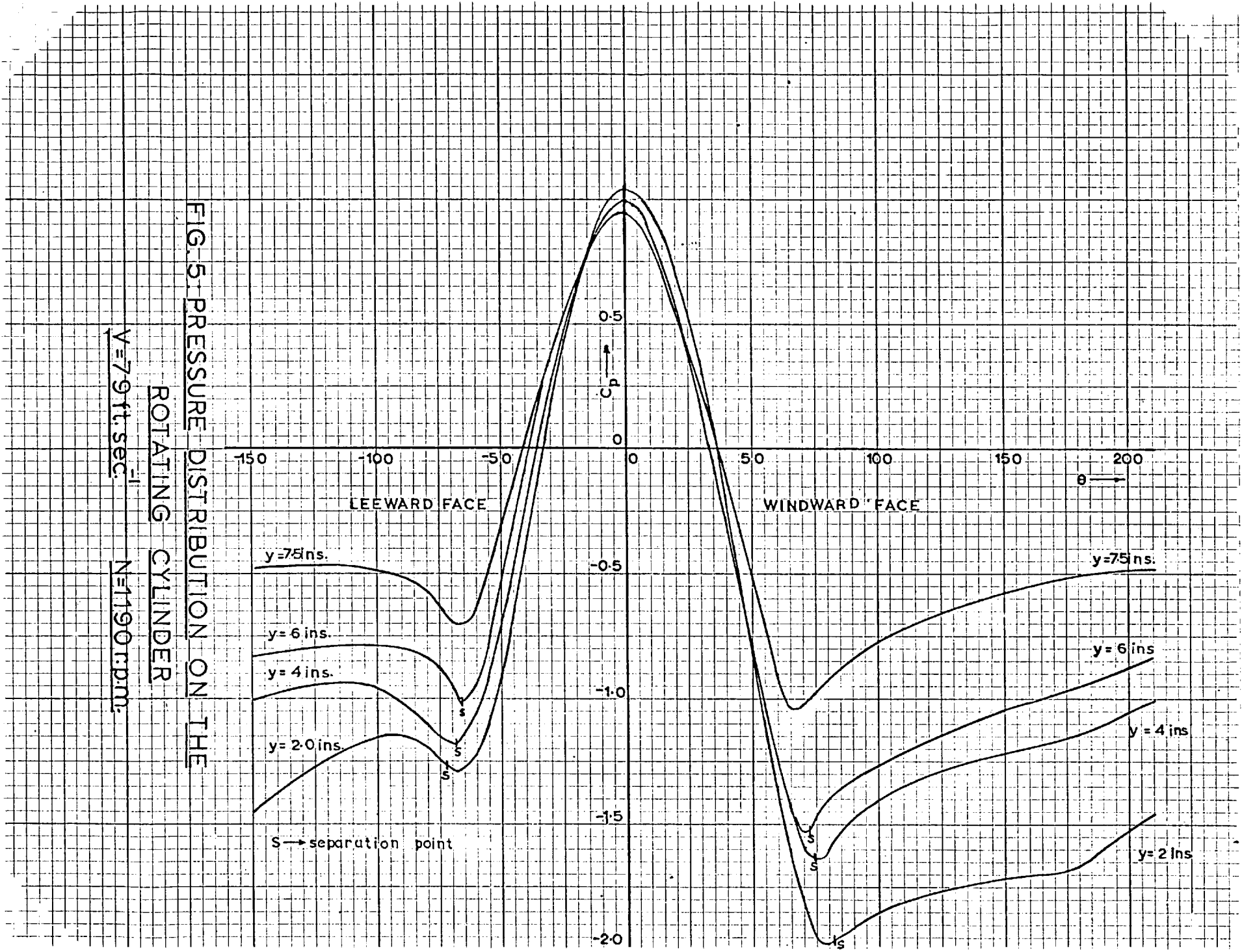

FIG. 5: PRESSURE DISTRIBUTION ON THE ROTATING CYLINDER

V=79 ft. sec.$^{-1}$ N=1190 r.p.m.

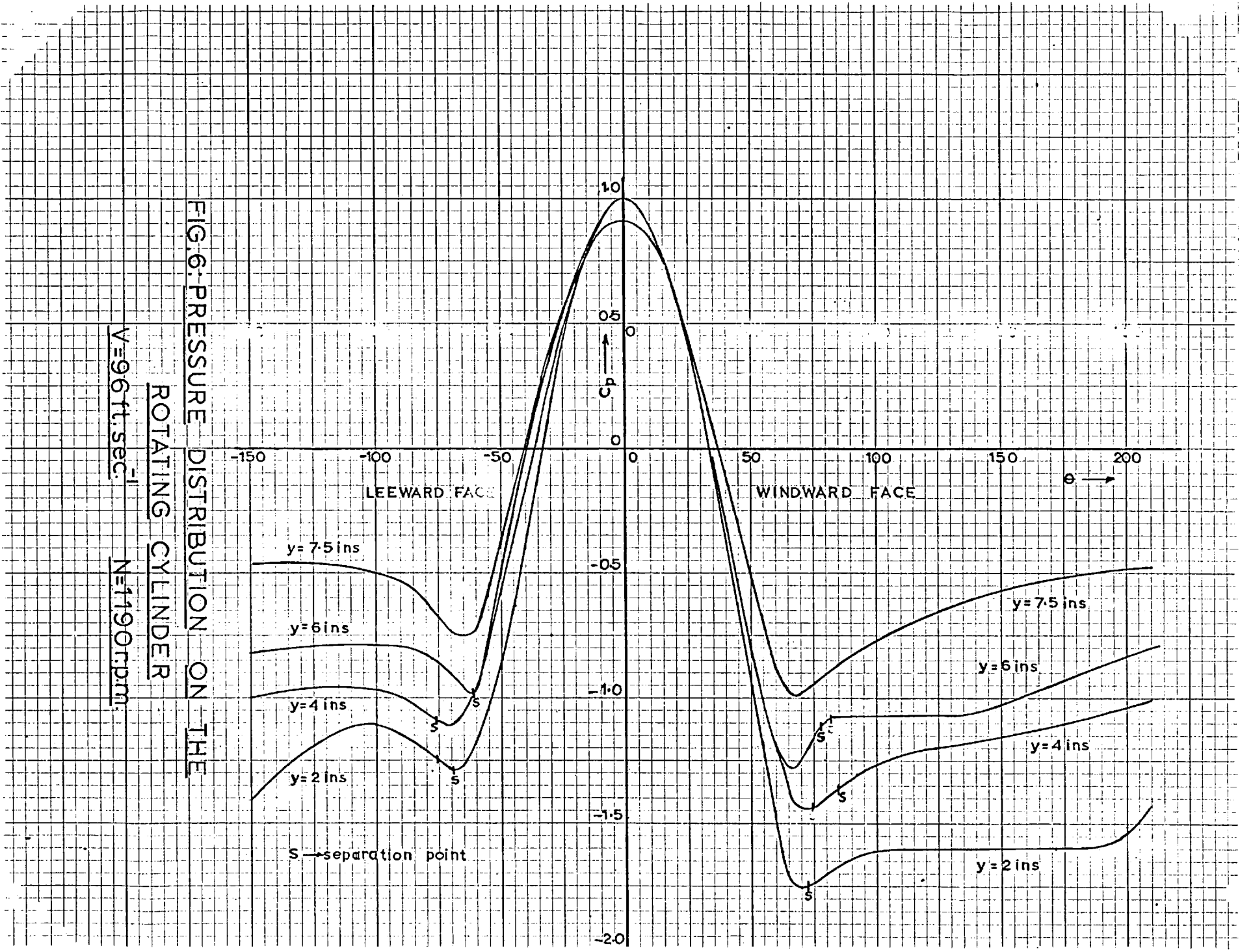

FIG. 6: PRESSURE DISTRIBUTION ON THE ROTATING CYLINDER

V = 96 ft. sec.$^{-1}$ N = 1190 r.p.m.

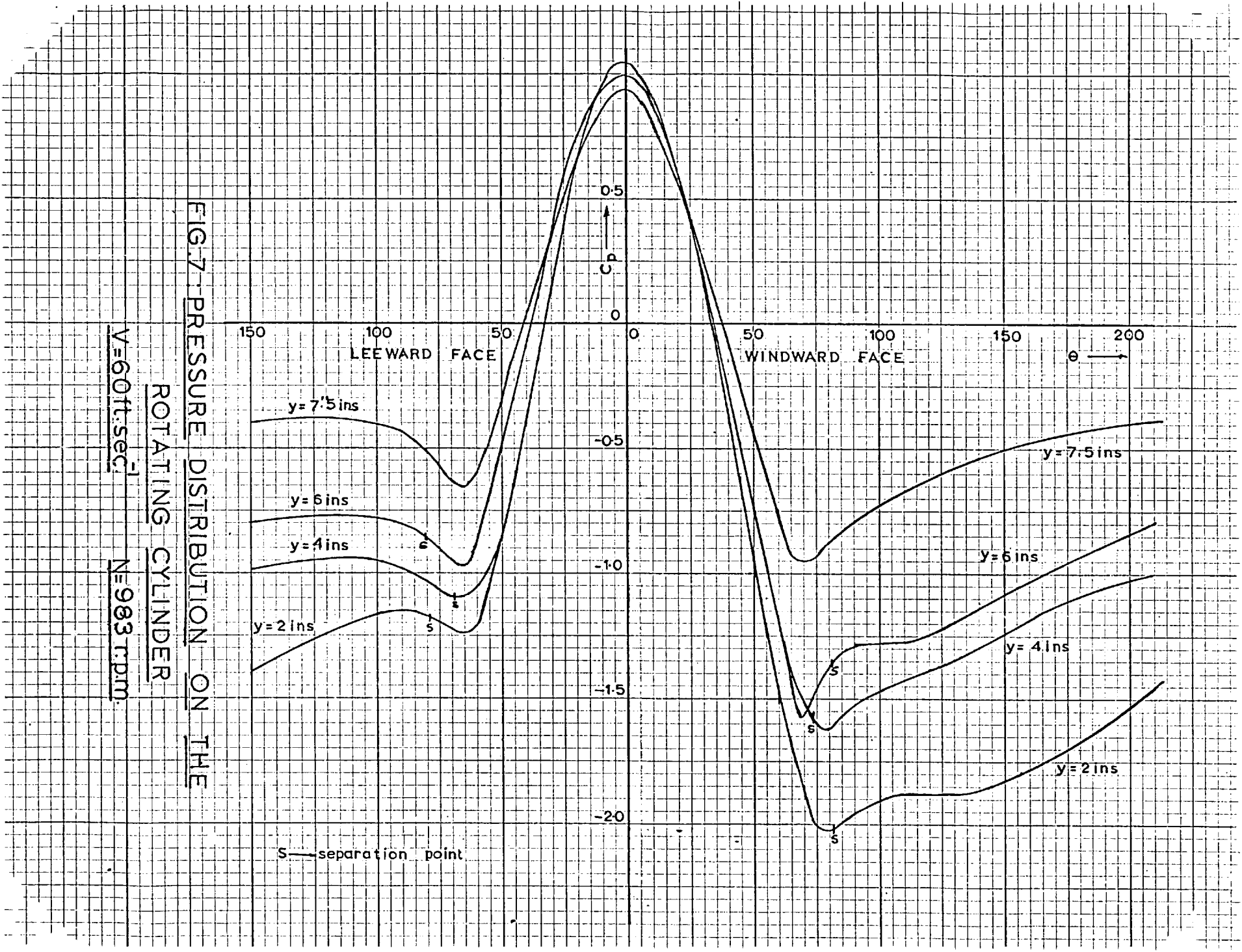

FIG. 7 : PRESSURE DISTRIBUTION ON THE ROTATING CYLINDER

V = 60 ft. sec.$^{-1}$ N = 983 r.p.m.

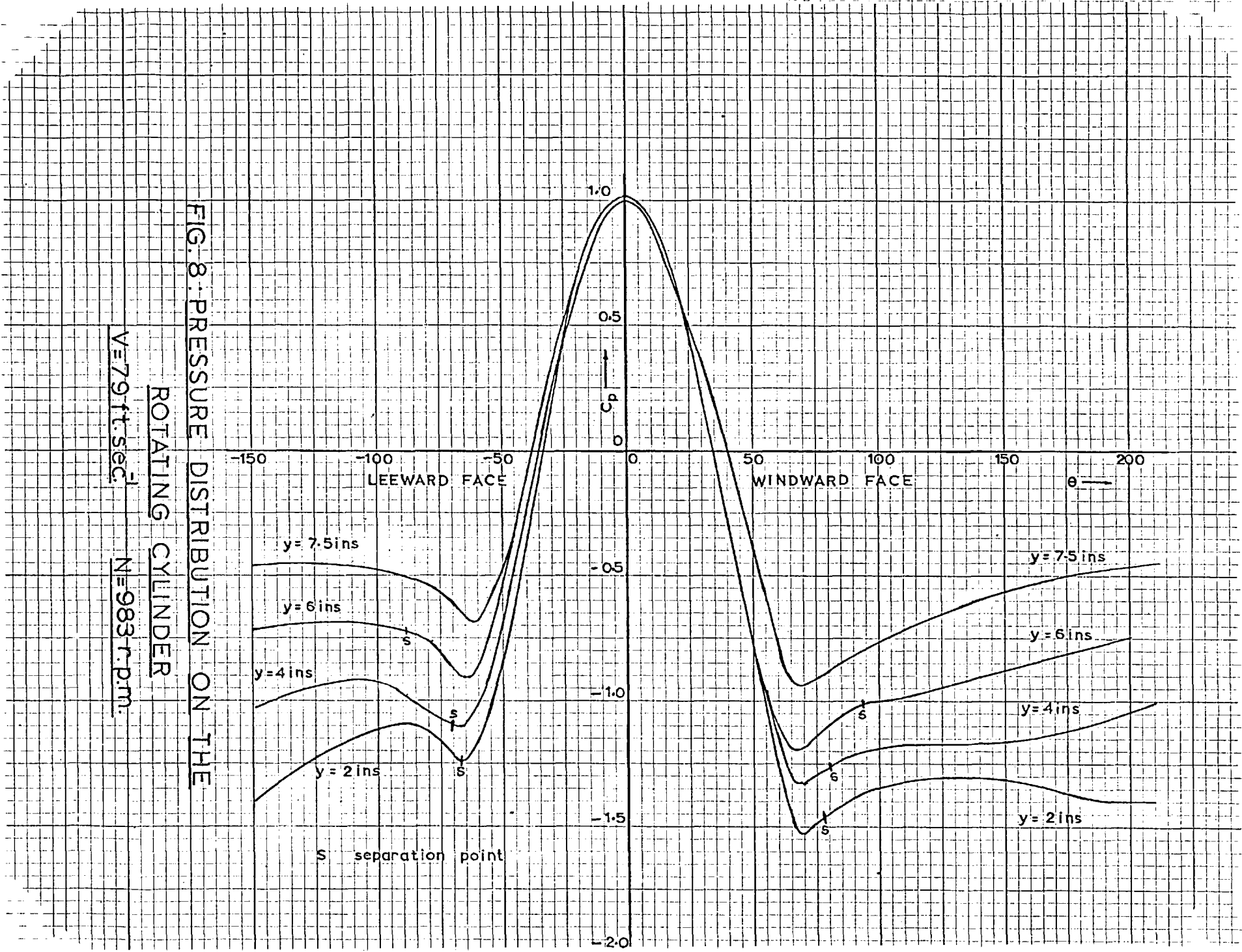

FIG. 8:- PRESSURE DISTRIBUTION ON THE ROTATING CYLINDER

V = 79 ft. sec.$^{-1}$ N = 983 r.p.m.

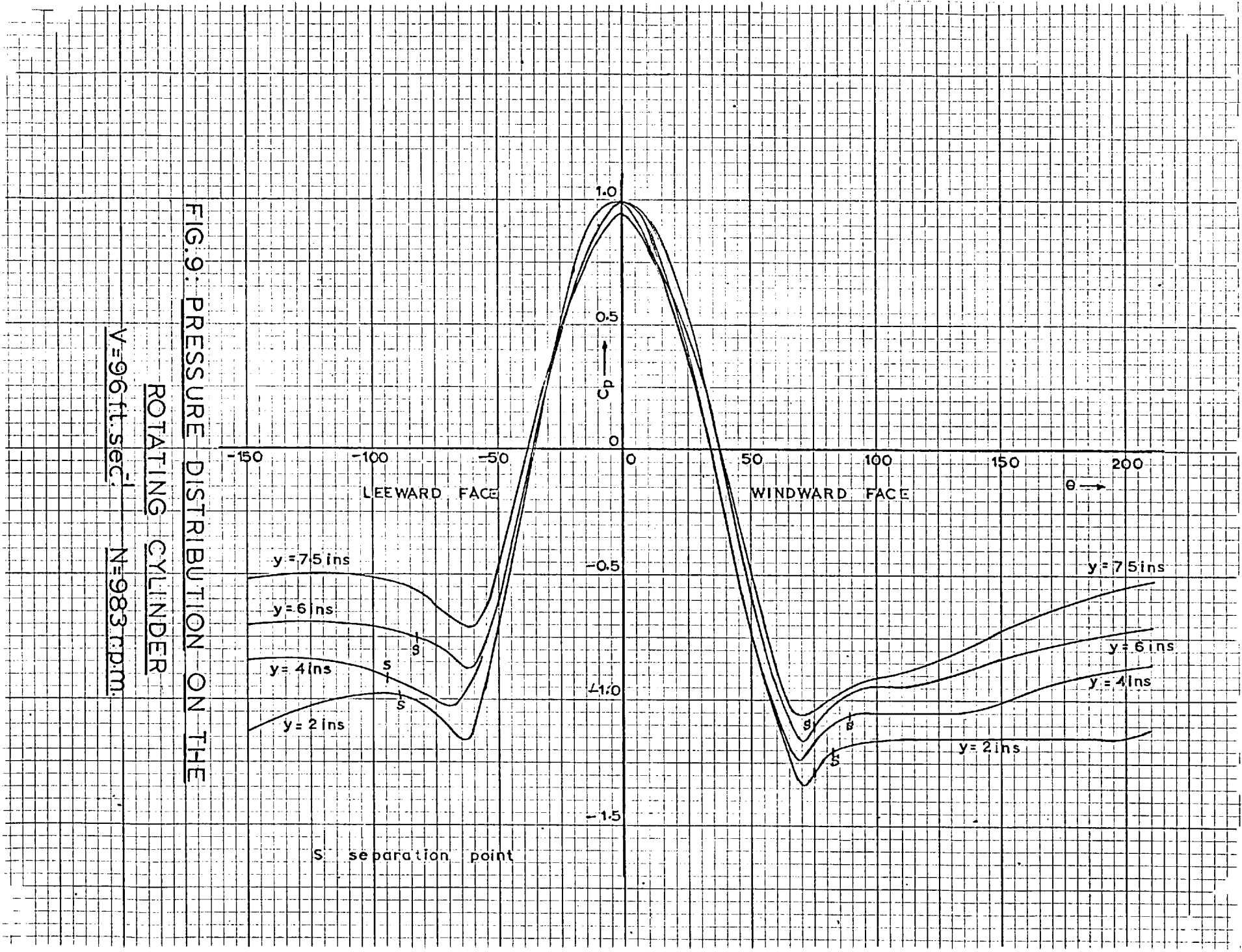

FIG. 9:- PRESSURE DISTRIBUTION ON THE ROTATING CYLINDER

V = 96 ft. sec.$^{-1}$ N = 983 r.p.m.

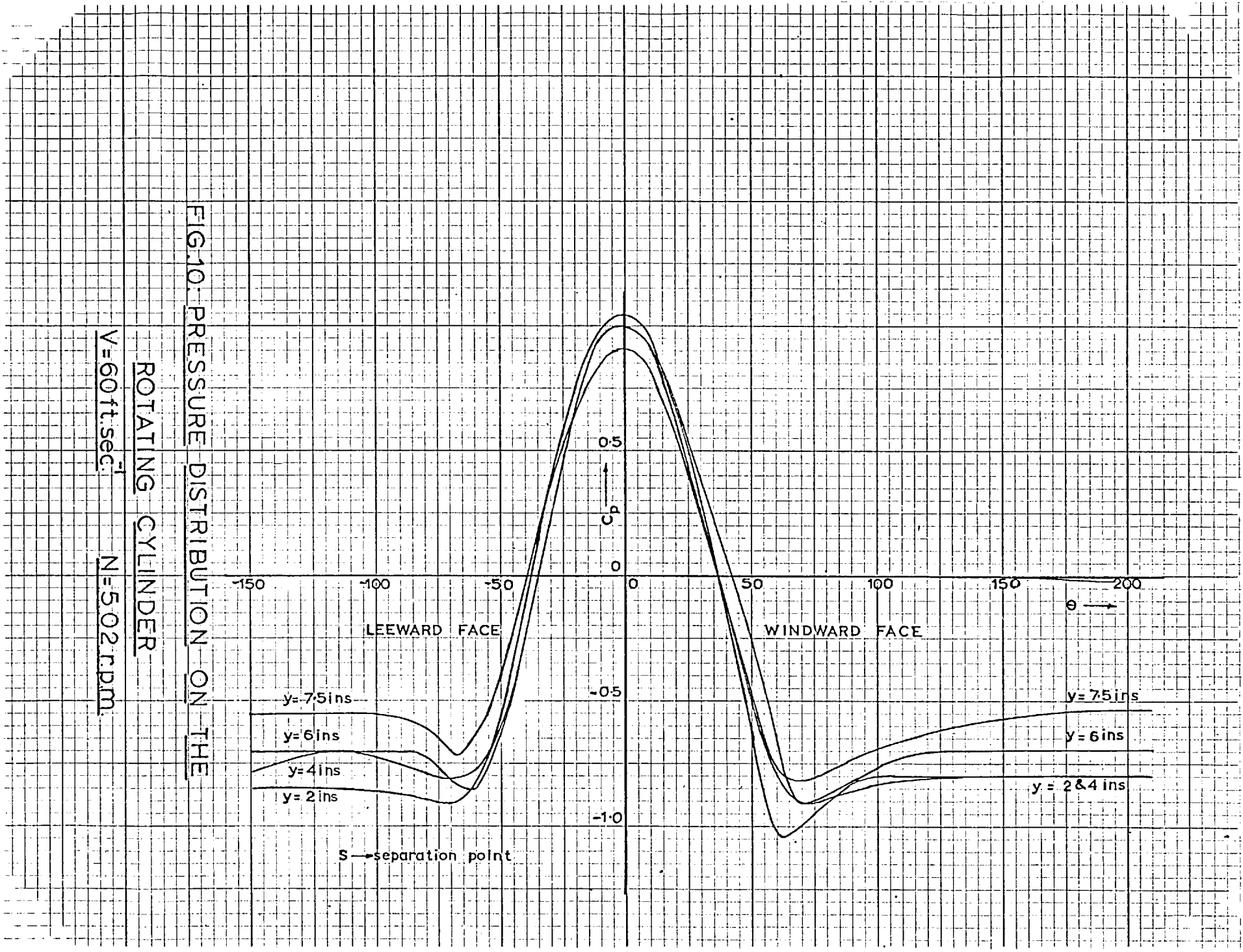

FIG. 10: PRESSURE DISTRIBUTION ON THE ROTATING CYLINDER

V = 60 ft. sec.$^{-1}$ N = 5·02 r.p.m.

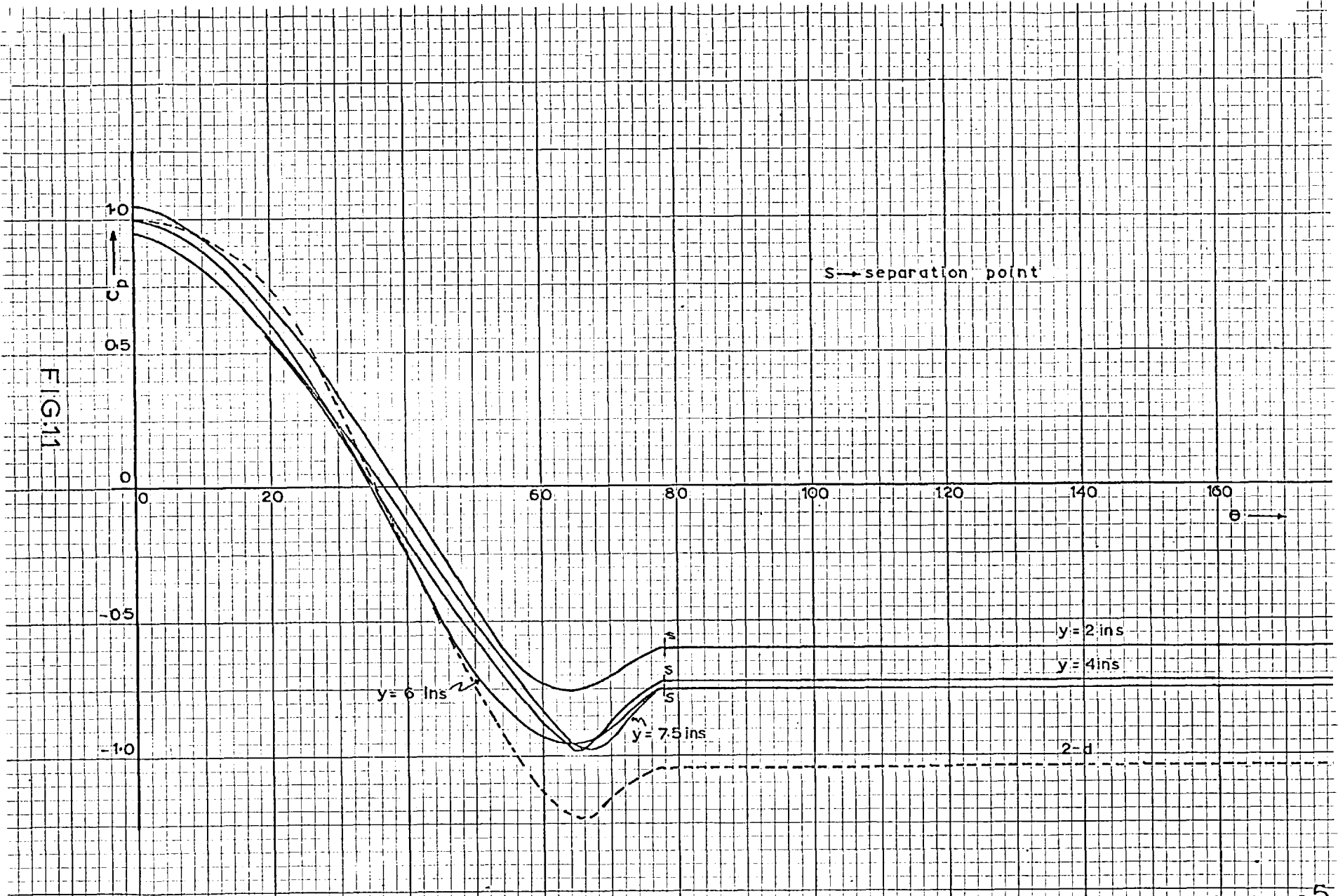

FIG.11

FIG.11: PRESSURE DISTRIBUTION ON STATIONARY CYLINDER $Re = 0{\cdot}77 \times 10^5$

V = 60 ft.sec^{-1} N = 0 r.p.m

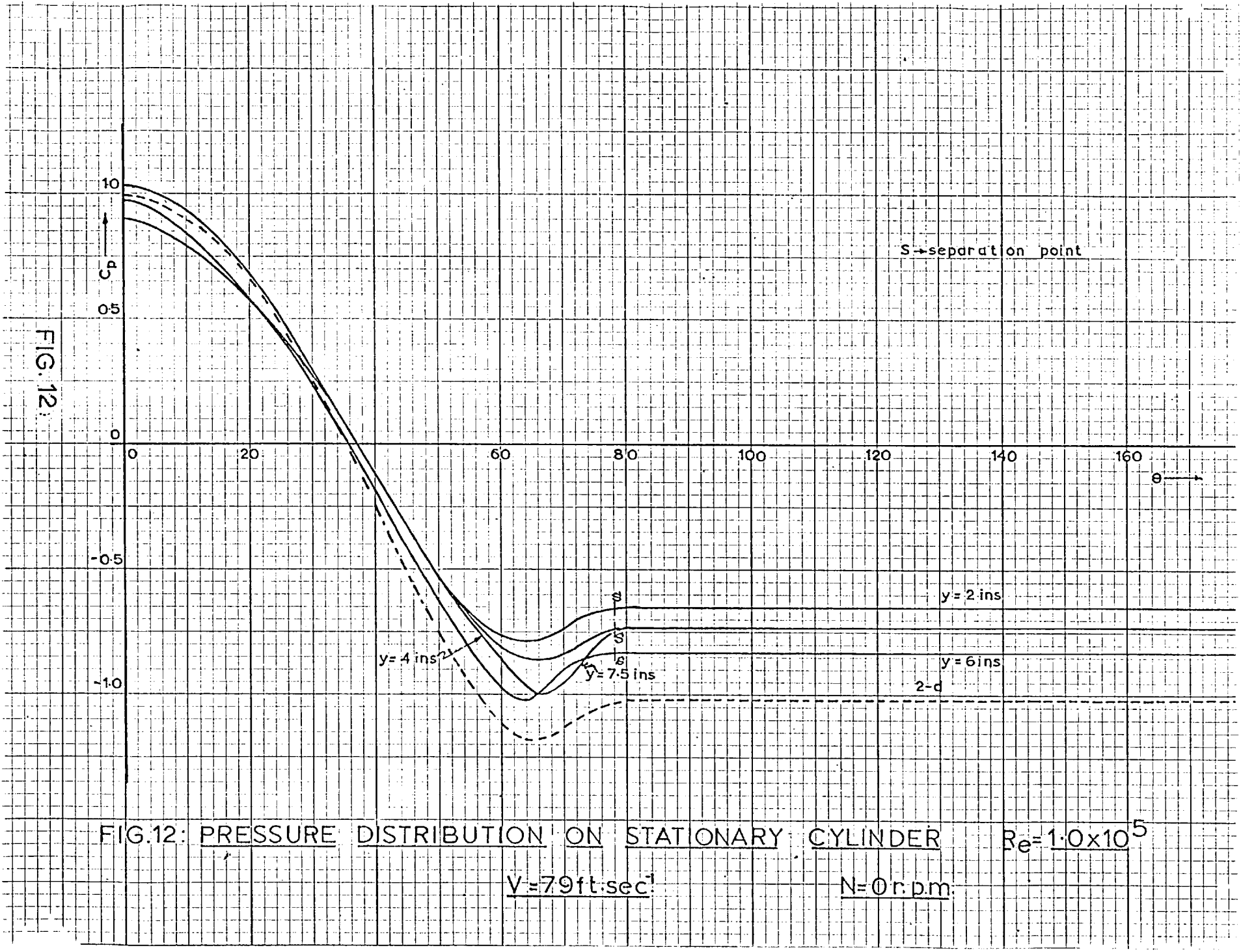

FIG. 12.

FIG.12: PRESSURE DISTRIBUTION ON STATIONARY CYLINDER $Re = 1{\cdot}0 \times 10^5$

V = 79 ft sec^{-1} N = 0 r.p.m.

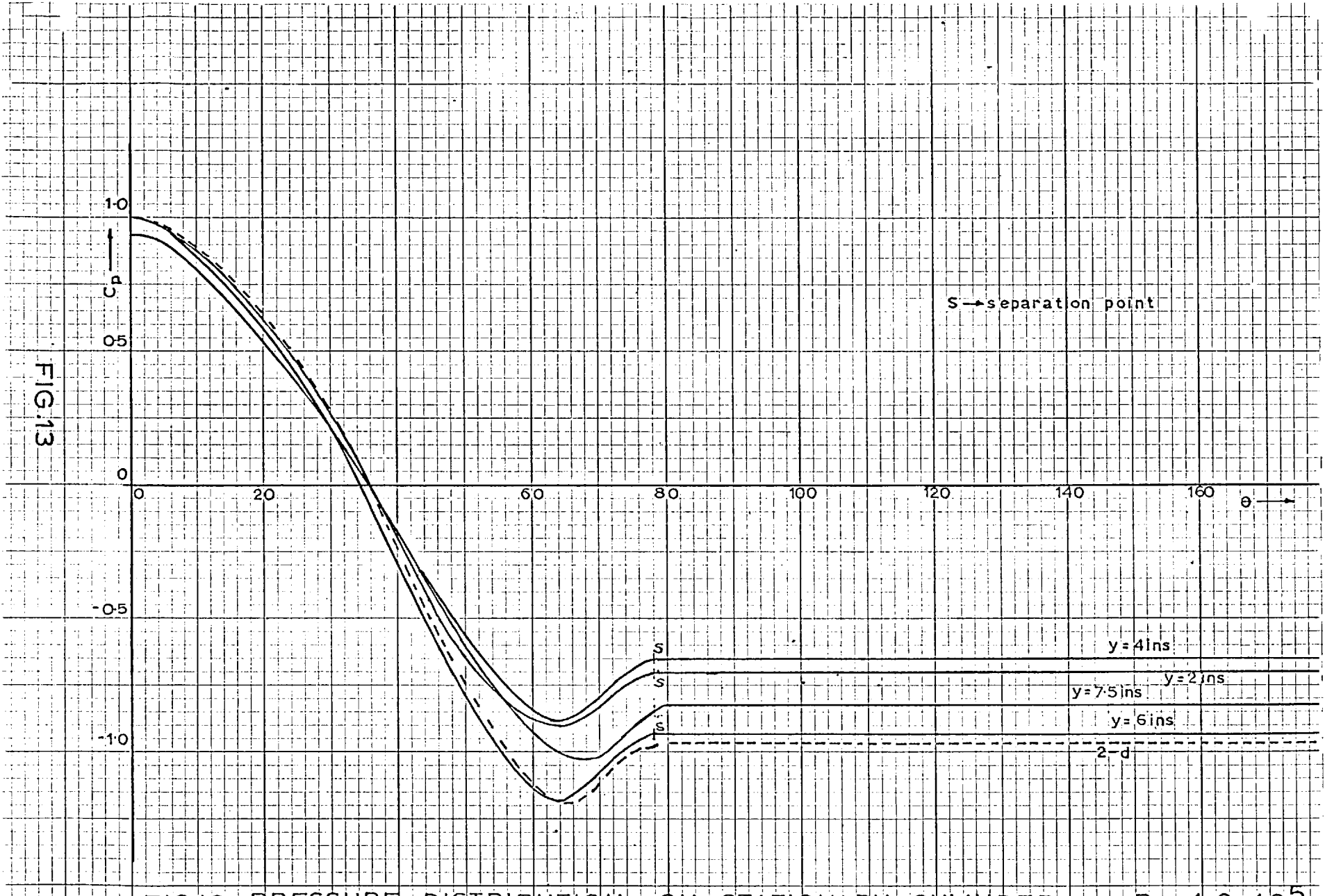

FIG.13

FIG.13: PRESSURE DISTRIBUTION ON STATIONARY CYLINDER $R_e = 1{\cdot}2 \times 10^5$

V = 96 ft. sec.$^{-1}$ N = 0 r.p.m.

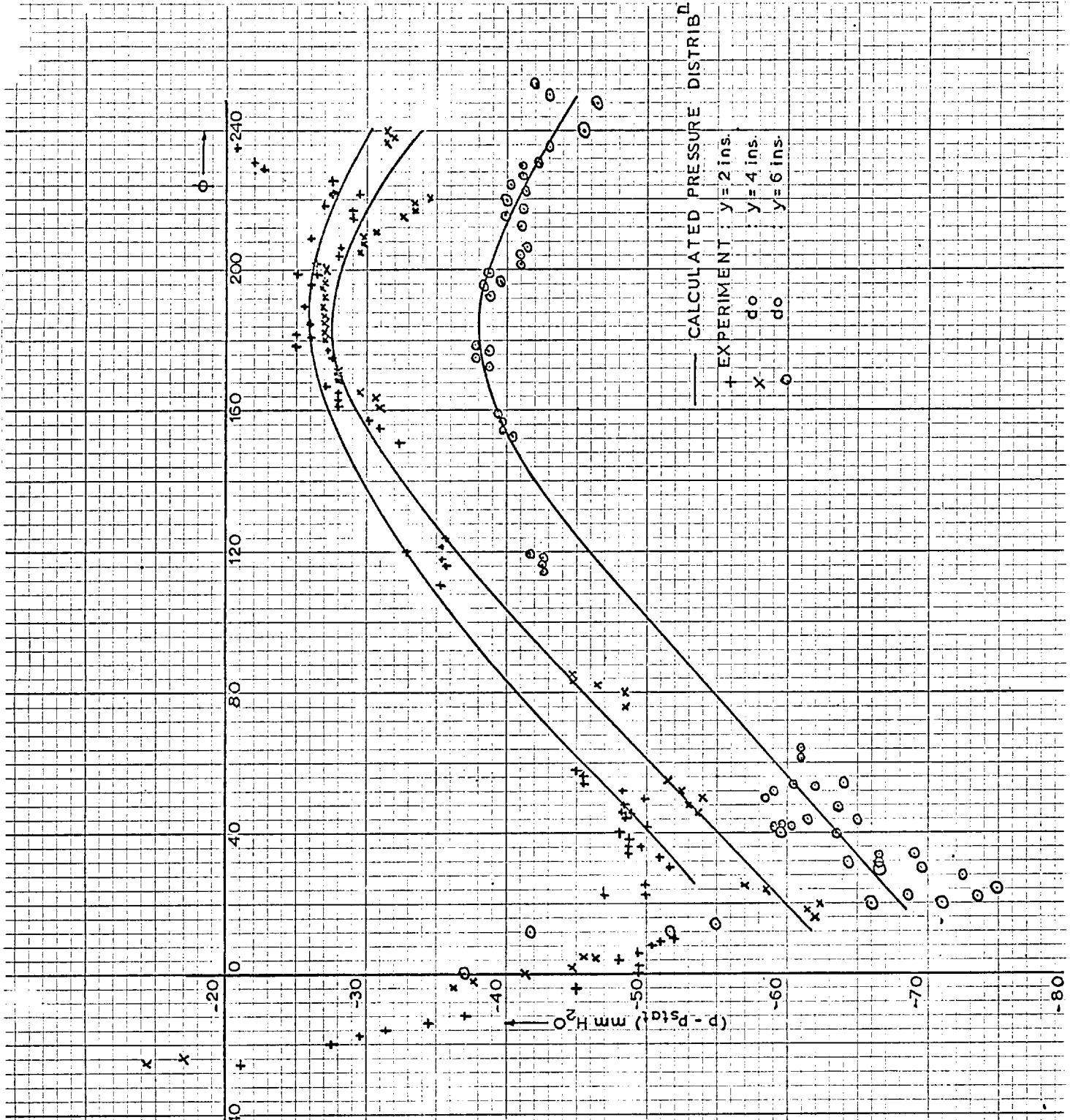

FIG. 14: PRESSURE DISTRIBUTION IN SEPARATED REGION OF ROTATING CYLINDER

V = 60 ft. sec.$^{-1}$ N = 1190 r.p.m.

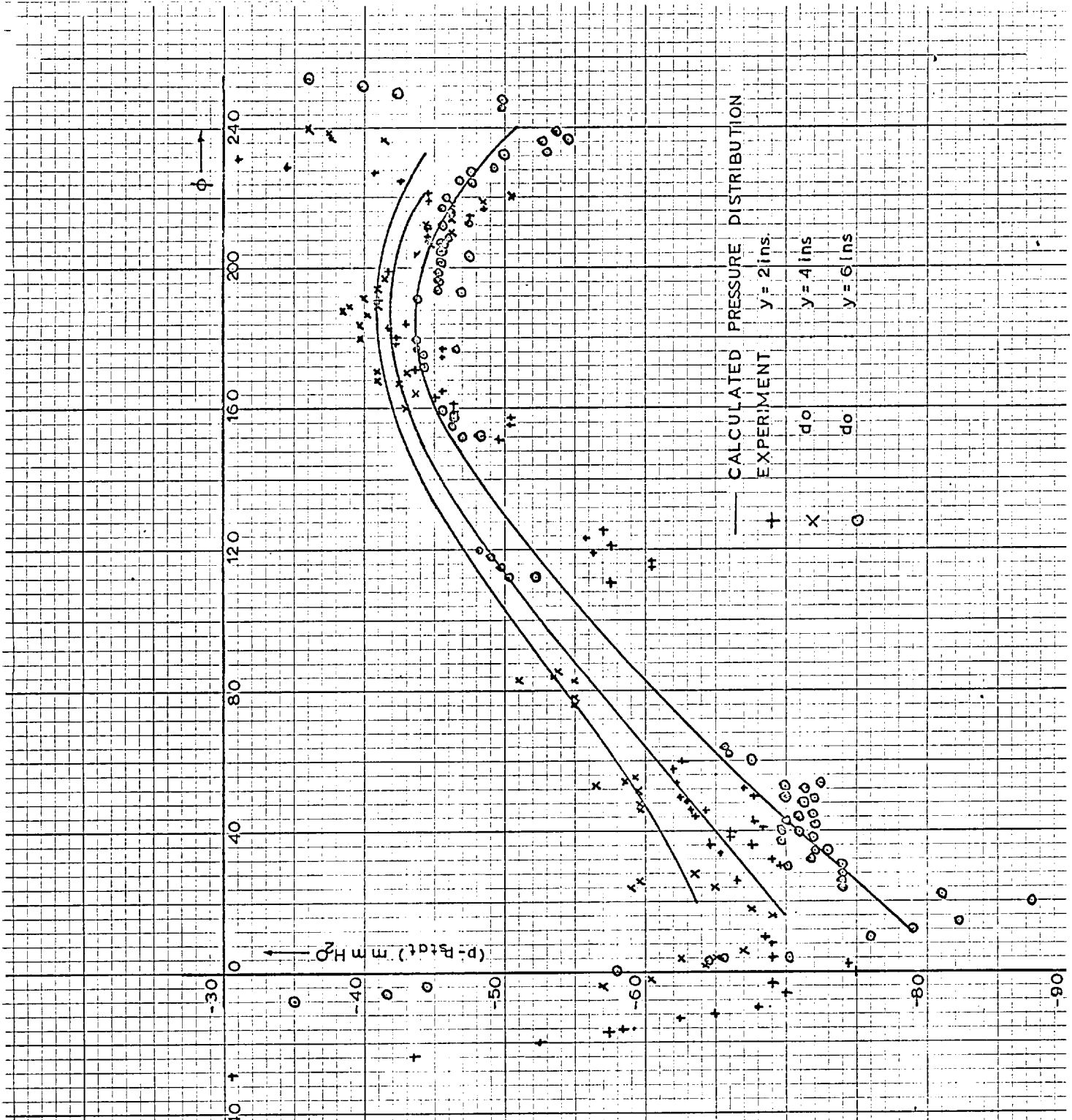

FIG. 15: PRESSURE DISTRIBUTION IN SEPARATED REGION OF ROTATING CYLINDER

V = 79 ft. sec^{-1} N = 1190 r.p.m

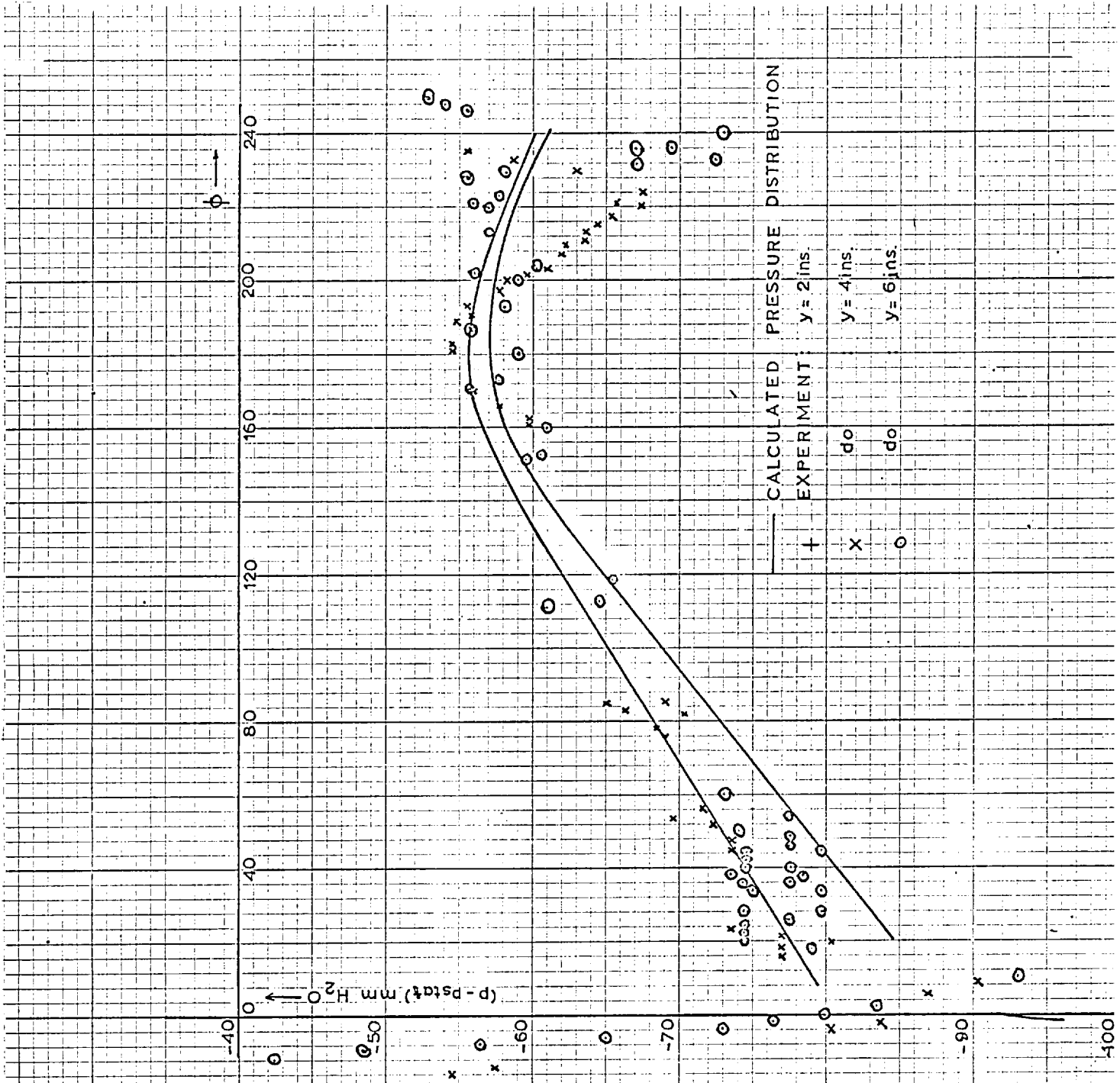

FIG. 16 : PRESSURE DISTRIBUTION IN SEPARATED REGION OF ROTATING CYLINDER

V = 96 ft. sec.$^{-1}$ N = 1190 r.p.m.

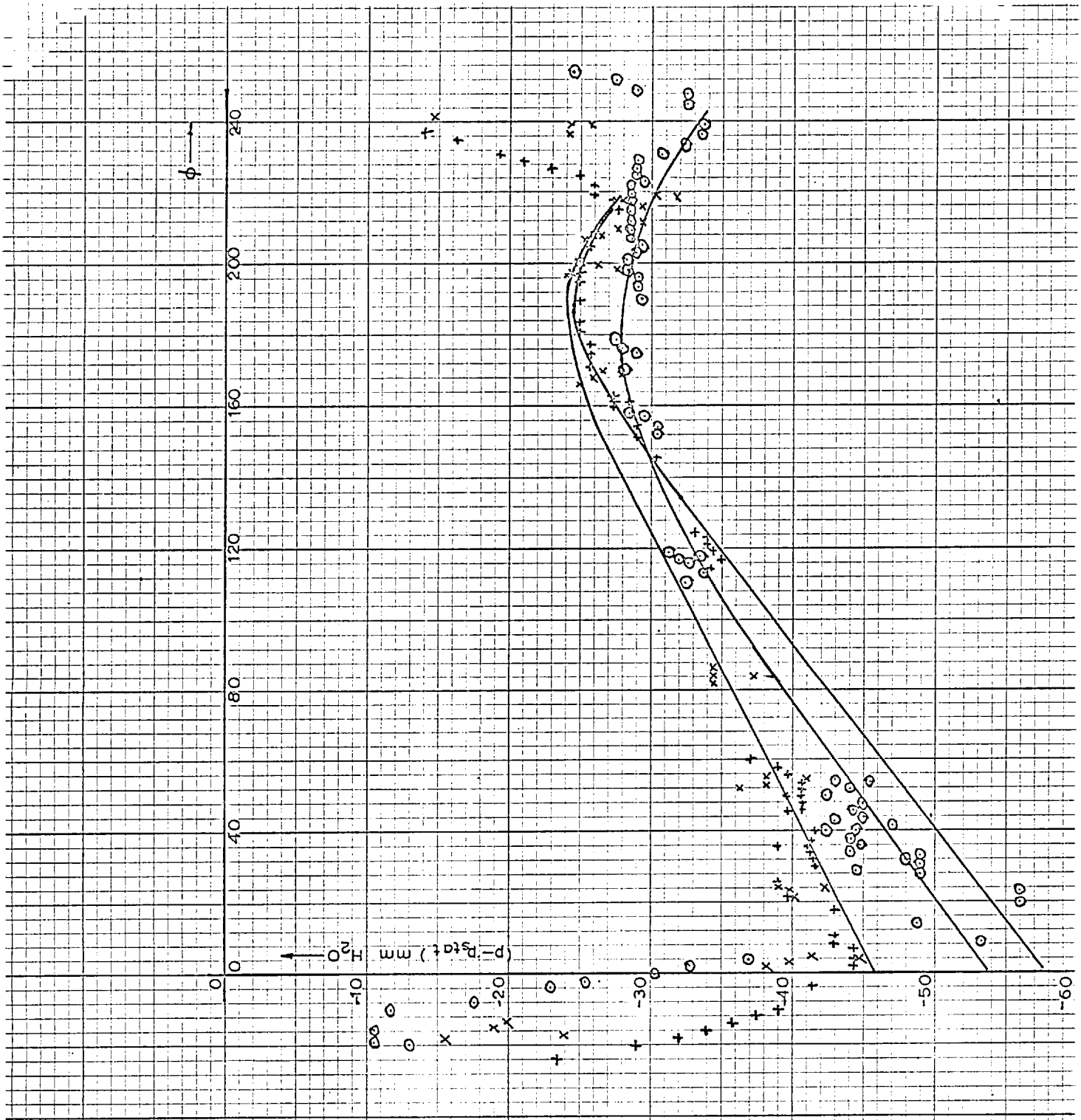

FIG.17: PRESSURE DISTRIBUTION IN SEPARATED REGION OF ROTATING CYLINDER

V=60ft.sec.$^{-1}$ N=983r.p.m.

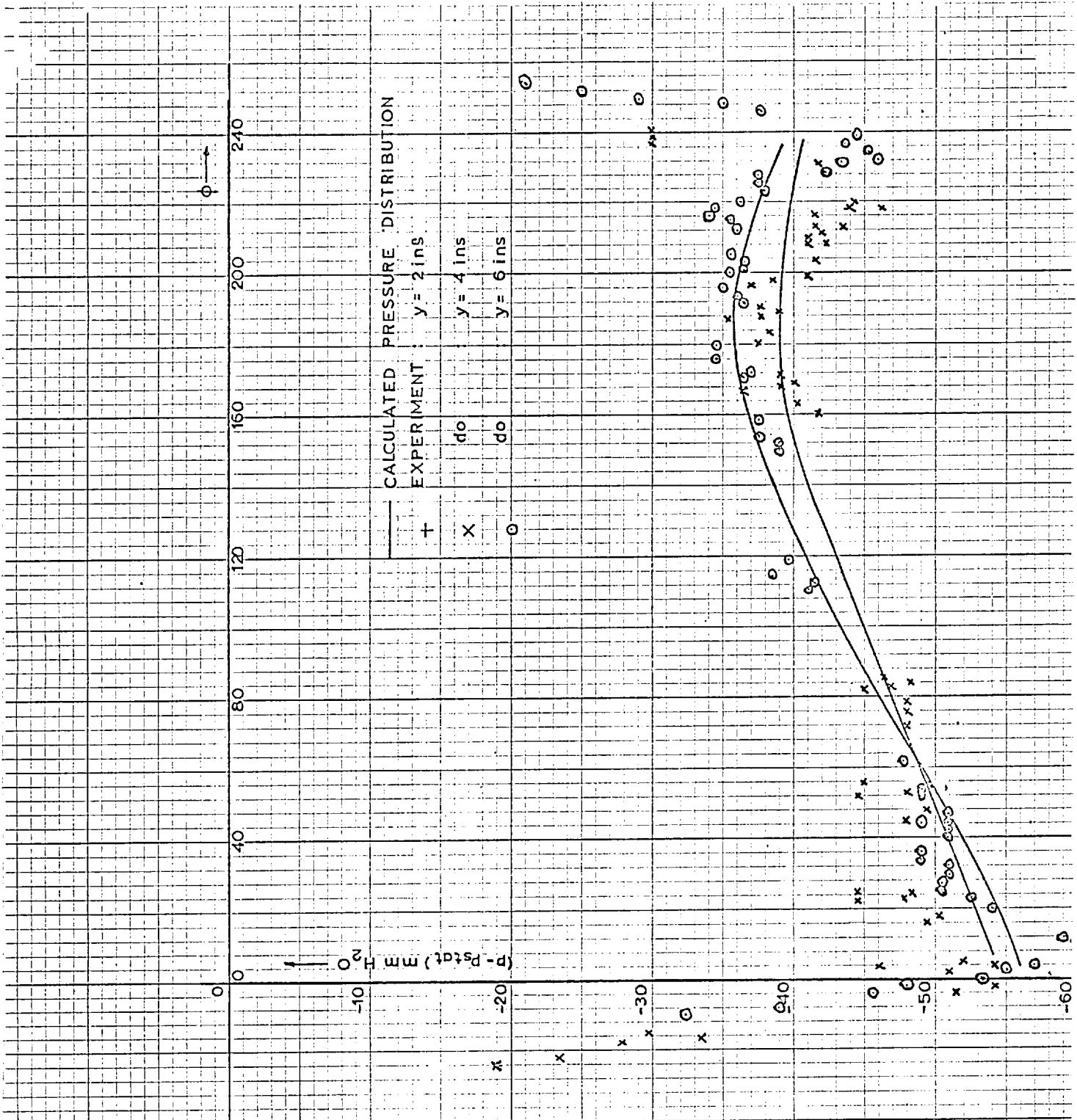

FIG. 18 : PRESSURE DISTRIBUTION IN SEPARATED REGION OF ROTATING CYLINDER

V = 79 ft. sec^{-1} N = 983 r.p.m.

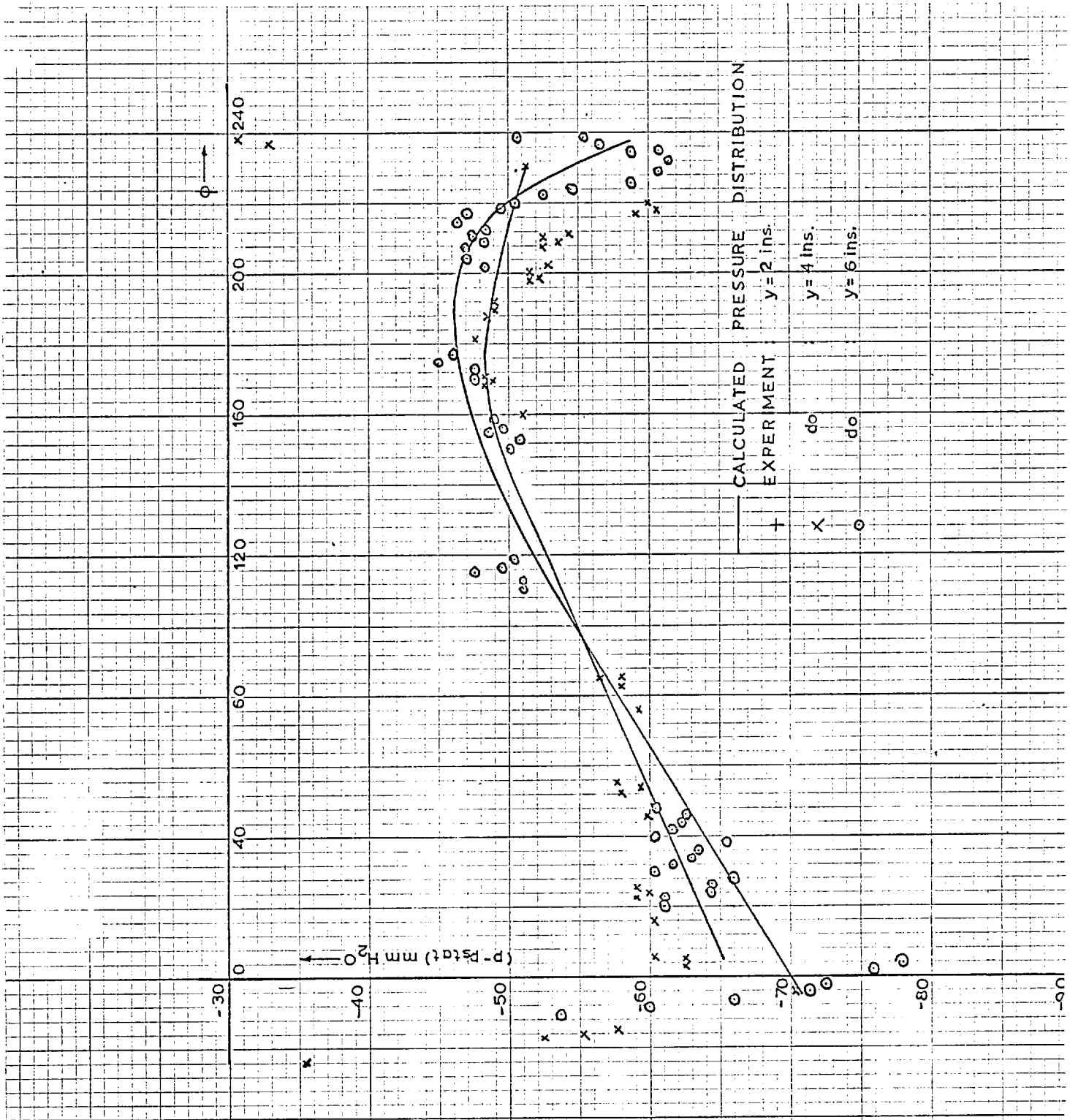

FIG. 19 - PRESSURE DISTRIBUTION IN SEPARATED REGION OF ROTATING CYLINDER

V = 96 ft. sec.$^{-1}$ N = 983 r.p.m.

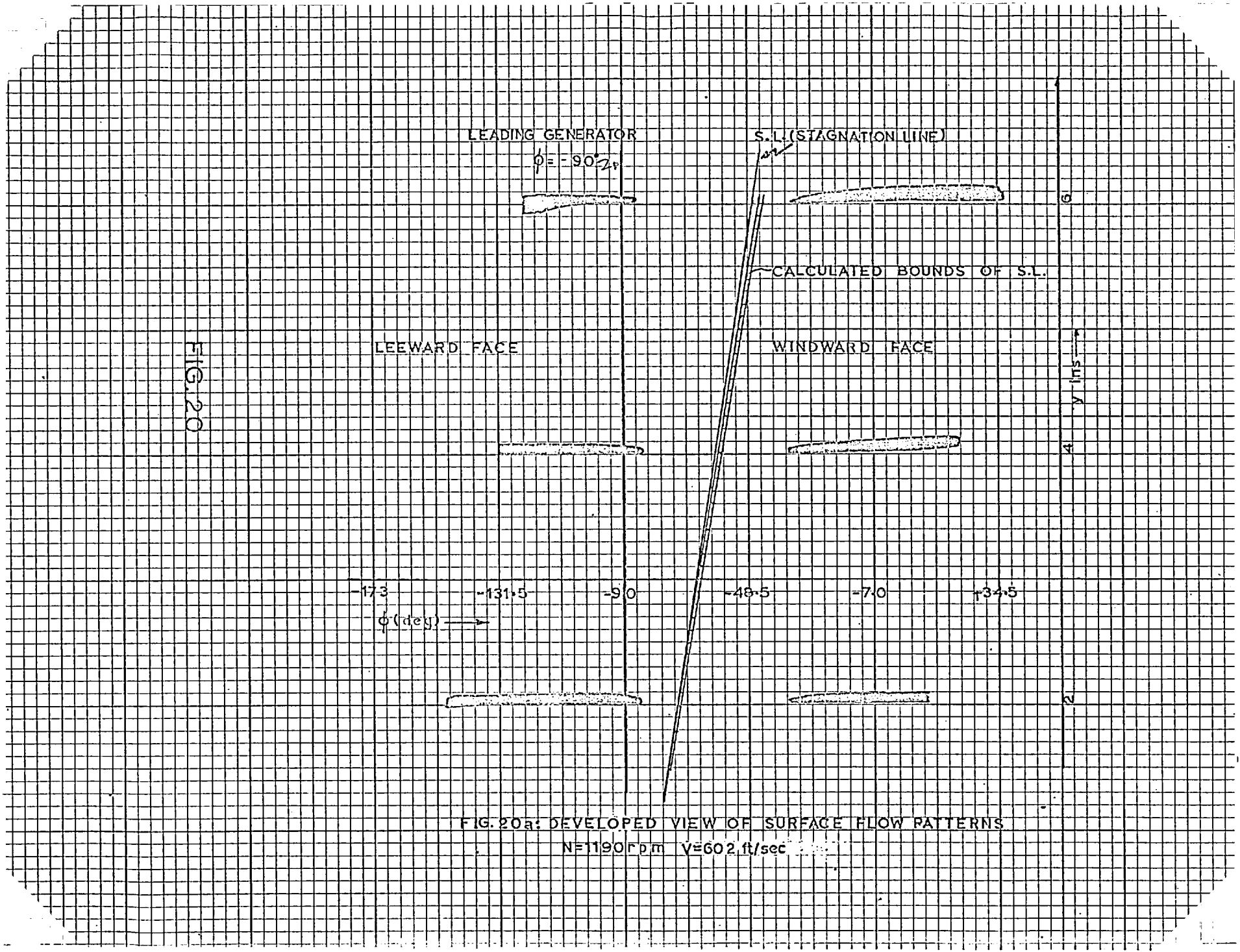

FIG. 20

FIG. 20a: DEVELOPED VIEW OF SURFACE FLOW PATTERNS
N=1190 r p m V=602 ft/sec

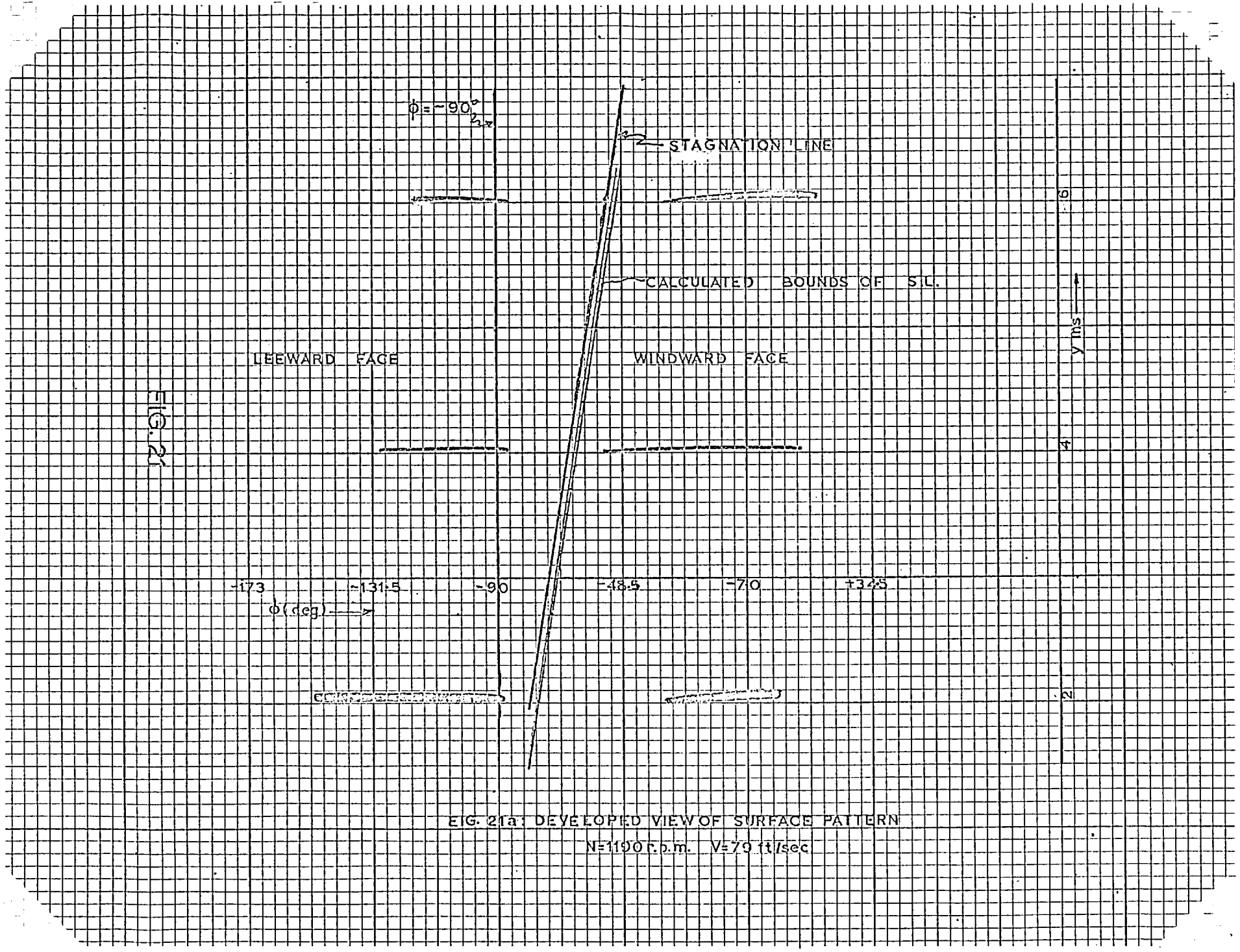

FIG. 21a: DEVELOPED VIEW OF SURFACE PATTERN
N=1190 r.p.m. V=79 ft/sec

FIG. 21

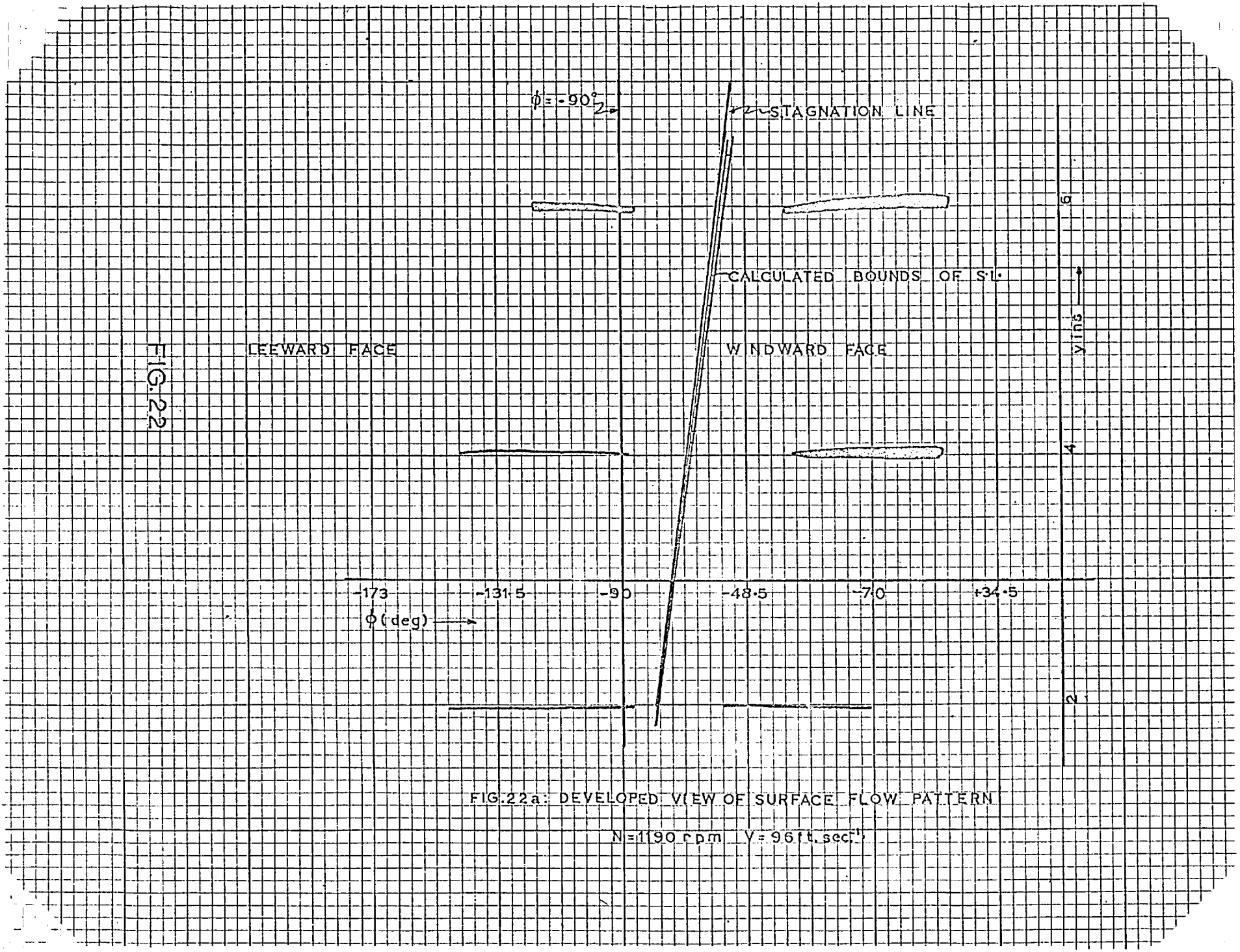

FIG. 22

FIG. 22a: DEVELOPED VIEW OF SURFACE FLOW PATTERN

N = 1190 rpm V = 96 ft. sec^{-1}

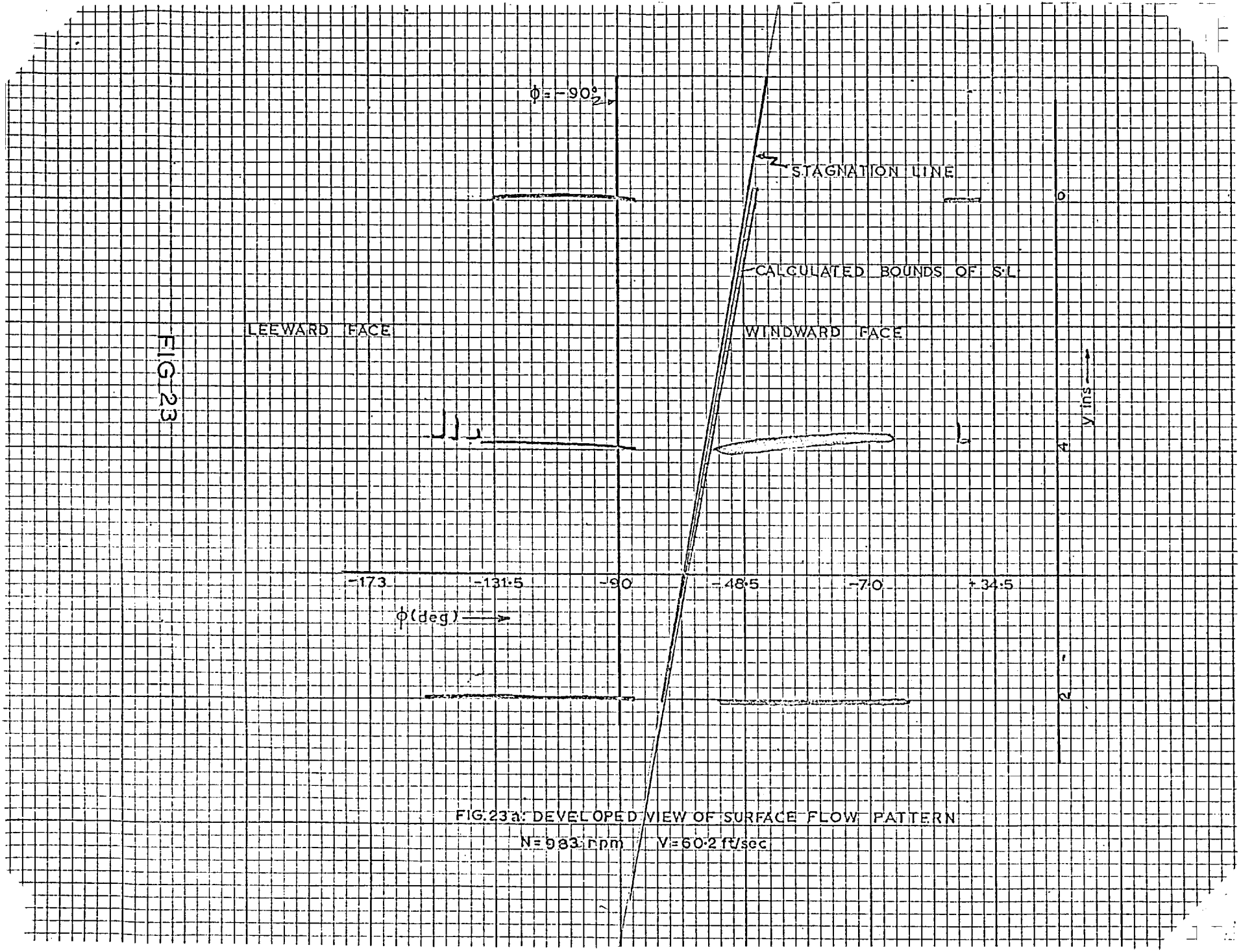

FIG. 23

FIG. 23a: DEVELOPED VIEW OF SURFACE FLOW PATTERN

N=983 rpm V=60·2 ft/sec

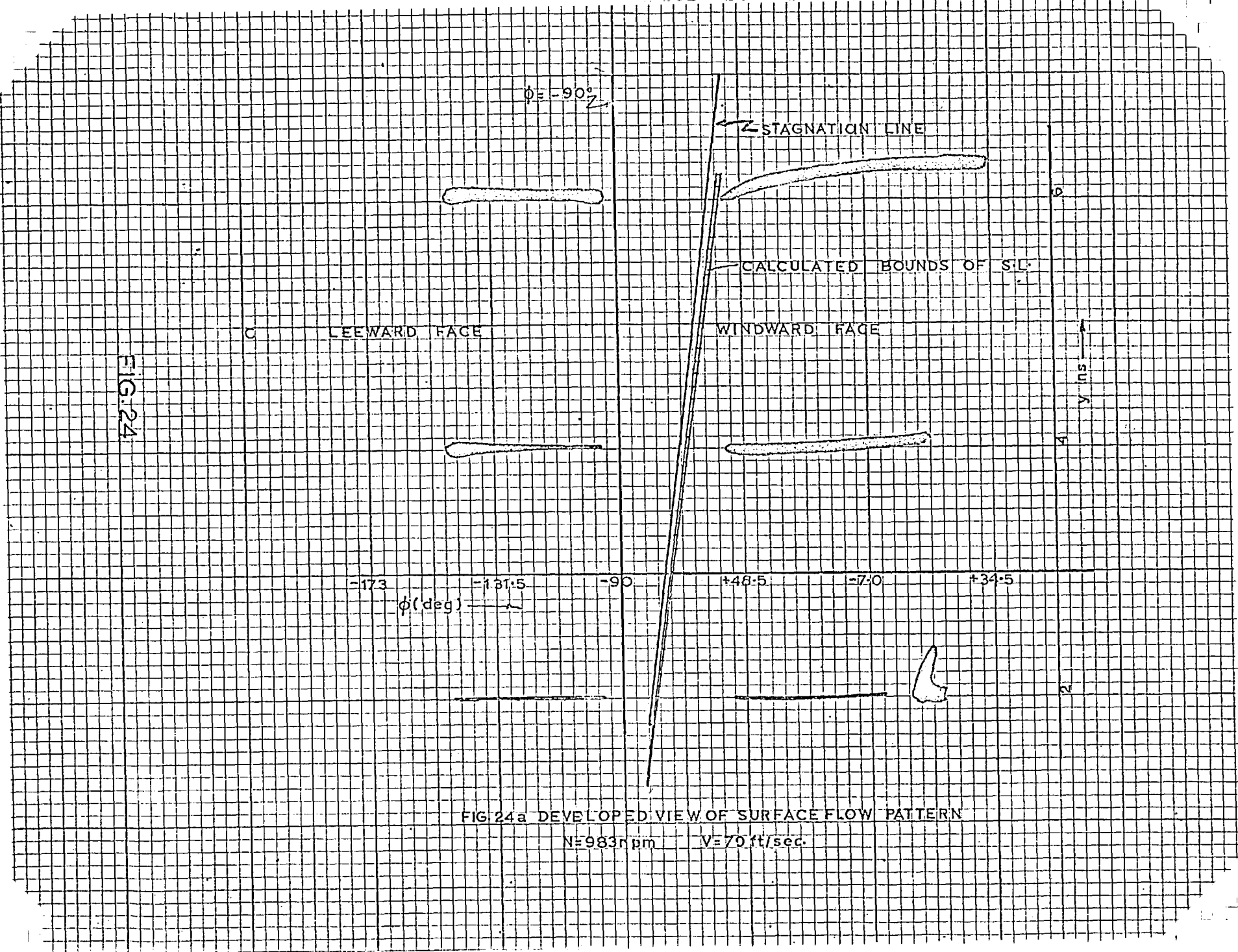

FIG. 24

FIG 24a DEVELOPED VIEW OF SURFACE FLOW PATTERN

N=983 rpm V=70 ft/sec.

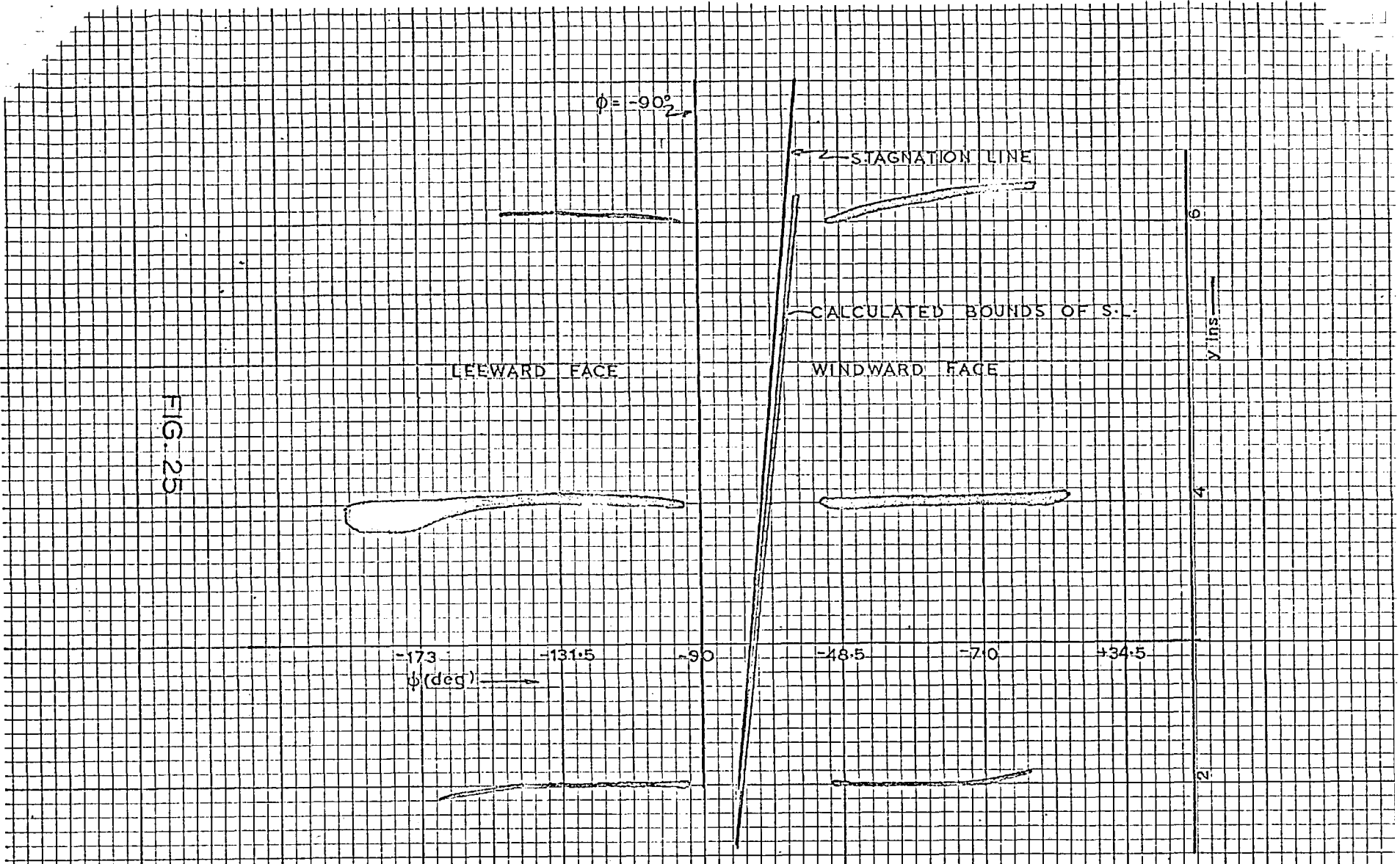

FIG 25a: DEVELOPED VIEW OF SURFACE PATTERN

N = 983 rpm V = 96 ft/sec.

FIG. 25

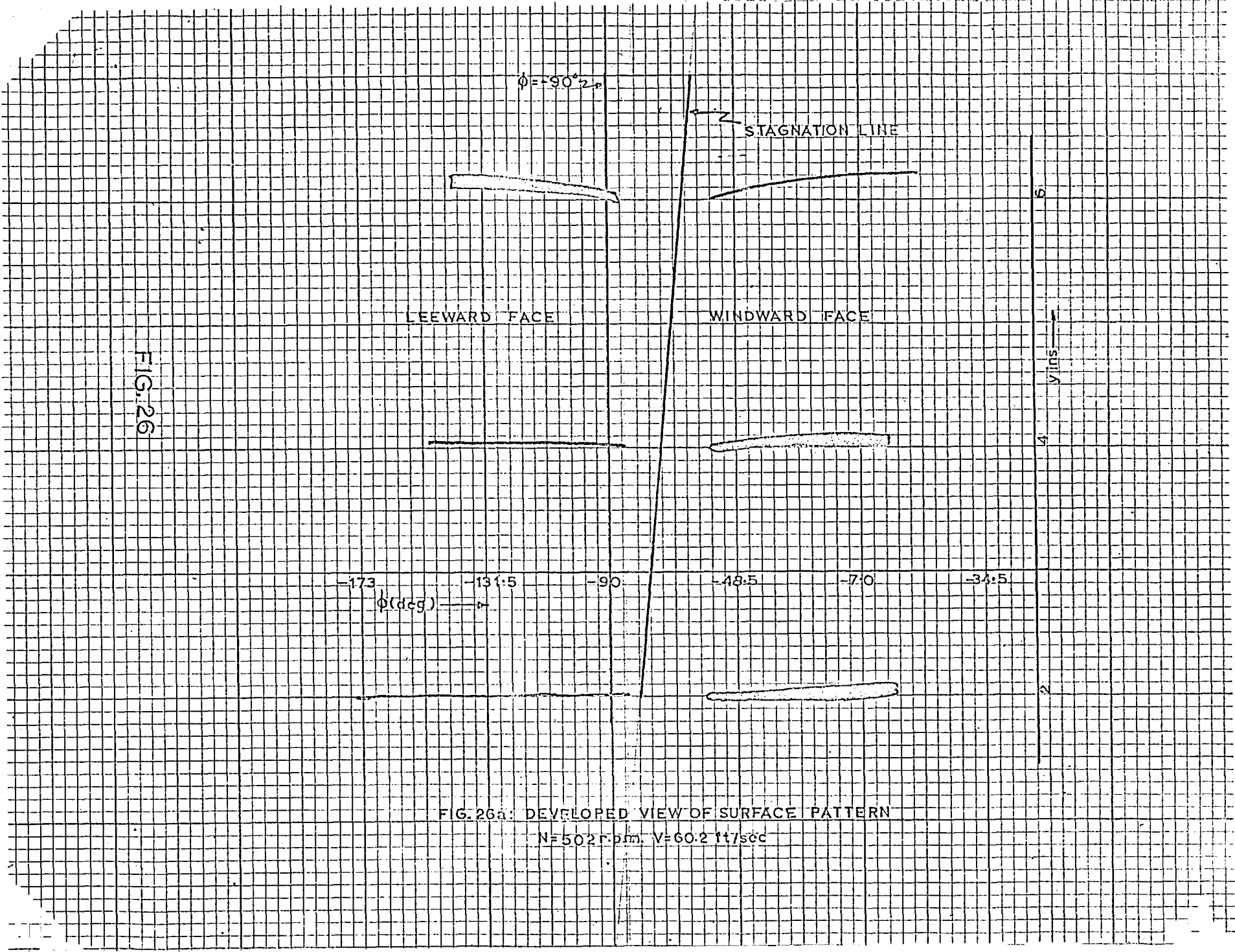

FIG. 26

FIG. 26a: DEVELOPED VIEW OF SURFACE PATTERN
N=502 r.p.m. V=60·2 ft/sec

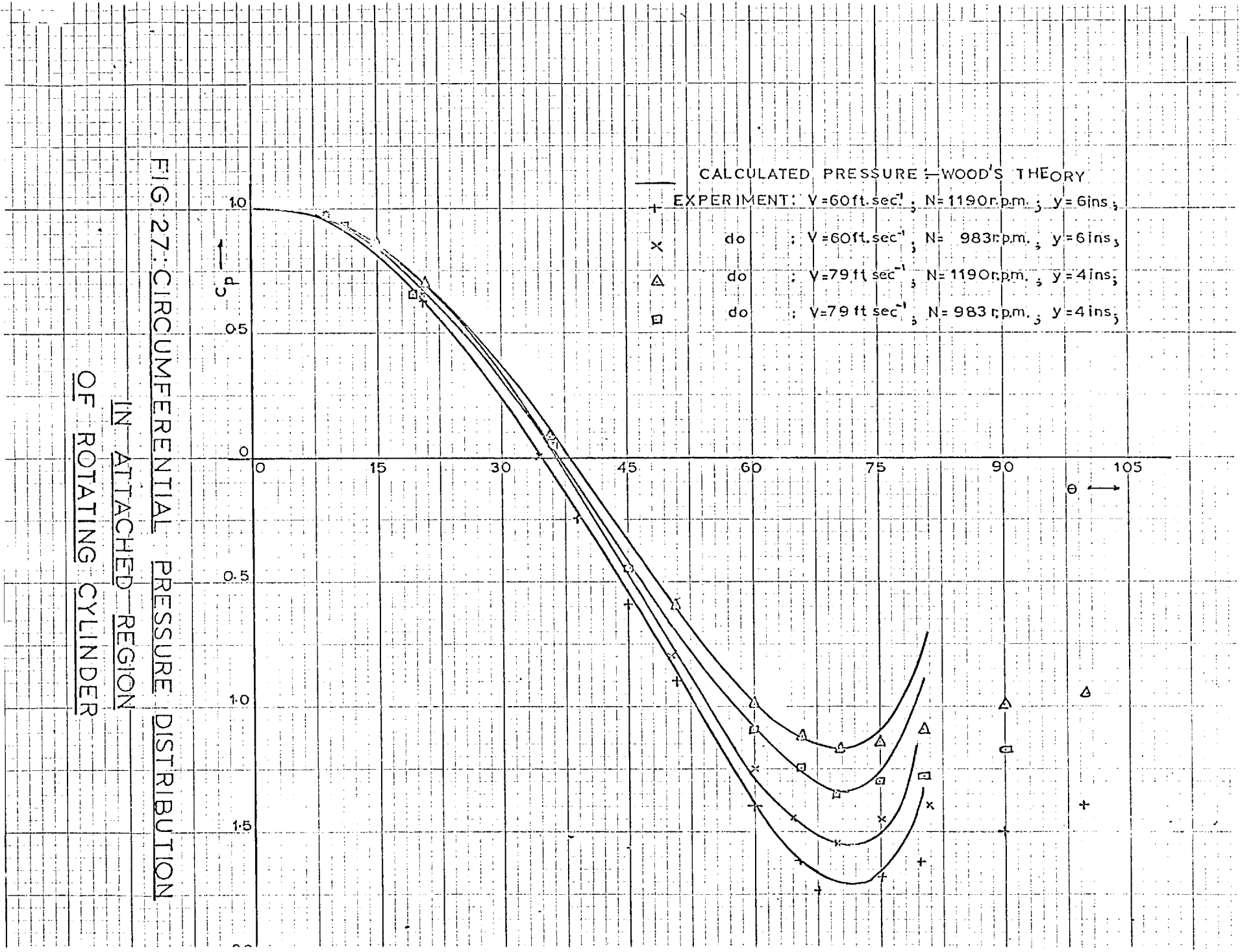

FIG. 27: CIRCUMFERENTIAL PRESSURE DISTRIBUTION IN ATTACHED REGION OF ROTATING CYLINDER

FIG. 27a: PRESSURE DISTRIBUTION ON CIRCULAR CYLINDER (TWO-DIMENSIONAL FLOW)

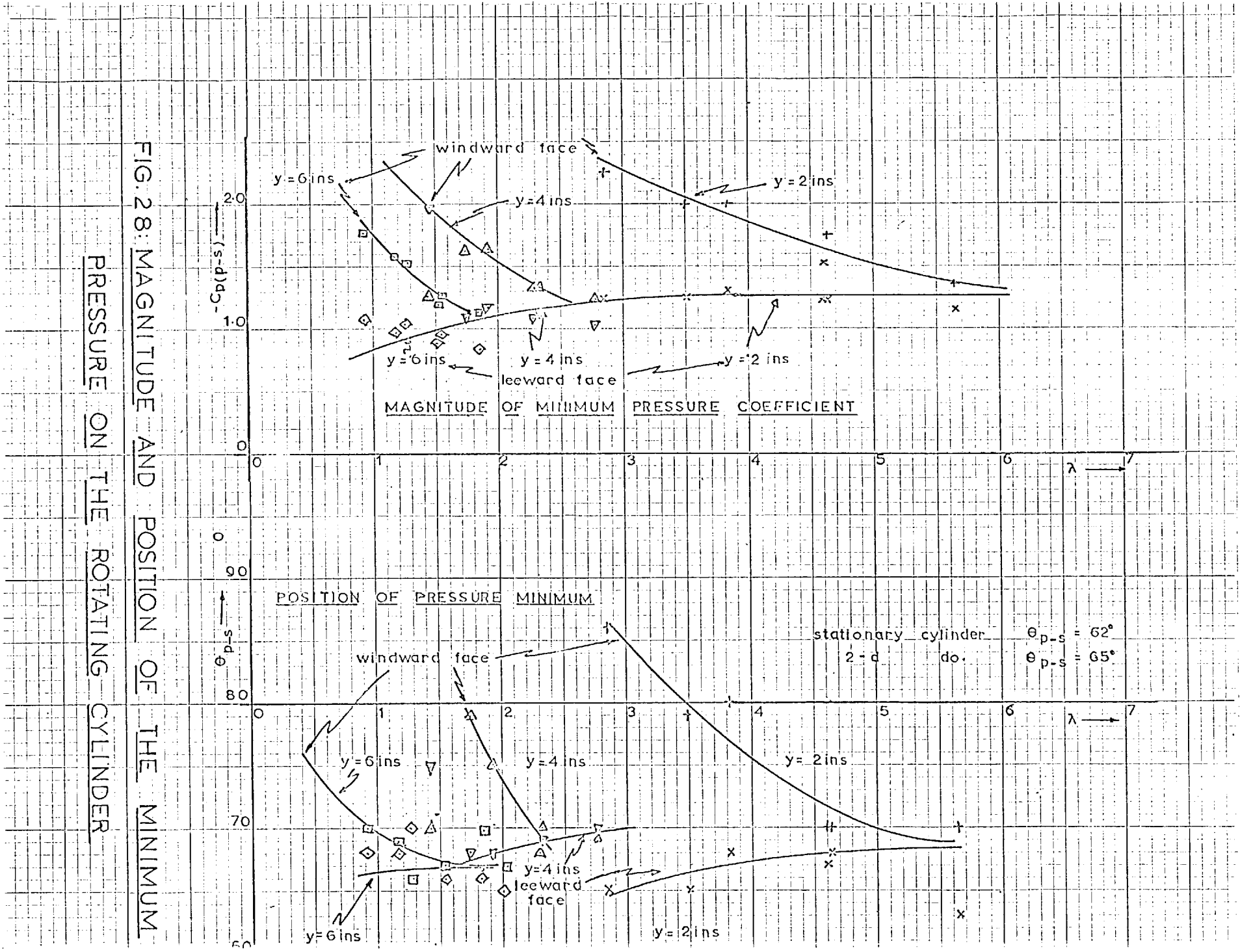

FIG. 28: MAGNITUDE AND POSITION OF THE MINIMUM PRESSURE ON THE ROTATING CYLINDER

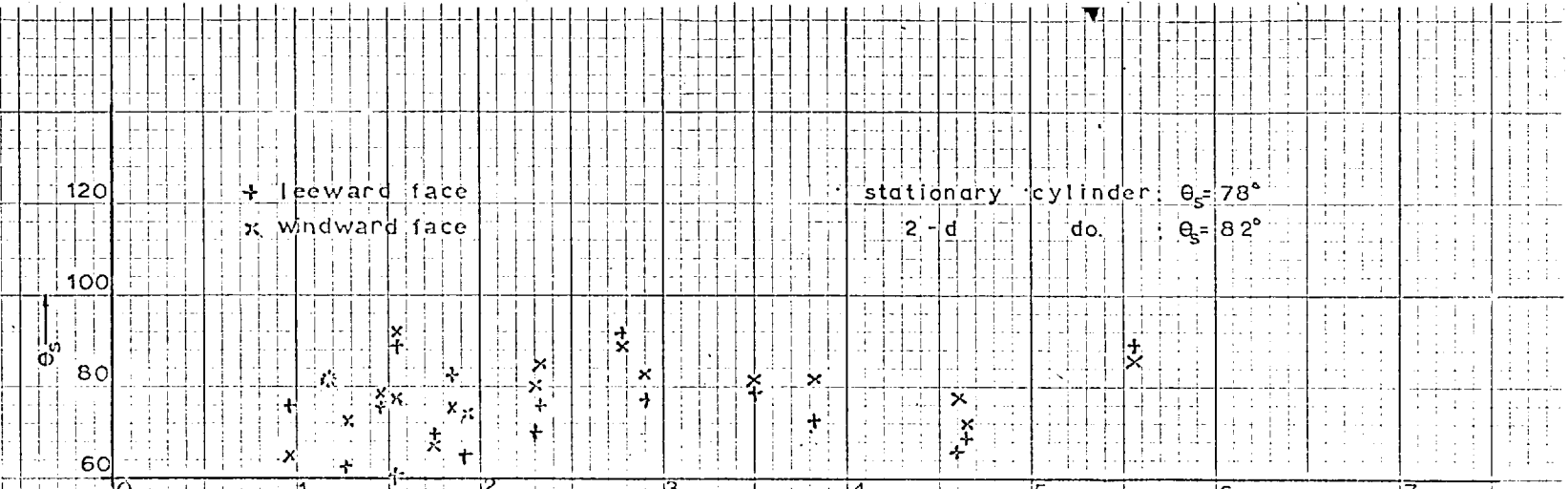

FIG.29: LOCATION OF SEPARATION POINTS ON ROTATING CYLINDER

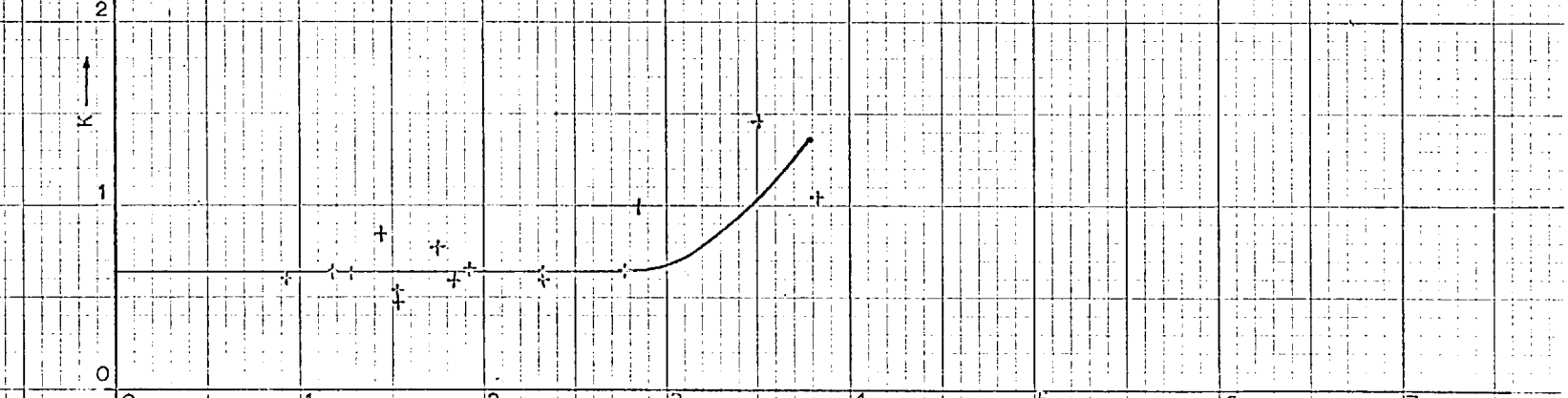

FIG.30: VARIATION OF K WITH THE ADVANCE RATIO

FIG. 29 & 30

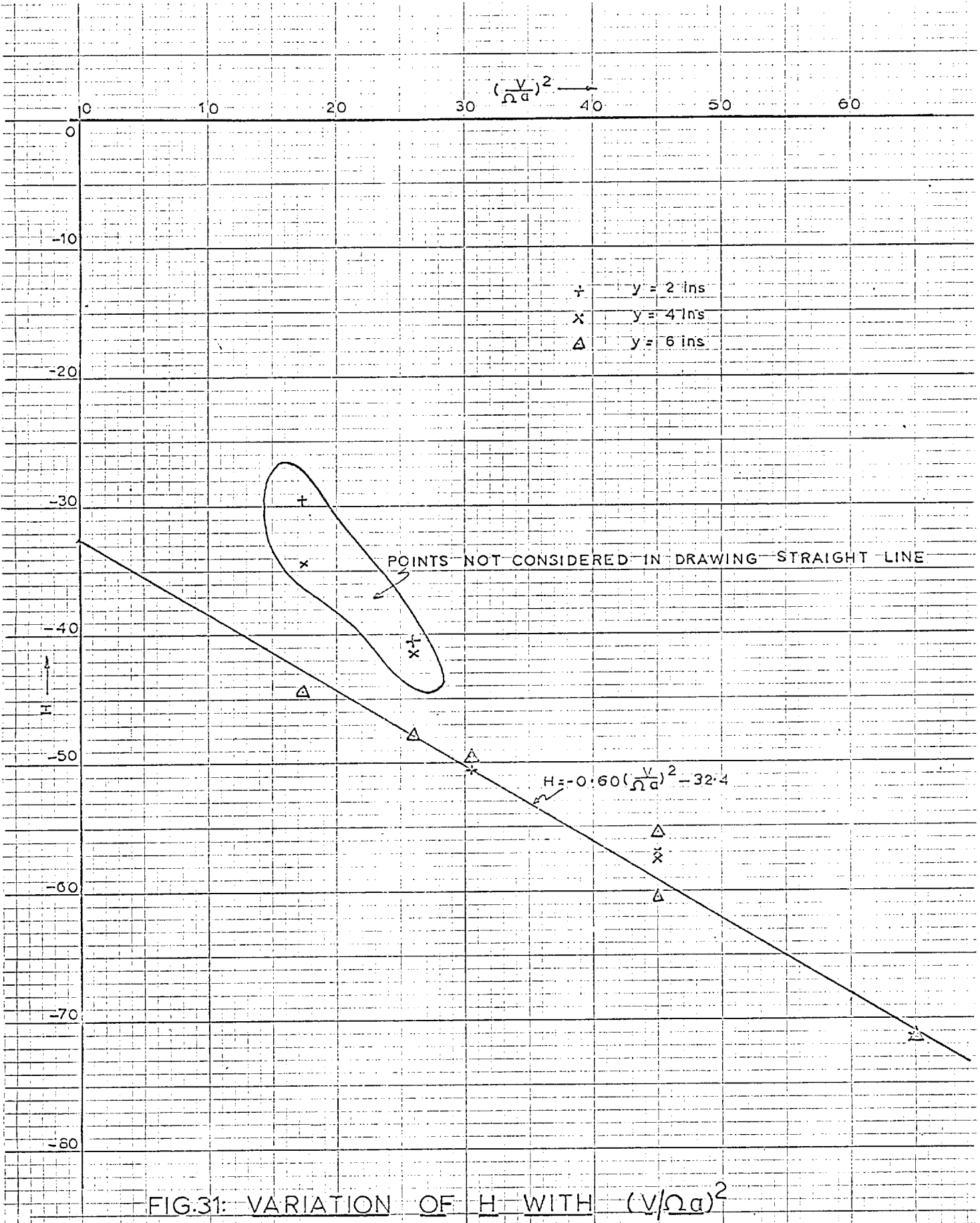

FIG.31: VARIATION OF H WITH $(V/\Omega a)^2$

FIG. 32 a, c & d

FIG. 32a : COORDINATE SYSTEMS USED IN INVESTIGATION

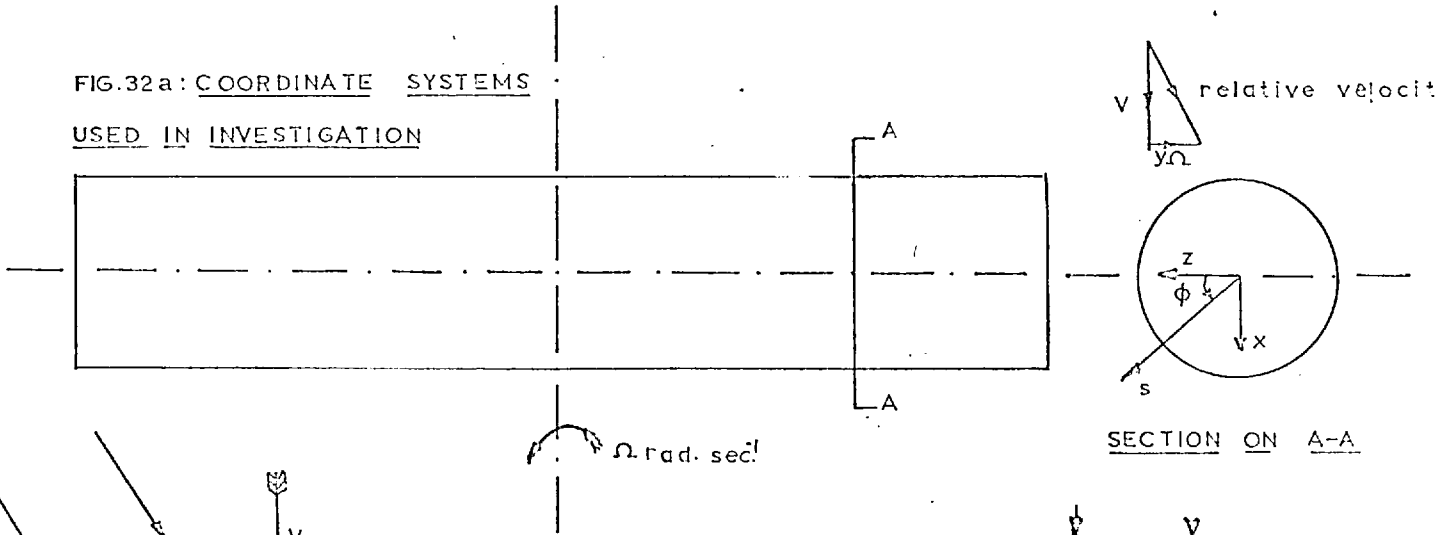

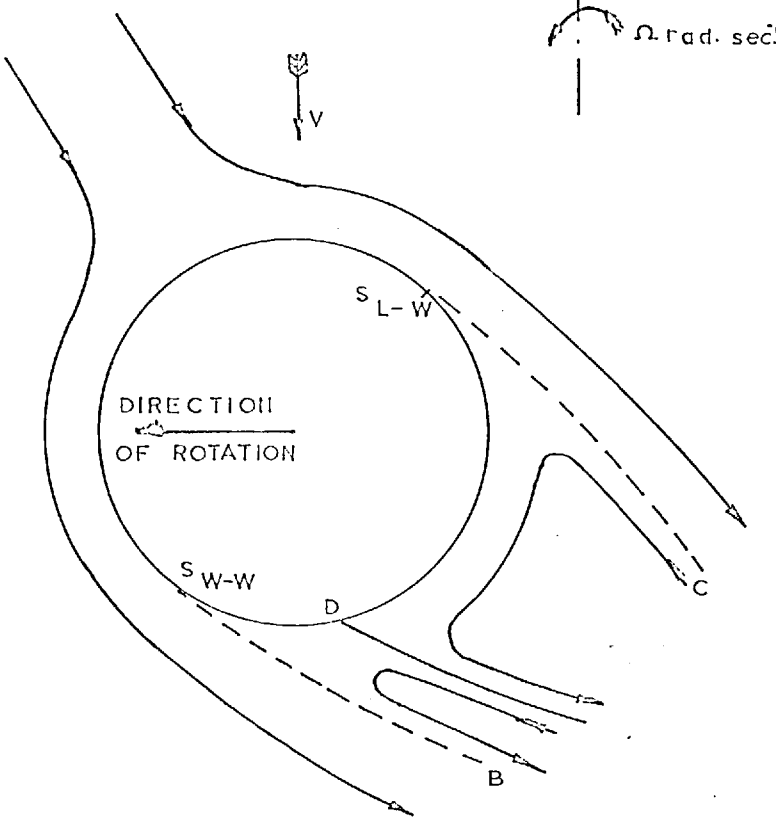

FIG. 32c : PROPOSED FLOW MODEL FOR ROTATING CYLINDER

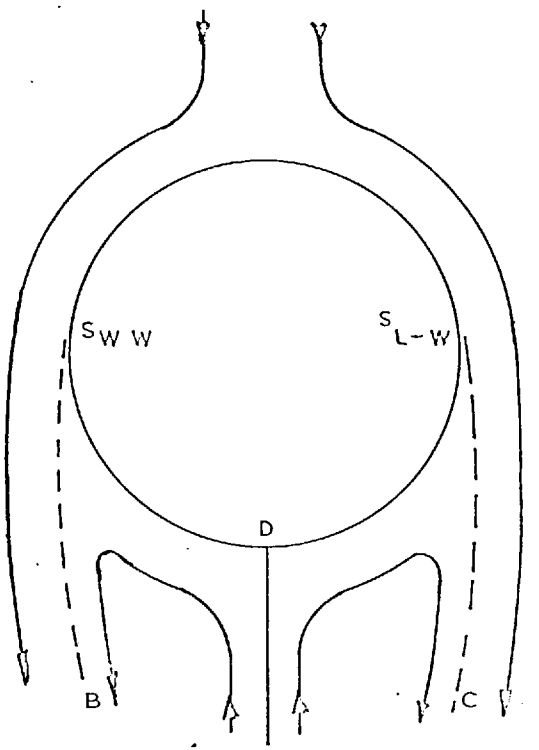

FIG. 32d : FLOW MODEL FOR STATIONARY CYLINDER

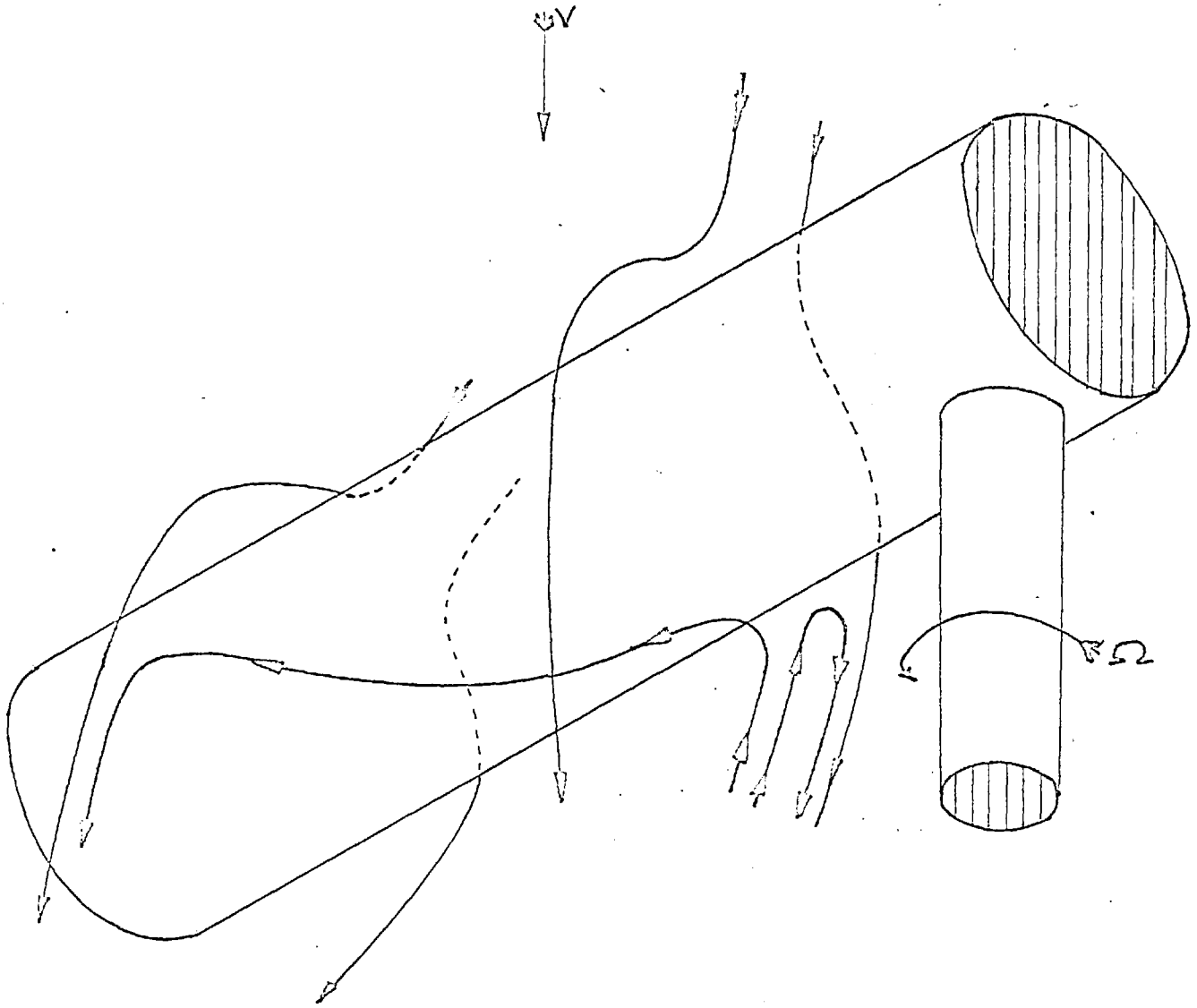

FIG.32b: ISOMETRIC VIEW OF THE FLOW PATTERN AROUND THE ROTATING CYLINDER

FIG. 32b:

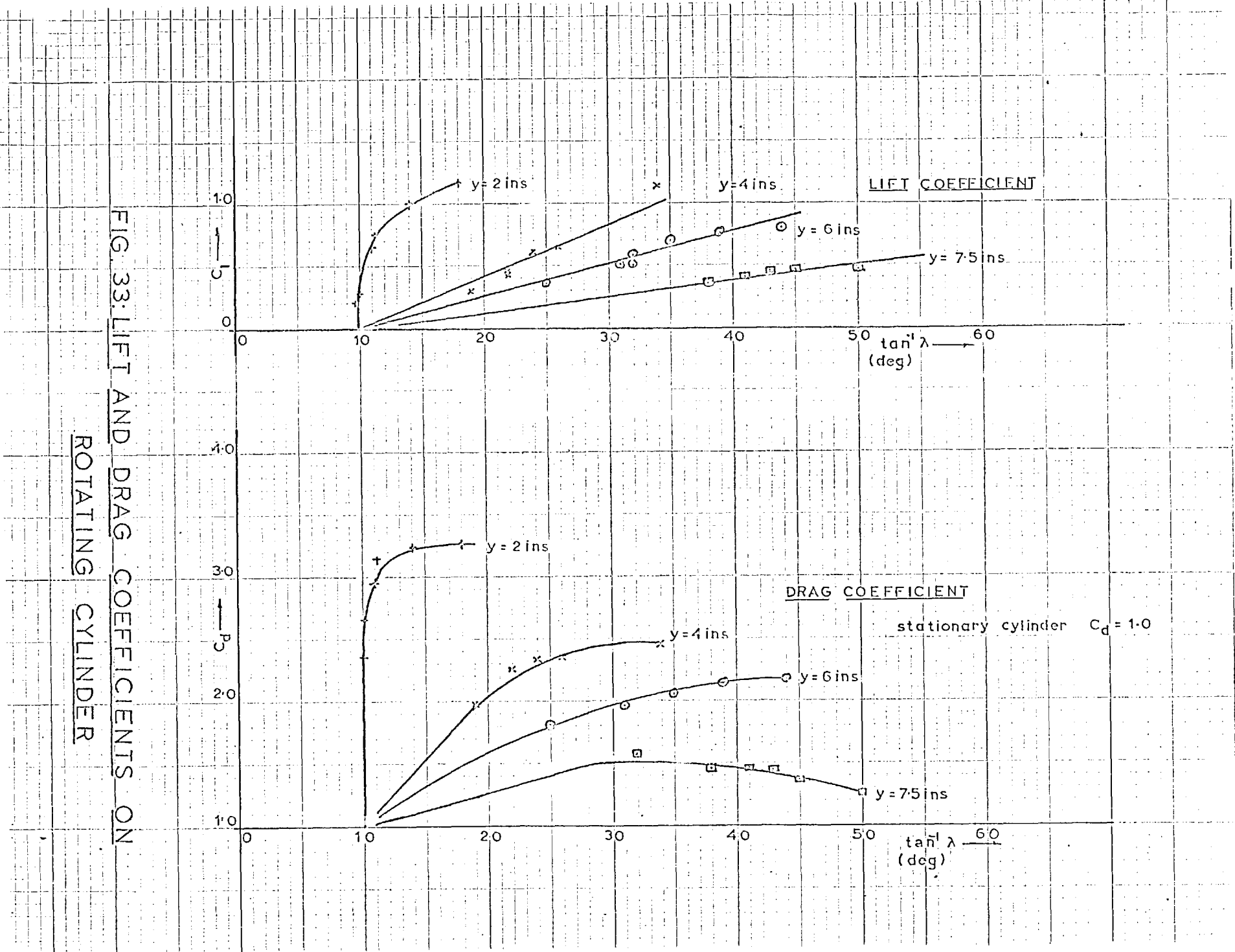

FIG. 33. LIFT AND DRAG COEFFICIENTS ON ROTATING CYLINDER

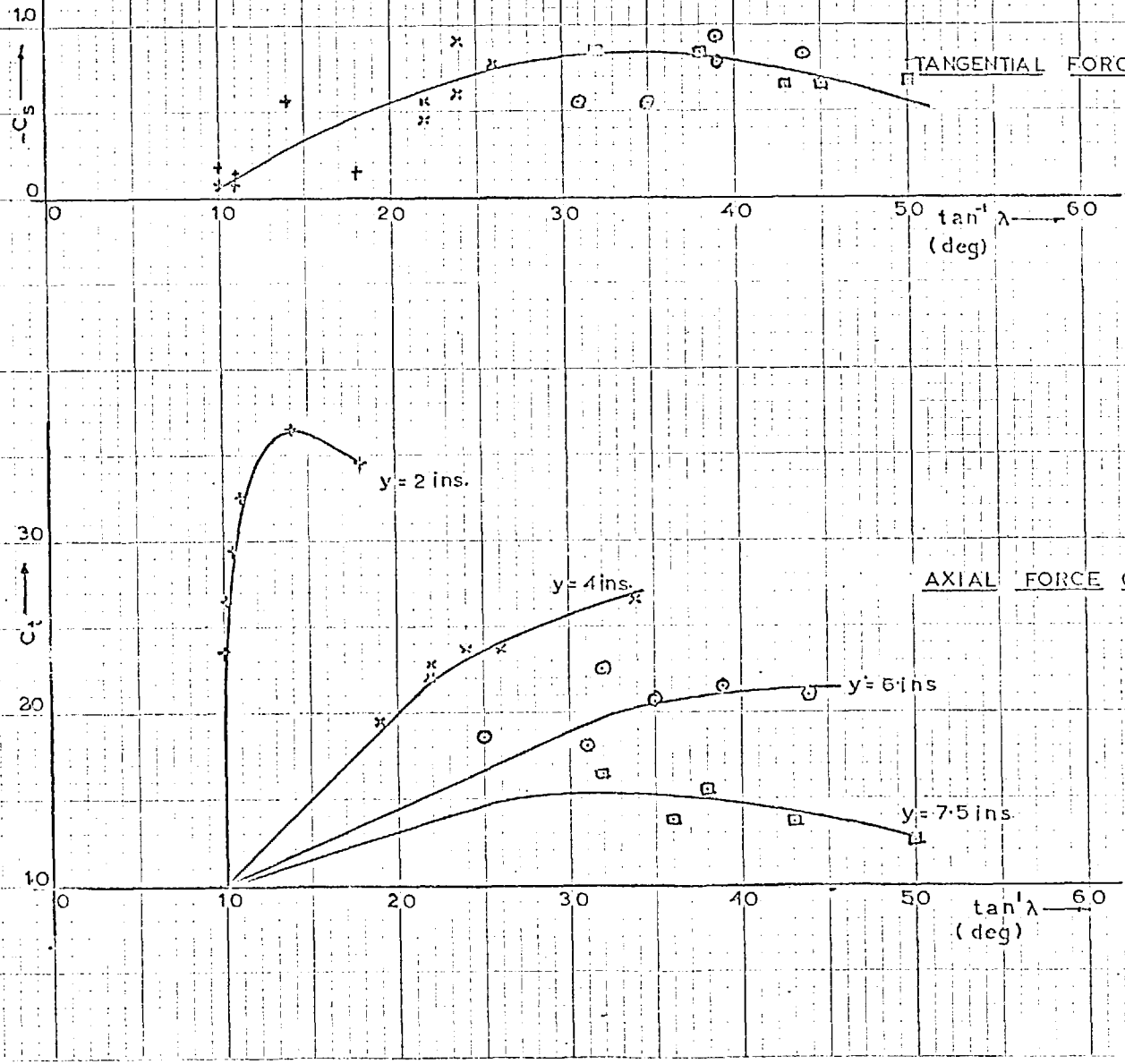

FIG. 34: AXIAL AND TANGENTIAL FORCE COEFFICIENTS ON ROTATING CYLINDER

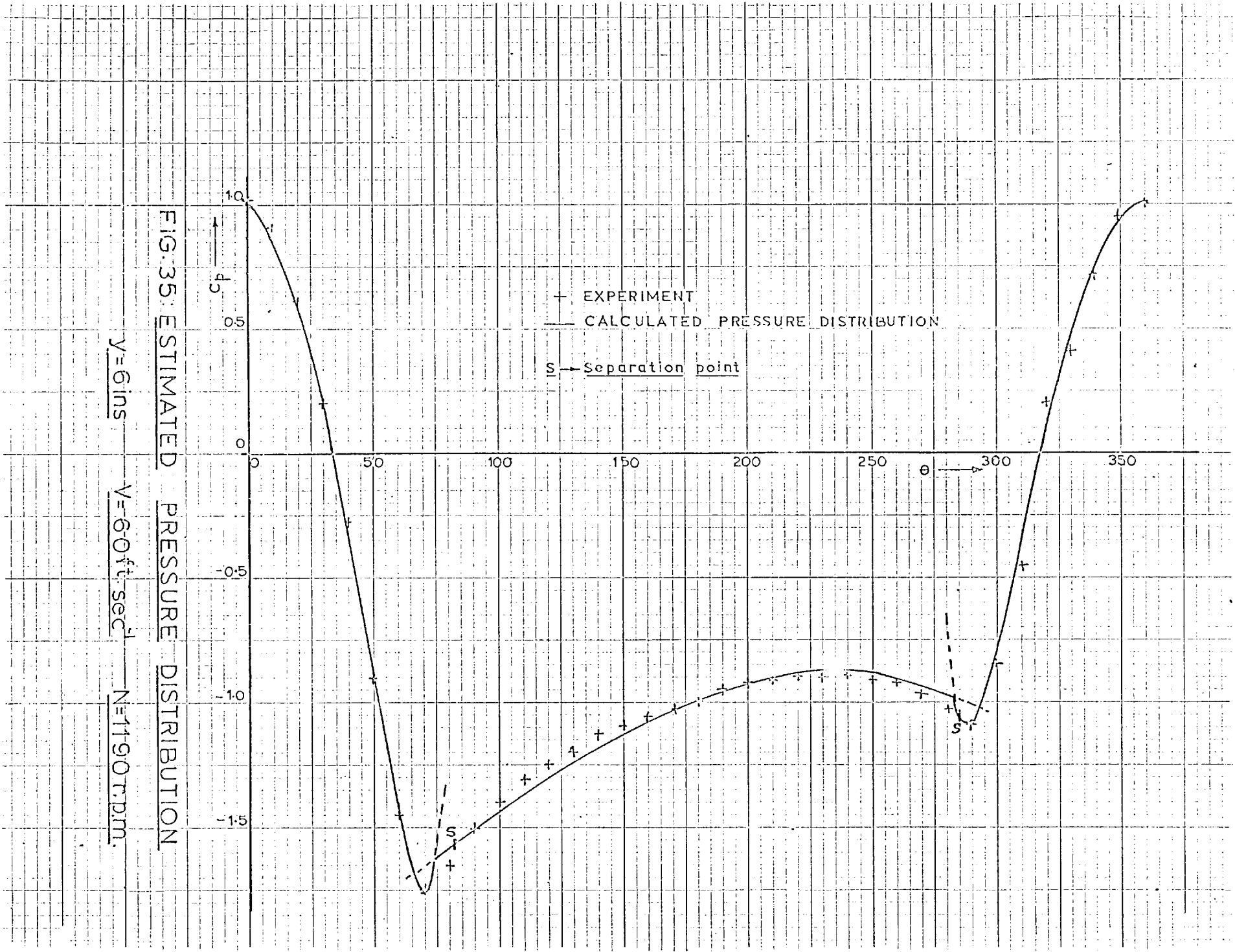

FIG. 35: ESTIMATED PRESSURE DISTRIBUTION

V=60 ft. sec^{-1} N=1190 r.p.m.

y=6 ins